Zirconia Based Supports for Rhodium for Automotive-Catalytic Reactions

Ian Burton

A thesis submitted in partial fulfillment of the requirements of The Nottingham Trent University for the Degree of Doctor of Philosophy

2001

Dedicated to the memory of

Richard Eaton

(1964-2001)

Abstract

Of the many factors investigated, the temperature of calcination and the ratio of ceria : zirconia in the bulk are the main variables that influence the character of the ceria / zirconia mixed oxide, when prepared by the coprecipitation route. The Plackett-Burman statistical approach used allows for a number of conclusions to be drawn. These include that mixed oxides calcined at 500°C have a surface area 85 m^2g^{-1} greater than those calcined at 900°C and reduce at a temperature 50°C lower. The use of the approach in preparing an 'optimised' catalyst has limited success.

Ternary additives, praseodymia, neodymia, lanthana and yttria, significantly influence the character ceria / zirconia mixed oxide. Ternaries at levels of 10 mol%, rather than at 3 mol%, offer greater stabilisation of surface area, the enhancement of which is greatest with lanthana and worst with yttria and this can be related to ionic radius.

As a support for rhodium, high temperature calcined supports significantly aid the catalyst in performing the CO-NO reaction. A ceria rich surface, high surface area and the addition of a ternary rare earth oxide into the support are also beneficial to the activity and selectivity of the catalyst. For N_2O decomposition, the surface area of the support, and hence the manner in which rhodium is supported on it, is directly related to catalytic activity.

The presence of rhodium species stabilises the surface area of tetragonal zirconia, when prepared as a 1wt% Rh / ZrO_2 mixed oxide by coprecipitation, and decreases the extent of the tetragonal to monoclinic phase transformation. Surface enrichment of rhodium under high temperature treatment improves the catalytic activity for N_2O decomposition.

The AlPO-5 structure is much less effective a vehicle for copper for the SCR of NO by propene than ZSM-5. The activity of each copper unit is much greater in the case of Cu-ZSM-5. The nature of the copper within the AlPO structure is shown to be different due to the mode of preparation and this is important to the catalytic nature of the material. A 1wt% Rh / ZrO_2 catalyst, when prepared by coprecipitation, is superior to Cu-AlPO in performing the SCR reaction.

Acknowledgements

I would like to thank my academic supervisor Professor Richard Joyner for his constant help, advice, support and encouragement throughout my Ph.D. studies. I am likewise grateful to my industrial supervisor Colin Norman.

I wish to thank MEL Chemicals Ltd. of Swinton, Manchester, for the support and funding that has allowed for the completion of this work. I would also like to thank Colin's colleagues at MEL, Peter Moles, Ian McAlpine and the technical staff for their suggestions and help.

Justin Hargreaves, now at the University of Liverpool, and Michael Stockenhuber, are gratefully acknowledged for their tireless work in the Catalysis Laboratory, their technical expertise, support and ideas.

To all the members of the Catalysis Laboratory and Research Office (1997-2000), I wish to say thank you for your friendship that has made my time in Nottingham so enjoyable.

Contents

Page Number

Page Number

List of Figures

List of Tables

Chapter 1:

Thesis Introduction:

Ceria / Zirconia Based Supports for Rhodium for Automotive Catalytic Application.

'Objects in the rear-view mirror may appear closer than they are.'

Meatloaf, from the album Bat Out Of Hell 2

1.1: General Introduction

A catalyst is described as a substance that increases the rate of reaction but is not itself consumed. A catalysts does not change the thermodynamics of a reaction and so does not change the equilibrium constant.

'Catalysis', from the Greek *katalysis* meaning a breakdown or loosening, was a word introduced in the early nineteenth century by Berzelius. This was around the time of great breakthroughs in this branch of physical chemistry. One notable breakthrough was the development of the miner's safety lamp by Humphrey Davy. Davy realised the potential of newly discovered, extracted and purified platinum. By catalytic oxidation, carbon monoxide caused glowing on platinum gauze, indicating to miners the danger of their surroundings. One hundred and fifty years on, catalysts are widely used in industry and the laboratory, and it is estimated that they contribute to the manufacture of one-sixth of all goods in industrialised countries (1,2,3).

This work deals with the preparation and testing of catalytic materials for the destruction of polluting gas from automotive sources. The requirement and method for the removal of these gases are discussed in the following sections.

1.2: Environmental and Legislative Requirements for Automotive Pollution Abatement

Atmospheric pollution caused by traffic volume came to prominence in 1950's Los Angeles, although it was known that coal burning had given rise to atmospheric pollution long before that. Oxides of nitrogen, from the combustion of nitrogen in air, and oxides of sulphur, from the combustion of sulphur containing fuel, for some time had been associated with acid rain. Hydrocarbons (HCs) and carbon monoxide from inefficient combustion processes and ozone and peroxyacetyl nitrate (P.A.N.) from photochemical reactions have now become associated with traffic volume. These pollutants act together and became linked with bronchitis, pneumonia and immune response suppression. The effects on health caused by the smogs led the Californian authorities to pass stringent legislation requiring the reduction in the levels of the

nitrous oxides (NOx), carbon monoxide (CO) and hydrocarbon (HC) pollutants, including particulate matter (4-6).

In the European Union strict air quality standards have been set (7). Directives applied to automotive sources of pollution have been enforced in order to achieve such standards (8,9).

Vehicle emission of NOx, CO and hydrocarbons are governed by a series of EC Directives which are enforced in the U.K. under the Motor Vehicles and Construction and Use and Type Approval Regulations. The Road Vehicles (Construction and Use) (Amendment No 2) Regulations 1990, implemented through Motor Vehicles (Tests) (Amendment No 3) Regulations 1991, require vehicle users to keep engines in tune, ensure that emission control equipment is functioning correctly and to have these tested annually.

EC Directive 94/12 came into force on 1st January 1996 for new models of light duty vehicles (cars and vans) and became applicable to all new cars from 1st January 1997. The current emission limits, for an average driving cycle, from this Directive are shown in table 1.1. (8-9).

Table 1.1. Automotive emission limits

Engine Type	**Emission Limit (g km^{-1})**		
	CO	**HC + NOx**	**Particulate Matter**
Petrol Engine	2.2	0.5	-
Direct and Indirect Injection Diesel	1.0	0.7	0.08

1.2.1: NOx: Source and Impact

Petrol consists of a mixture of hydrocarbon compounds, which, when combusted in sufficient air will produce carbon dioxide and water. Assuming the average molecular formula for petrol is C_8H_{18}, then the equation can be written thus:

$$C_8H_{18} + 12\,½\,O_2 + 47\,N_2 \rightarrow 8CO_2 + 47\,N_2 + 9\,H_2O$$

The typical concentrations of exhaust gas constituents however are 750 ppm of hydrocarbons, 1050 ppm of NOx, 0.68 vol% carbon monoxide, 0.23 vol% hydrogen, 13.5 vol% carbon dioxide, 0.51 vol% oxygen and 12.5 vol% water, with the balance mostly being nitrogen (6).

The major product, carbon dioxide, is not directly harmful to the atmosphere with no direct effect on health. Global concentrations of carbon dioxide in the atmosphere are about 350 ppm and are rising at the rate of 1 ppm per year. The gas is an infra-red radiation absorber and as such acts as a heat sink. Excessive CO_2 levels are thus contributing to the "greenhouse effect", the unnatural warming of the earth.

In 1995, the Intergovernmental Panel on Climate Change Working Group 1 concluded that there was evidence suggesting influence on the global climate by the activities of man. In 1997 the Kyoto Protocol was approved, resulting in a number of industrialised nations agreeing to reduce "greenhouse gas" emissions (10,11).

Reduction of carbon dioxide emissions from automotive sources can be achieved by a number of strategies (12). Battery powered electric vehicles and fuel cell powered cars have the long term potential to replace the existing internal combustion engine powered automobile. Such strategies would also cause reduction in the overall emissions of the other previously mentioned pollution gases. Recently, hybrid vehicles i.e. petrol / battery powered cars have become available to the British public with the arrival of the Honda Insight and Toyota Prius (13). Vauxhall has unveiled a Vectra model that runs on liquid petroleum gas (LPG). This car produces 75% less CO, 40% less NO and 85% less hydrocarbons than the equivalent diesel powered model (14).

Carbon monoxide is a colourless, odourless, tasteless gas produced by inefficient carbon combustion processes. Along with small particulates and

hydrocarbons, CO can enter the lungs, threatening the health of individuals with existing respiratory problems (10). It is the presence of CO in the exhaust gas which offers the best method for the removal of NOx, as will be discussed in the following section.

NO and NO_2 are the major constituents of what is described as NOx. NOx is formed by high temperature and pressure combustion of fuel in the automobile engine with both fuel bound nitrogen and nitrogen from the air being oxidised. NO formation results from a chain reaction mechanism.

$$N_2 + O \Leftrightarrow NO + N \quad \textit{and} \quad N + O_2 \Leftrightarrow NO + O \quad \textit{and} \quad N + OH \Leftrightarrow NO + H$$

Other pathways involving N_2O intermediates and CH radicals are also claimed to be of importance. As exhaust gas cools upon leaving the exhaust pipe, NO is slowly, but readily, converted to NO_2.

NO_2 can irritate the lungs, lowering the resistance to infection It is an important precursor in acid rain formation, and can cause nutrient enrichment of the aquatic environment, leading to algal blooms and ecosystem destruction. It is the contribution to photo-oxidant ozone and photochemical smog formation that has caused much concern in recent times. Ozone and photochemical smog are known to exacerbate symptoms for people with respiratory problems, affect crop yield, general plant growth and the durability of materials. The effect of ozone and smog on the local environment is dependent upon climactic and geographical conditions (6,10,11,15).

1.3: The Automotive Three-Way Catalytic Converter (TWC): Form, Function and Chemistry

1.3.1: The Form and Function of the TWC

From the previous sections it is seen that there are both legal and environmental necessities for the removal of carbon monoxide and nitrogen oxides from the exhaust of petrol driven motor cars. Catalysis offers a route by which this requirement may be met.

The 'Three Way Catalytic Converter' (TWC) is now found in every new car

sold in the U.S., Australia, Japan and in the European Union. The encased catalyst is found between the engine manifold and the silencer box. The term TWC is used as three major reactions are catalysed, shown below.

1. $CO + {}^{1}/_{2}\, O_2 \rightarrow CO_2$
2. $Hydrocarbons + O_2 \rightarrow CO_2 + H_2O$
3. $2NO + CO + H_2 \rightarrow N_2 + CO_2 + H_2O$

The TWC technology has been the main source of automotive pollution abatement for 25 years. The process involves advanced catalysis and material science in conjunction with engine management systems and onboard diagnostics (3-6).

The extent to which a petrol engine emits atmospheric pollutants depends on a number of factors, the most important is commonly the ratio of air to fuel that is injected into the cylinders. This ratio is designated lambda, and a value of $\lambda = 1$ is assigned to the stoichiometric ratio of air required to completely combust the petrol fuel. With excess fuel ($\lambda<1$) greater levels of CO and HC's are emitted. At higher λ values, less CO and HCs but more NO are emitted. The catalysis of NOx removal in lean conditions will be discussed in chapter 6.

The TWC has been designed to function in an environment of $\lambda=1$, as shown in figure 1.1. and only functions well close to this point. The stoichiometric ratio is maintained by the electronically controlled engine management system which, by the use of oxygen sensors and monitors, controls the concentration of oxygen entering the engine. Sudden, rapid acceleration and deceleration leads to the air-fuel ratio being decreased and increased respectively for a short while, until the control systems can adjust the settings. Over time, to improve efficiency when the TWC is working under non-optimal, transient conditions, further components have been added to the catalyst.

Fig 1.1. Catalyst efficiencies around the λ=1 point.

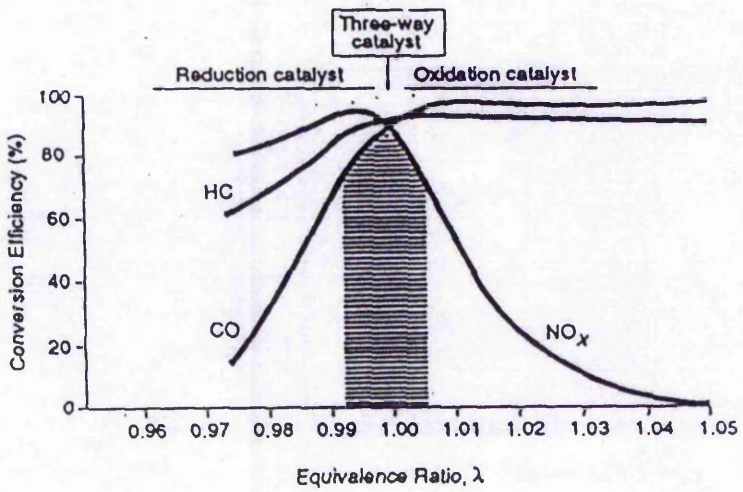

The monolith catalyst is now the most common in use. The honeycomb structure that supports the active constituents is made from the mineral cordierite $(Al_3Mg_2Si_5Al)O_{18}$. There are approximately 400 axial openings per inch^2 through which exhaust gases traverse longitudinally with rapid velocity and little pressure drop (3-6, 16-18). Figure 1.2 shows the structure and general functions of the TWC.

Figure 1.2. Structure and function of the TWC (3).

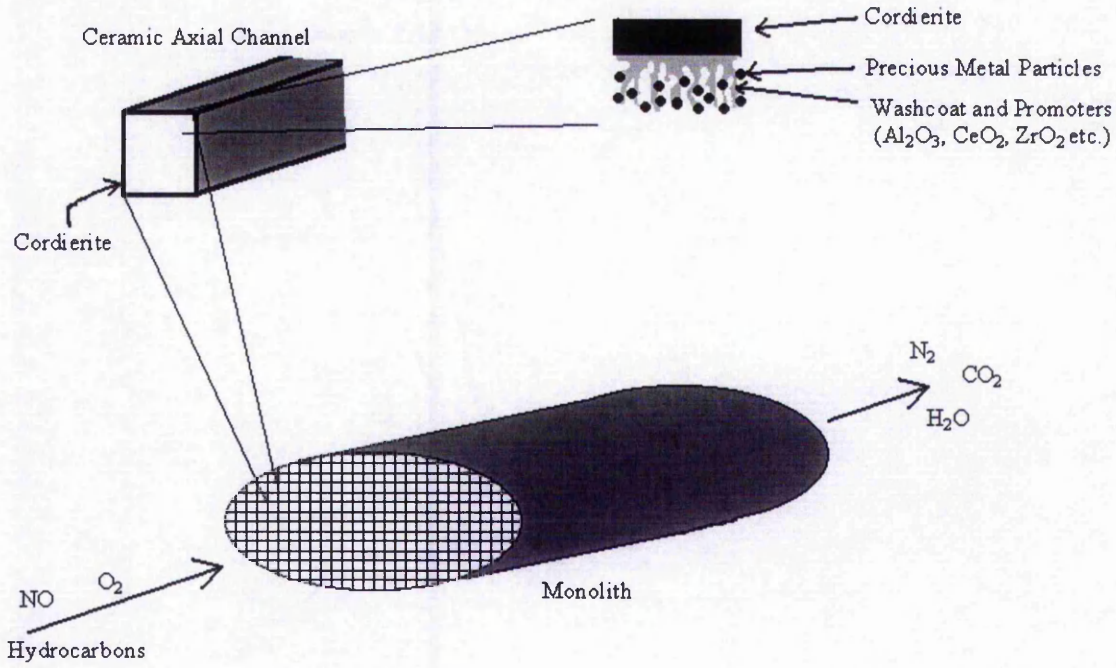

A thin alumina washcoat is applied to the cordierite surface, and acts as the support for the noble metal catalyst. The typical precious metals are rhodium (Rh) plus platinum (Pt) and /or paladium (Pd). Rh promotes the reduction of nitrogen oxides (NO_2, NO, N_2O_4 and N_2O), commonly referred to as NOx, to nitrogen (N_2). Pd and /or Pt are primarily responsible for the oxidation of carbon monoxide (CO) and hydrocarbons (HC's). Ceria as part of the washcoat promotes the water-gas shift reaction, stabilises the metal dispersion against thermal damage, improves precious metal reduction, catalyses steam reforming and NO reduction and participates as an oxygen storage compound. Zirconia is commonly used to retard Rh agglomeration, improving the thermal stability of the alumina and to promote the activity of ceria. Other oxide stabilisers such as lanthana, silica and barium for NOx storage may also be found in the modern catalyst (3-6,16,17).

The automotive catalytic converter works in the range 300-900°C and must maintain high conversion over the life time of the engine, typically 150,000 miles. To be thoroughly effective, optimal pore size distribution, optimal metal particle size and excellent distribution of the active metals within the pores is required. The mechanical strength and thermal shock resistance are provided by the monolith (3-6,16-18).

1.3.2: Rhodium as a Component of the TWC

Rhodium is a transition metal and one of the group of platinum group metals. It is used in numerous catalytic processes (18). Here the chemistry of the metal is reviewed with regards its presence in the TWC.

NO is removed in the TWC by the reaction shown below:

$$2\,CO + 2\,NO \rightarrow 2\,CO_2 + N_2$$

The reaction is catalysed by the noble metals (4). Of all the noble metals rhodium has been shown to be the most effective as a component in the TWC for this reaction. The dissociation of NO (a prerequisite for the CO + NO reaction) on the metal surface has been argued to be the reason for this (19). Figure 1.3. shows the comparative ability of

platinum and rhodium surfaces to dissociate NO. The graph shows nitrogen and oxygen desorption upon heating following NO absorption.

Ruthenium has been shown to be active for the CO + NO reaction when supported on alumina. Total conversion of NO to N_2 has been observed at temperatures below 250°C. The order of activity has been shown to be Ru > Rh > Pd > Pt (20). The presence of oxygen was shown to be detrimental to ruthenium activity because of volatility issues. Iridium is active for the reaction in the presence of oxygen. Results indicate the Ir has the ability to absorb NO well in the presence of oxygen with results comparable to that of rhodium (20,21). The metals of choice for the reaction are susceptible to sintering, over oxidation of the surface and deactivation in highly oxidising environments, and so NOx conversion decreases in lean burn conditions (4). Other catalytic strategies are thus required for NOx removal in such environments, these are discussed in chapter 6.

Fig 1.3. Graph of the ability of metal surfaces to dissociate NO.

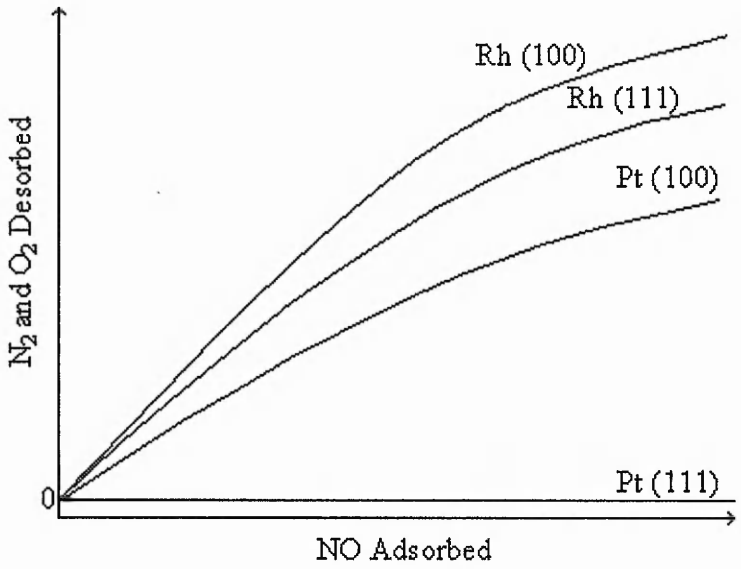

Many investigations have been undertaken to determine both kinetics and mechanism of the CO + NO reaction. Studies have dealt with adsorption and desorption of the components of the reaction and the importance of formation of N_2O in the

production of nitrogen and carbon dioxide (4,6,15,22-25). N_2O is stable at room temperature and temperatures above 650°C for cleavage of the N-O bond in the gas phase are required, in the absence of a catalyst (26,27). The presence of reducing agents can further aid removal. The reactions are exothermic and irreversible (28,29). Decomposition of nitrous oxide by use of a rhodium catalyst has been reported (30). The CO-NO and N_2O decomposition reactions are discussed further in chapter 5.

1.3.3: Supported Rhodium

The interaction between rhodium particles and a γ-alumina support has been investigated with regards to NO adsorption (31). The metal-support interface was suggested to be a site for NO dissociative adsorption. The loading and particle size distribution of rhodium on the support have also been shown to important to the activity of the catalyst (6,32,33).

The manner in which the catalyst is treated severely affects the physical characteristics. Rhodium dispersion is not drastically influenced by reducing conditions at temperatures as high as 700°C but is in oxidising conditions as alluded to earlier. In such conditions rhodium is rapidly oxidised resulting in dissolution into the support, resulting in a decrease in the amount of surface rhodium present. The higher the temperature the more rapid the process. Upon reduction of the catalyst only partial recovery is attained and the rhodium is present as sintered particles (34,35).

The introduction of zirconia into the washcoat favours the formation of Rh – O – Zr bonds retarding agglomeration of rhodium and improving the thermal stability of the support, maintaining catalytic activity (16,36-39). Although washcoat stabilisation is not the main reason for ceria use in the TWC, it has been shown to retard alumina phase change and surface area loss at high temperature (40). Platinum dispersion has been shown to be stabilised at high temperature against sintering by the formation of a surface complex of Pt - O - Ce (41).

1.4. Zirconia and Ceria

1.4.1: Zirconia and Ceria Stabilised Zirconia

Zirconium is found in the second row of the transition metals with an atomic mass of 91.22 and an atomic radius of 1.45Å. The metal is hard and corrosion resistant. It is relatively abundant but is not found in concentrated deposits and only in the combined state. It bonds preferably with oxygen and occurs naturally as the oxide baddeleyite or as part of a complex of oxides containing silicon (18,27).

Zirconia (ZrO_2) is polymorphic. The monoclinic form (baddeleyite) changes at around 1100°C to the tetragonal form and at around 2300°C to the cubic form which has the fluorite structure. Figure 1.4. shows the phase changes that occur in zirconia. The diagrams represent 8 oxygen ions surrounding a Zr^{+4} ion placed at the centre of each cube.

Fig 1.4. The polymorphism of zirconia

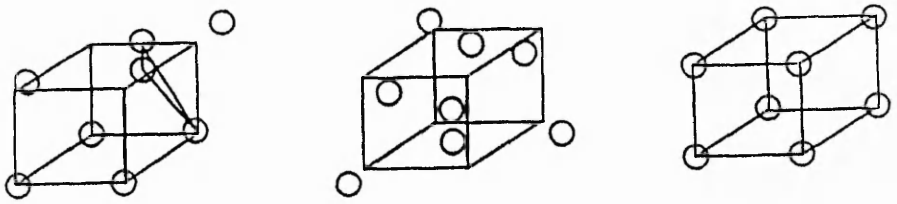

The tetragonal form, the structure most relevant to this work, has a distorted fluorite structure. 8 O^{2-} neighbours are not equidistant from the Zr^{4+} centre. There are 4 sets of 2 oxygen neighbours at 2.065 and 2.455Å, respectively, away from the centre (16,27).

The high temperature tetragonal phase cannot be retained upon rapid cooling to room temperature, but the tetragonal structure can exist at room temperature if prepared by precipitation from aqueous solution or by low temperature calcination of zirconium salts. This is important, as it is the tetragonal form which is generally of interest as a

high surface area catalyst or catalyst support. Prepared by this method, from the hydroxide, zirconia is wholly tetragonal at temperatures of 500-700°C and monoclinic over 900°C. Between 700 and 900°C there is often a mixture of tetragonal and monoclinic phases present (42,43).

The aqueous chemistry of zirconium compounds is based on Zr – O bonds and polymeric structures (16,44,45). Upon precipitation a number of possible hydroxides / hydrous oxides can be formed, depending on how the hydroxide is prepared and treated (44,45). The preparation chemistry of zirconia is complex and numerous factors have been investigated with regards to the nature of the final product. The pH of precipitation (46,47), nature of precipitant (48-53) and aging time and temperature of the precipitate in solution (44,54) have been studied. Such variables, along with the drying and calcining of the hydroxide / hydrous zirconia, are discussed in chapter 3.

The 'critical size argument' has been used in an attempt to explain the transformation of tetragonal zirconia to the monoclinic polymorph (42,54). The argument states that phase is determined by the energy of the bulk, surface and strain effects. Tetragonal zirconia at room temperature is characterised by small mean crystallite size, large surface area and excess energy. Upon heating of the zirconia there is a decrease in excess energy, surface area decrease and crystallite growth and phase transformation. It was stated that at the point of transformation the free energies are equal, and the point corresponds to a crystallite 'critical size' of 30nm.

Ceria has been used to stabilise tetragonal zirconia (43). Here the critical size argument was supported as both 2 and 4% ceria in zirconia, calcined at 950°C had a percentage tetragonal phase of 85% with a mean crystallite size of 22 nm. In this zirconia phase the cation network is strained and oxygen overcrowding exists. The tetragonal phase is stabilised against monoclinic transformation by the addition of the oversized tetravalent dopant Ce^{4+}. The Ce^{4+} cation forms a random substitutional solid solution with zirconia. The 8-fold oxygen co-ordination around the oversized Ce^{4+} and the dilation it causes stabilises the tetragonal structure by relieving strain and oxygen overcrowding (55).

1.4.2: Ceria and Rare Earth Oxides

1.4.2.1: The Chemical Nature of Ceria and Rare Earth Oxides

Cerium is a member of the rare earth group of elements. The rare earths are a group of elements having similar chemical properties, consisting of the lanthanide group (Ln's), lanthanum and yttrium. Scandium is sometimes also considered a rare earth. Figure 1.5. shows the rare earth group of elements, shaded.

Figure 1.5. The rare earth elements

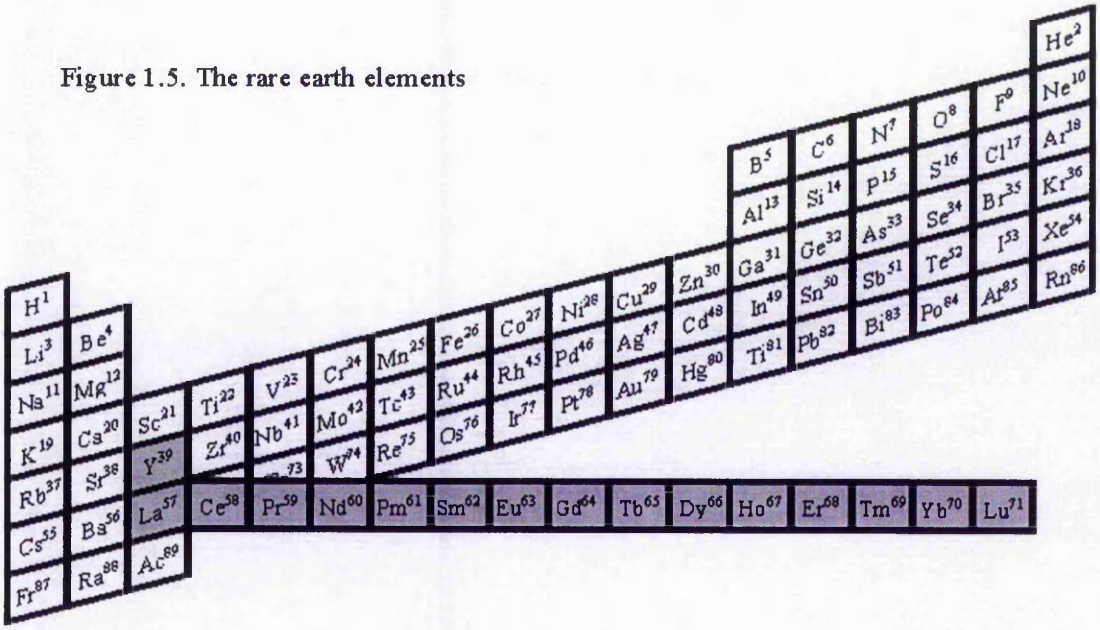

The name itself is a misnomer, they are not exceptionally rare, except promethium. Yttrium is more abundant than lead and the rarest are more common than the platinum group metals. The metals are obtained from the minerals monazite, xenotime and bastnasite, amongst others. The metals can be leached out by acid; precipitation and ignition then gives a rare earth mixed oxide.

The 'lighter' rare earth oxides used in this thesis are those of the metals yttrium, lanthanum, cerium, praseodymium and neodymium, with the atomic weights and radii of 88.91 and 1.88Å, 138.91 and 1.88Å, 140.12 and1.846Å, 140.91 and 1.828Å and 144.24 and 1.821Å respectively (18,27,56,57).

Of the rare earth oxides investigated in this work, Y^{3+} is 6-coordinated and La^{3+}, Ce^{3+}, Pr^{3+} and Nd^{3+} are 7-coordinated. Yttria has a hexagonal structure. The other, 3+, 7-coordinated oxides consist of LnO_7 units as shown if figure 1.6. Ceria in the 4+ state exists in the fluorite (CaF_2) structure, whereas Pr_6O_{11} exists as a fluorite-like structure in which one twelfth of the anions have been removed. Figure 1.7. shows the fluorite structure of ceria 4+ (58-60).

Figure 1.6. The LnO_7 structure of and La^{3+}, Ce^{3+}, Pr^{3+} and Nd^{3+}

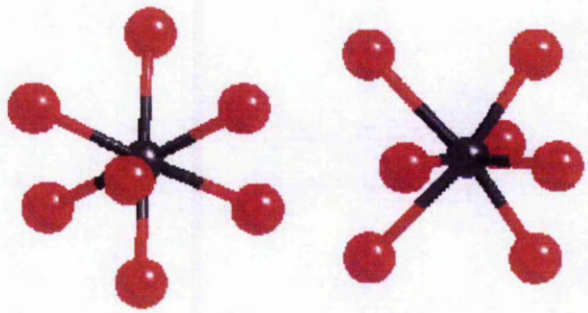

1.7. The fluorite nature of ceria 4+.

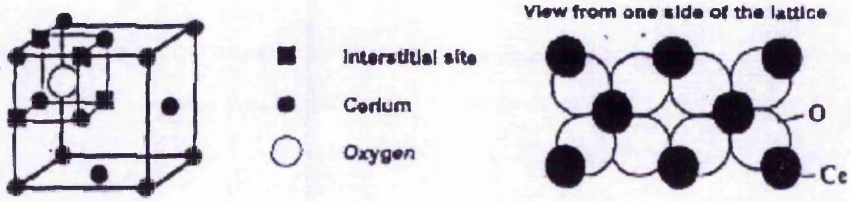

1.4.2.2: The Role of Ceria and Rare Earth Oxides in the TWC

Ceria is used in three-way catalysts for a number of reasons (61,62), which are now discussed.

The reduction of CeO_2 to Ce_2O_3 was thoroughly investigated and reported almost half a century ago (63) but it wasn't until the 1980's that this was applied to automotive three-way catalytic converter technology (64).

From figure 1.1. it was seen that the TWC operates optimally at the stoichiometric air to fuel ratio, λ =1. The oxygen storage capacity (OSC) of ceria provides oxygen for the oxidation of HCs and CO when the car is transiently running fuel rich, and it takes up oxygen when the car is running fuel lean: -

(1) Partial Ce^{4+} reduction to Ce^{3+} (oxygen release)

$$xCO + CeO_2 \rightarrow xCO_2 + CeO_{2-x}$$

(2) Reverse reaction (oxygen storage)

$$0.5xO_2 + CeO_{2-x} \rightarrow CeO_2 \quad (where\ x = 0 - 0.5)$$

The OSC widens the air-fuel ratio window where all the major pollutants can be removed (60). From figure 1.1. it was seen that high air : fuel ratios ($\lambda > 1$) result in decreased NO removal. It is the ability of ceria containing materials to reduce and reoxidise which is of benefit here (65-69) and is thus described.

Addition of ceria also reduces the rate of rhodium deactivation, and so prolongs the life of the three-way catalyst. Accumulation of surface oxygen species resulting from NO decomposition is one explanation that can be offered for this. Reduced ceria can allow excess oxygen from the metal to 'spill over' allowing further NO decomposition. Bulk oxygen vacancies in the ceria / zirconia mixed oxide are implicated in further enhancing NO decomposition by the promotion of the oxygen vacancy gradient.

Section 1.3.3. discussed the ability of NO to decompose on the rhodium – zirconia interface. It has been argued that ceria spreads onto the metal surface allowing

oxygen migration between the two entities creating a large interface where the CO + NO reaction can occur (70,71).

The oxygen storage capacity and support function of ceria is dependent on surface area and thermal stability at high temperatures commonly experienced in the catalytic converter. The type of ceria originally used sintered at 800°C and showed decrease in redox efficiency. Thus an improvement of the material was sought. This was achieved by a number of routes (60,70-75):-

1. improving the process by which ceria was made
2. adding zirconia to the ceria
3. adding dopants to stabilise the ceria

The temperature programmed reduction (TPR) of ceria shows the benefit of zirconia addition. Ceria (4+) reduction has been shown to be a 2 step process due to limited oxygen diffusion in the oxide. The magnitude of the first step, at about 400-500°C, is dependent upon the surface area of the sample. The second step, at approximately 750-950°C, represents the bulk reduction of CeO_2 to Ce_2O_3 (63,76-78). Zirconia addition changes the reduction characteristics. The presence of a single reduction peak, at temperatures lower than that of the second reduction step of pure CeO_2, indicates that zirconia has a key role in linking surface and bulk reduction (60). Zr^{4+} has an effective ionic radius of 0.84 Å, compared to Ce^{4+} which has an effective ionic radius of 0.97 Å. This small difference allows the possibility for the substitution of Ce by Zr in the CeO_2 cubic phase (60). Structural disorder has been shown in a ceria / zirconia mixed oxide because of the insertion of ZrO_2 into the CeO_2 cubic lattice (79). The disorder was explained in terms of a decrease in the number of nearest neighbour oxygens associated with Zr^{4+} from 8 to 6, with the two missing oxygens having a Zr-O bond distance greater than 2.7 Å. These distortions generate mobile oxygen ions which are responsible for improved redox properties at moderate temperatures. Computational methods have been used to investigate the doped system. Reduction energy is significantly reduced in the mixed oxide and the activation energy for oxygen migration in the bulk is low, implying facile oxygen diffusion through the bulk catalyst, resulting in a decrease in reduction temperature (80-82).

The crystal phase is important when considering OSC of the mixed oxides (48,60,83). For the crystalline state, the OSC increases in the following manner...

Pure cubic CeO_2 < Phase separated ceria / zirconia < Discrete solid solution.
mixed oxide

The ceria / zirconia mixed oxide has been prepared by numerous routes, including incipient wetness (43), coprecipitation (84), high energy milling (86), and sol-gel methods (86). The mode of preparation route may strongly influence the crystal phase and hence OSC.

OSC has been shown to be very good with zirconia at concentrations of 15-50% but best at 30%. This corresponds to the optimum amount of zirconia, homogeneous in the mixed oxide, for the enhancement of oxygen mobility (60). The ratio of the components in the mixed oxide also determines surface area and reduction temperature (61,87). Figure 1.8. shows the general influence composition has on surface area and reduction temperature. The materials were calcined at 900°C.

From figure 1.8. it can be seen that ceria stabilises the surface area of zirconia, as previously described, and zirconia at low levels stabilises the surface area of cubic ceria. The latter occurs by inhibition of sintering and prevention of grain growth at high temperatures, improving thermal stability (83). As with OSC, the temperature of reduction is lowered by an optimal oxide ratio similar to that previously described.
The characteristics of ceria / zirconia mixed oxides are investigated and further discussed in chapter 3.

Figure 1.8. Composition of the mixed oxide, surface area and reduction temperature (61,87)

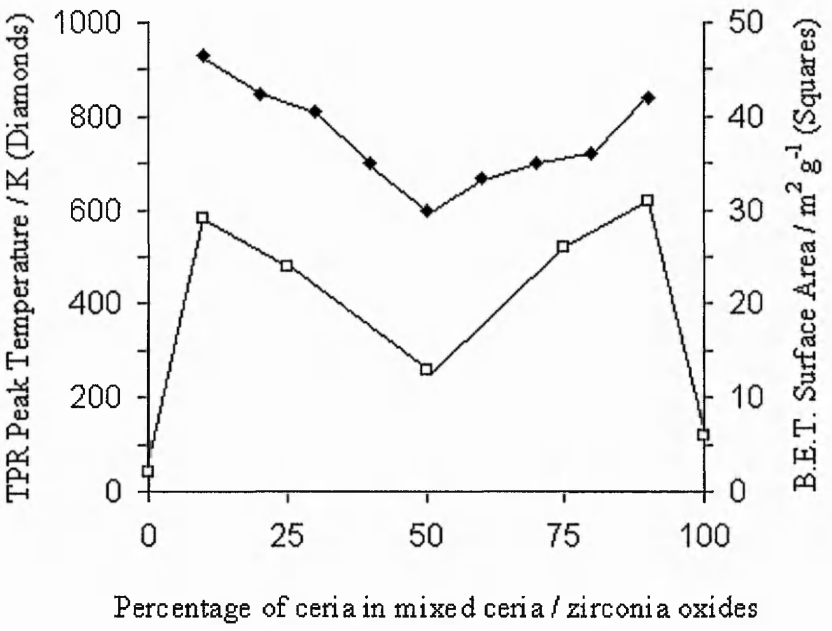

The rare earth oxides lanthana, yttria, praseodymia and neodymia have been shown to both stabilise the surface area of zirconia (43, 88-93) and stabilise and enhance the redox characteristics of ceria (70-75, 94-99). In chapter 4 these ternary additives are investigated, and further discussed, with respect to the characteristics of the ceria / zirconia mixed oxides.

The presence of the rare earth La^{3+} ion is reported to stabilise γ-alumina, the preferred support for the precious metals, from transforming into α-alumina by the formation of $LaAlO_3$ (88,89). In the presence of ceria the formation of $LaAlO_3$ prevents the interaction between CeO_2 and γ-alumina, forming $CeAlO_3$. When cerium is present as a cerium aluminate oxygen storage capacity is lost.

The zirconia tetragonal structure has been shown to be stabilised by incorporation of ceria, lanthana and yttria, and the nature of the dopant and method of preparation are both important (90).

The lanthana stabilized zirconia system has received some attention (43,75,91-93). It has been observed that at 700°C, 4 and 8 mol% La_2O_3/ZrO_2 had surface areas of

58 and 74 m^2g^{-1}, compared to only 29 m^2g^{-1} for the undoped sample (92). An extensive investigation of lanthana / zirconia mixed oxides (43) has lead to a number of conclusions, including that 2.8% lanthana will form a single phase solid solution of tetragonal zirconia which is stable up to 900 C, dopant addition retards crystallisation of zirconia, and upon crystallisation the samples maintain high surface areas.

Both lanthana and yttria (43) have been investigated with regards to stabilising the surface area of tetragonal zirconia. Lanthana has been shown to be the more effective when the rare earths were doped at 2.8 mol%. The specific areas and crystal phase and structures of the 2.8 mol% doped zirconias were shown to be almost identical when the lanthana and yttria doped materials were calcined at 600°C and 500°C respectively.

Ceria surface area loss, due to crystallite growth, has been described by a process involving the diffusion of cerium and oxygen (71-73). The stabilisation of the surface area at high temperature was explained in terms of foreign cations being strongly associated with oxygen vacancies or Ce^{3+} ions, thus inhibiting diffusion and thus inhibiting crystallite growth. Surface area stabilisation of ceria was achieved by lanthana, neodymia, and yttria doping (74). It was shown that doping ceria with 10% rare earth oxide offered a six-fold improvement when calcined at 980°C for 1 hour. A 25% surface enrichment of the rare earth oxide was observed, by the use of x-ray photoelectron spectroscopy, after the calcination procedure and it was stated that the stabilisation mechanism involved the formation of a stabiliser rich surface phase that impedes crystallisation. The use of lanthana as a dopant, rather than yttria or neodymia, was shown to offer the greatest stabilising influence. Doping ceria with praeseodymia has been shown to increase the surface area of the mixed oxide as compared to pure ceria alone (97).

Lanthana and yttria dopants have been investigated with the aim of increasing the OSC of ceria as the 3+ nature enhances the redox cycling of the cerium cations (88,89,94-96) by the formation of defects and oxygen vacancies. The addition of lanthana to ceria is said to generate defects which enhance both oxygen exchange rate and the total extent of oxygen exchange. The maximum increase in oxygen storage capacity is reached when the relative amount of lanthanum in ceria is 25%. A possible

drawback of this application however is observed under severe reducing conditions. A phase transformation is observed which reduces capacity for oxygen exchange (94).

An example of a trivalent cation substitution for the Ce^{4+} is shown below:

$$2La_2O_3 + 3Ce^{4+} = 3CeO_2 + 4La^{3+} + 2Vo$$

The Ce4+ is the cerium cation on the Ce site of the ceria lattice, the La^{3+} is the lanthanum trivalent cation occupying a cerium site in the cerium lattice and Vo are the vacancies formed (98).

Praseodymia has been investigated as it can be oxidised and reduced in a similar way to ceria (98,99).

1.5: References

1. H.E.Avery, Basic Reaction Kinetics and Mechaninsms, 12th Ed, MacMillan Education Ltd. London. 1991 113
2. D.F.Shriver, P.W.Atkins, C.H.Langford, Inorganic Chemistry, Oxford University Press, Oxford. 1990 542
3. M.V.Hardveld, Ph.D. Thesis, Eindhoven University of Technology. 1997
4. M.Bowker and R.W.Joyner, in 'Insights into Speciality Inorganic Chemicals',ed.D.Thompson, Royal Society of Chemistry, Cambridge. 1995 145-167
5. J.Armor, 'Environmental Catalysis', American Chemical Society, Washington D.C. 1994 90-93.
6. K.C.Taylor, Catal.Rev-Sci.Eng. 1993 457-481
7. National Society for Clean Air, Fact Sheet, 'EC Air Quality Standards' 1997
8. National Society for Clean Air, Fact Sheet, 'UK Air Quality Standards and Objectives' 1997
9. National Society for Clean Air, Fact Sheet, 'Vehicle Emissions – EU Directives' 1997
10. M.P.Walsh, Plat.Met.Rev, 2000 44(1) 22-30
11. R.Gould. Volvo Leaflet "Building Cars for a Better Environment" 1989
12. Chemistry and Industry, Power and Pollution: Cars of Tomorrow, 1995 15 589

13. BBC Television UK. BBC2. Top Gear. 01.03.2001.
14. ITV Television UK. Teletext. P324. 20/03/2001.
15. V.I.Parvulescu, P.Grange, B.Delmon, Catalysis Today 1998 46 233
16. P.Moles, 'Zirconia – Current and Future Uses' MEL Leaflet
17. R.J.Farrauto, R.M.Heck, Catalysis Today 1999 51 351-360
18. McGraw-Hill Encyclopedia of Science and Technology, 7th Ed. 1990
19. M.Shelef, G.W.Graham, Catal.Rev.Sci.Eng. 1994 36 431
20. T.P.Kobylinski, B.W.Taylor, J.Catal. 1974 33 376
21. R.L.Klimish, K.C.Taylor, Env.Sci.Tech. 1993 7 127
22. W.C.Hecker, A.T.Bell, J.Catal. 1983 84 200
23. W.C.Hecker, A.T.Bell, J.Catal. 1984 85 389
24. W.C.Hecker, A.T.Bell, J.Catal. 1983 84 220
25. R.W.McCabe, C.Wong, J.Catal 1990 121 422
26. J.C.Bailar et al Eds. Comprehensive Inorganic Chemistry, Pergamon Press, Oxford, 1984 316
27. N.N.Greenwood and Earnshaw, Chemistry of the Elements. 1984
28. G.Zwang, T.Yamguchi, H.Kawakami, T.Suzuki, Appl.Catal.B.Env. 1992 1 L15
29. E.Giammello et al J.Catal. 1992 136 510
30. T.W.Dann, K.H.Shulz, M.Mann, M.Collings, Appl.Catal.B.Env 1995 6 1
31. T.R.Ward, P.Alemany, R.Hoffman, J.Phys.Chem 1983 97 7691
32. J.Kaspar, C.D.Leitenburg, P.Fornasiero, A.Trovarelli, M.Graviani, J.Catal. 1994 146 136
33. S.H.Oh, C.C. Eikel, J.Catal. 1990 128 526
34. D.D.Beck, C.J.Carr, J.Catal. 1993 144 296
35. J.G.Chen, M.L.Colaianni, P.J.Chen, J.T.Yates, G.B.Fisher, J.Phys.Chem. 1990 94 5059
36. European Patent EP 0262962 Engelhard Corp.
37. United States Patent USP 4233289 Ford Motor Co.
38. Japanese Patent JP 63,077,544
39. Japanese Patent JP 63,020,036
40. B.Harrison, A.F.Diwell, C.Hallett. Plat.Met.Rev. 1988 32(2) 73-83

41. K.Maruya, K.Ito, K.Kushihashi, Y.Kishida, K.Domen, T.Onishi. Cat.Lett. 1992 14 123
42. R.C.Garvie. J.Phys.Chem 1969 65 1238
43. M.Keenan Ph.D Thesis. The Nottingham Trent University. 1996
44. T.Yamaguchi. Catal.Today 1994 20 199-218 and references therein
45. A.Clearfield, G.P.D.Serrette, A.H.K.Syed. Catal.Today 1994 20 295-312 and references therein
46. B.H.Davis, Comm.Am.Ceram.Soc 1984 C-186
47. B.H.Davis, R.Srinivasan and R.DeAngelis, J.Mater.Res, 1986 4 1-12
48. C.E.Hori, H.Permana, K.Y.S.Ng, A.Bremner, K.More, K.M.Rahmoeller and D.Belton, Appl.Catal.A.Gen. 1991 16 105-117
49. K.Hashimoto, N.Touka, R.Hamada and S.Imamura, Cat.Lett. 1998 50 193-198
50. E.Luccini, S.Merriani and O.Sbaizero, Int.J.Materials and Product Technology 1989 4 167-175
51. G.K.Chuah, S.Jaenicke, Appl.Catal.A.Gen, 1997 163 261-273
52. M.A.Aramenda, V.Borau, C.Jimenez, J.M.Marinas, A.Porras and F.J.Urbao, J.Chem.Soc.,Faraday Trans, 1997 93 1431-148
53. G.K.Chuah, S.Jaenicke, S.A.Chong and K.S.Chan, Appl.Catal.A.Gen, 1996 145 267-284
54. R.C.Garvie. J.Phys.Chem 1978 82 218
55. L.Ping, I.W.Chen, J.E.P.Hahn. J.Am.Ceram.Soc. 1994 77(5) 1281-88
56. J.Emsley. The Elements. Clarendon Press, Oxford. 1989
57. K.S.Pitzer. Accounts of Chemical Research. 1974 12 271-276
58. F.A.Cotton, G.Wilkinson, Advanced Inorganic Chemistry, 5th Ed. Wiley, New York, 1988
59. F.A.Cotton, Lanthanides and Actinides, Macmillan, London, 1991
60. J.P.Cuif, G.Blanchard, O.Touret, A.Signeurin, M.Marczi, E.Quemere. SAE Paper 970468 1997
61. C.J.Norman. SAE Paper 970463 1997
62. A.F.Diwell, R.R.Rajaram, H.A.Shaw, T.J.Truex. CAPOC2 Ed. A.Crucq, Elsevier Science Publications. 1991
63. D.J.M.Bevan.,J.Inorg.Nucl.Chem. 1955 1 49-55.

64. J.Kaspar, P.Fornasiero, M.Graziani. Catal.Today 1999 50 285-298
65. G.Srinivas, S.S.C.Chuang, S.Debnah. in 'Environmental Catalysis' Ed. J.Armor, A.S.C. Washington D.C. 1994 157-167
66. R.S.Fenoglio, R.Cataluna, J.Soria, J.S.Conesa. EuropaCatI Book of Abstacts. 1993
67. G.RangaRoa, P.Fornasiero, R.DiMonte, J.Kaspar, G.Vlaic, G.Balducci, S.Meriani, G.Gubitosa, A.Cremona, M.Graziani. J.Catal. 1996 162 1-9
68. G.RangaRoa, P.Fornasiero, J.Kaspar. S.Meriani, R.DiMonti, M.Graziani. COPAC4 Reprints. 1997 73-83
69. G.RangaRoa, J.Kaspar, S.Meriani, R.DiMonte, M.Graziani. Cat.Let. 1994 24 107-112
70. J.P.Cuif, G.Blanchard, O.Touret, M.Marczi, E.Quemere. SAE Paper 961906
71. M.Pijolat, M.Prin, M.Soustelle, O.Touret ,P.Nortier. Faraday Trans. 1995 91(21) 3941
72. M.Pijolat, M.Prin, M.Soustelle, O.Touret ,P.Nortier. Solid State Ionics 1993 63 781
73. M.Pijolat, M.Prin, M.Soustelle, O.Touret ,P.Nortier.CAPOC3. Elsevier Science Publications 1995 325
74. J.E.Kubsh, J.S.Rieck, N.D.Spencer. CAPOC2. Elsevier Science Publications 1991 125
75. M.Ozawa, M.Kimura, A.Isogai. J.Alloys.Comp. 1993 193 73-75
76. L.A.Bruce, M.Hoang, A.E.Hughes, T.W.Turney, Appl.Catal.A Gen 1996 134 351-362
77. H.C.Yao and Y.F.Yu Yao,.J.Catal, 1984 86 254-265
78. P.Fornasiero, G.Balducci, R.DiMonte, J.Kaspar, V.Sergo, G.Gobitosa, A.Ferrero, M.Graziani.,J.Catal. 1996 164 173-183
79. G.Vlaic, P.Fornasiero, S.Geremia, J.Kaspar, M.Graziani. J.Catal. 1997 168 386
80. G.Vlaic, R.Dimonte, P.Fornasiero, E.Fonda, J.Kaspar, M.Graziani, CAPOC4, Poster Reprints 1997
81. G.Balducci, J.Kaspar, P.Fornasiero, M.Graziani, M.S.Islam, J.D.Gate,. J.Phys.Chem.B, 1997 101 1750-1753
82. G,Balducci, P.Fornasiero, R.DiMonte, J.Kaspar, S,Meriani, M.Graziani. Cat.Let. 1995 33 193-200

83. H.Permana, D.N.Belton, K.M.Rahmoeller, S.J.Shnieg, C.E.Hori, K.Y.S.Ng, A.Brenner. SAE Paper 970462 1997
84. C.D.Lieitenburg, A.Trovarelli, J.Llorca, F.Cavani, G.Bini. Appl.Catal.A.Gen. 1996 139 161
85. D.Michel, L.Mazerolles, P.Berthet, E.Gaffet. J.Am.Ceram.Soc. 1993 76 2884
86. Y.Sun, P.A.Sermon. J.Mater.Chem. 1996 6 1025
87. T.Yamada, T.Kobayashi, K.Kayano, M.Funabiki. SAE Paper 970466 1997
88. G.W.Graham, P.J.Schmitz, R.K.Usmen, R.W.McCabe. Cat.Lett. 1993 17 175-185
89. R.K.Usmen, G.W.Graham,W.L.H.Watkins, R.W.McCabe. Cat.Lett. 1995 30 53-63
90. T.H.Etsell, S.N.Flengas. Chem.Rev. 1970 70 339
91. P.D.L.Mercera PhD Thesis University of Twente 1991
92. R.Franklin, P.Goulding, J.Haviland, R.W.Joyner, I.McAlpine, P.Moles, C.Norman, T.Nowell. Catal.Today. 1991 10 405
93. C.K.Loong J.W.Richardson, M.Ozawa. J.Catal. 1995 157 636
94. S.Bernal, G.Blanco, M.A.Cauqui, G.A.Cifredo, J.M.Pintado, J.M.R.Izquierdo. Cat.Letters. 1998 53 51-57
95. S.Bernal, G.Blanco, M.A.Cauqui, G.A.Cifredo, J.M.Pintado and J.M.R.Izquierdo. J.Alloys and Comp. 1997 250 449-454
96. W.M.O'Neill, M.A.Morris. Chem.Phys.Lett. 1999 305 389-394.
97. M.Y.Sinev, G.W.Graham, L.P.Haack, M.Shelef. J.Mater.Res. 1996 11 8 1960-1971
98. A.D.Logan, M.Shelef, J.Mater.Res. 1994 9 2 468-475
99. S.B.Adler, J.W.Smith. J.Chem.Soc.Faraday.Trans. 1993 89 16 3123-3128

Chapter 2 :
Experimental Techniques.

"The test of all knowledge is experiment."

Richard P Feynman

"If we knew what were doing, it would not be called research, would it?"

Albert Einstein

2.1 : Application of the B.E.T. Approach for Surface Area Determination

Surface area determination is a useful tool in catalyst characterisation, since it indicates the available area of a solid for the adsorption of molecules in heterogeneous reactions, or in some cases the capacity of an adsorbent to remove particular components from a gaseous or liquid mixture. It is possible to calculate a specific surface area from a knowledge of the adsorption isotherm.

Adsorption isotherms are plots of the amount of gas adsorbed at equilibrium as a function of the partial pressure, at constant temperature. Brunauer, Deming, Deming and Teller (B.D.D.T.) proposed 5 types of isotherm which result from physical adsorption; these are shown in figure 2.1.

Figure 2.1. The five B.D.D.T. isotherms

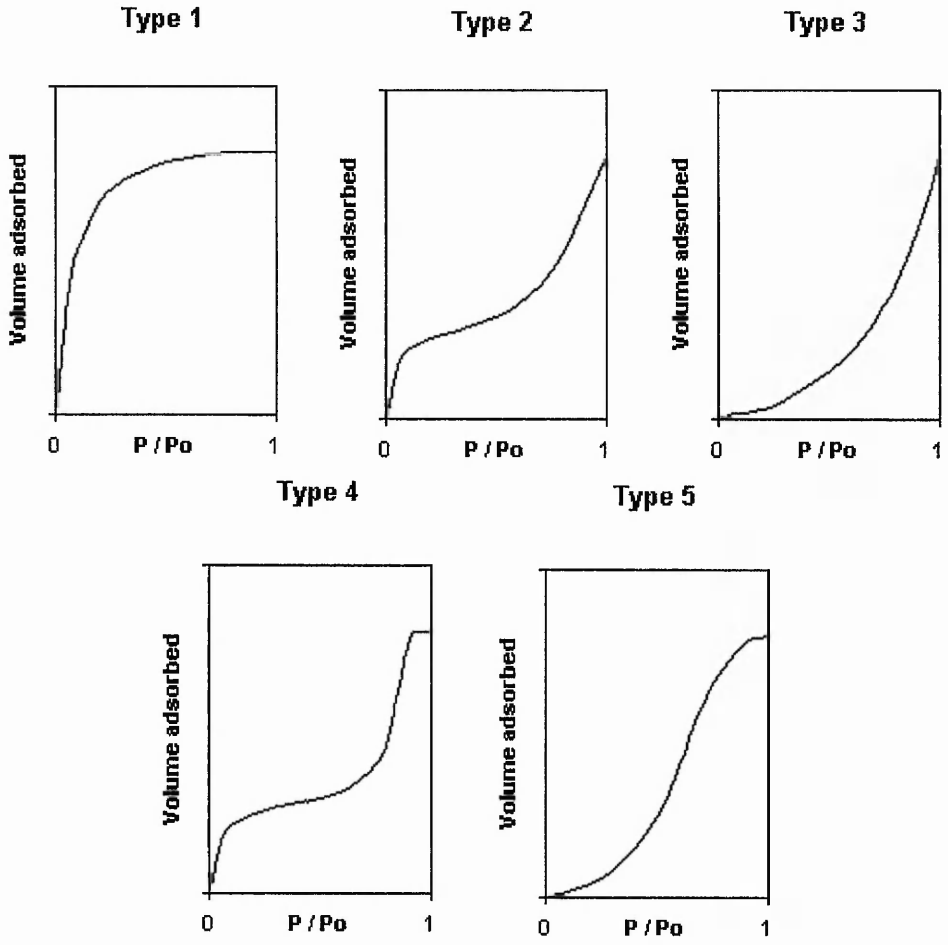

Type 1 is of the form of the Langmuir isotherm given, coincidentally, by microporous solids, such as zeolites, with the plateau representing the complete filling of very small pores by the condensed gas. Types 2 and 4 represent isotherms of multilayer physisorption on a flat surface and multilayer adsorption accompanied by capillary condensation in mesopores respectively; the monolayer capacity is equated with the low pressure shoulder. Type 4 usually shows a hysteresis loop; the isotherm not following the same path for desorption as it does adsorption. This is due to the fact that evaporation of condensed gases in fine pores does not occur as readily as its condensation. Types 3 and 5 are generally regarded as uninteresting as theoretically they are not well understood. They are generally explained by strong adsorbate – adsorbate interactions and where the adsorbate – adsorbate interactions are greater than adsorbate – adsorbent interactions respectively.

The Brunauer, Emmett, Teller (B.E.T.) equation can be applied to type II and IV isotherms to determine the monolayer coverage of an adsorbate on the surface of a sample, and hence surface area if the size of the adsorbing molecule is known. The B.E.T. equation is shown below.

$$P / [V (P_0 - P)] = 1 / V_m.C + (C - 1 / V_m C).P/P_o \qquad \text{equ.2.1.}$$

Where,

P = Equilibrium pressure

V = Volume of gas adsorbed at equilibrium pressure

P_o = Saturated vapour pressure of the adsorbed gas at measurement temperature

V_m= Monolayer coverage volume

C = Constant

The C constant in the equation is a function of the net heat of adsorption given by..

$$C = \exp [(H_a - H_l) / RT] \qquad \text{equ.2.2}$$

H_a and H_l being the enthalpy of adsorption in the first layer and the enthalpy liberated on forming subsequent layers respectively.

Plotting $P/V(P_o-P)$ versus P/P_o, should give a straight line of gradient (C-1) / V_mC, and the intercept is $1/V_mC$. The monolayer coverage, determined by 1/ (intercept + slope), is then used to obtain the surface area of the sample with a knowledge of the cross-sectional area of the adsorbing molecule, $0.162nm^2$ for nitrogen. The isotherm is expected to be linear over the range 0.05 – 0.30 P/P_o. The B.E.T. equation is only valid over this range (1-3).

Specific surface area determinations were performed using an automated computer controlled gas adsorption apparatus using nitrogen as the adsorbate at 77K. A sample was weighed accurately in a glass bulb and degassed in the region of 150C for at least 2 hours, down to a pressure in the region of 6×10^{-2} Torr. The sample volume was calibrated by the use of helium at room temperature and at 77K. The dosing of nitrogen then allowed for the automatic determination of surface area and C constant.

A number of previous studies have shown zirconia based catalysts displaying type 2 isotherm characteristics with the absence of microporosity (4-6), and so the BET equation has been applied with confidence, in the measurement of surface areas, to many ceria / zirconia mixed oxides prepared by coprecipition (7-9).

To ensure the materials produced by this route were applicable to analysis by the B.E.T. method, a full isotherm analysis was carried out, using the same apparatus manually controlled, on a typical sample (sample 8 in chapter 3). Figure 2.2 shows the isotherm produced, this isotherm is typical of isotherm 2 in the classification proposed by Brunauer, Deming, Deming and Teller. Materials showing this type of isotherm can be considered non-porous and thus the B.E.T. method can be applied (1).

Figure 2.2. Nitrogen adsorption isotherm of sample 8

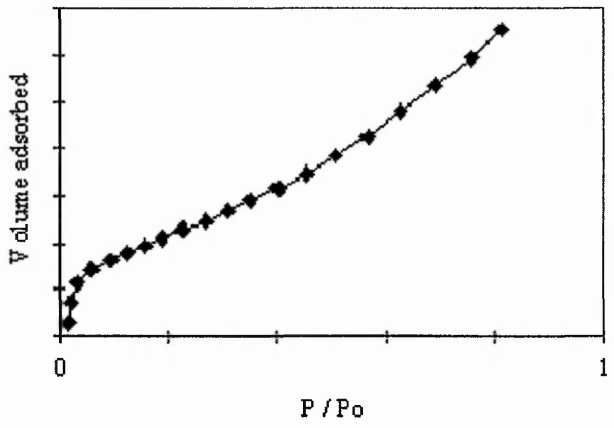

A further indicator of a type 2 isotherm is that when the B.E.T. method is applied to the material the B.E.T equation C constant is within the expected range (1). As previously mentioned, the C constant is a function of the enthalpy of adsorption. The higher the C constant the stronger the first layer is held. Materials which have type 3 isotherms will display a C constant below 2 but greater than 0 because of the strong adsorbant – absorbant interaction. The ceria / zirconia mixed oxides produced in chapter 3 have C constants in the region of 8 - 60, well within the region of acceptability for the application of the B.E.T. method to materials displaying an non-porous type 2 adsorption characteristics (2).

2.2 : Temperature Programmed Reduction

Temperature programmed reduction (TPR) is employed to study the reducibility of both bulk and supported catalysts. It is a highly sensitive method for discriminating the reducibility of any species in relation to its chemical states.

A reactor for the study of the reduction process is now described. The reactor containing a catalyst is situated in a furnace equipped with a temperature programmable controller. The reactor effluent is then typically analysed by a thermal conductivity detector (TCD) for hydrogen consumption. The TCD measures the uptake of hydrogen by the sample by the difference in thermal conductivity of the gas pre- and post-reactor.

Any changes in the environment of the detector filaments cause a current to flow, which is recorded as a peak. The peak profile is the hydrogen concentration as a function of temperature. To obtain a quantitative signal, the H_2O produced during the reaction is trapped before the gas mixture reaches the detector. The reducing gaseous mixture consists of H_2 and an inert gas that does not react with H_2 or the solid. Figure 2.3 shows the apparatus used during experimentation.

Fig 2.3. TPR apparatus

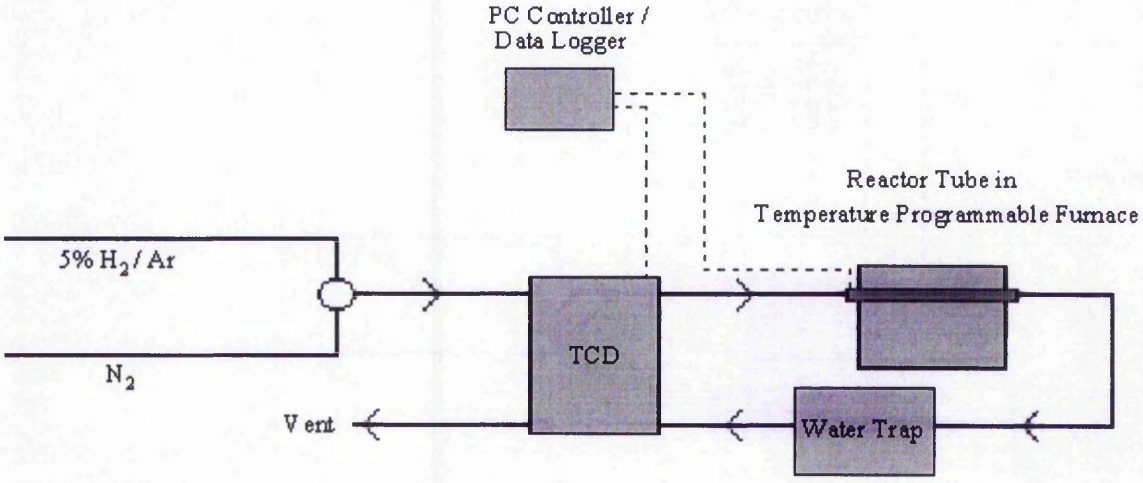

The shape of the resulting TPR profiles are markedly affected by experimental operating variables and mass transfer limitations. A characteristic K number has been defined to aid in selecting the values for the operation variables which should be chosen in order to obtain the optimum reduction profiles. The Monte and Baiker equation is shown below (10).

$$K = S_o / (V.C_o) \qquad \text{equ.2.3.}$$

where,

K = constant for the calculation of optimum parameters (s)

S_o = amount of reducible species (umol)

V = total flow rate of the gas stream (ml s^{-1})

C_o = initial concentration of the reducing gas (umol ml^{-1})

The K number, with optimum parameters, has a value of 100s or at least between 55 and 140. Heating rates of between 0.1 and 0.3° ks^{-1} are recommended. Improved sensitivity of the TPR method has been claimed to be obtained with low feed rates of hydrogen. Taking into account this approach, artefacts have been shown to perturb profiles at high K values (3,10,11).

Using the information obtained from the Monte and Baiker equation, the following experimental procedures were applied. A 5% hydrogen in argon gas flow rate of 40ml/min was used. Approximately 40mg (22mg of reducible ceria (IV) in the 40mol % mixed oxide samples) of the sample was inserted into a silica cell and was held in place by small quantities of silica wool. Silica rods were placed on the exit side of the cell, so as to reduce dead space. Samples were pretreated under nitrogen at 500°C for 1 hr. A CuO standard was run to calibrate the apparatus and so allow for the quantification of hydrogen reducing the ceria component of the mixed oxide.

The heating system used was a Carbolite furnace with a Eurotherm temperature controller, which was set to increase the temperature by 5°K min^{-1} up to 1000°C, allowing satisfactory peak resolution. A Gow-Mac thermal conductivity detector was used. The TCD signal and catalyst bed temperature, determined by thermocouple, were simultaneously recorded by 386 PC running Quicklog PC, a data acquisition programme by Strawberry Tree. Data was transferred to the Galactic Industries Corporation programme 'Grams' for analysis. The reduction peak was integrated and the calculation of peak height, width and area was done automatically within the programme.

2.3 : X-ray Diffraction

Powder XRD can be used to determine the structural of crystalline materials. Crystalline materials composed of any element can be studied, but the procedure is most sensitive to elements of high atomic number. Figure 2.4 shows the basic experimental set-up.

Figure 2.4. Schematic illustration of the powder x-ray diffractometer

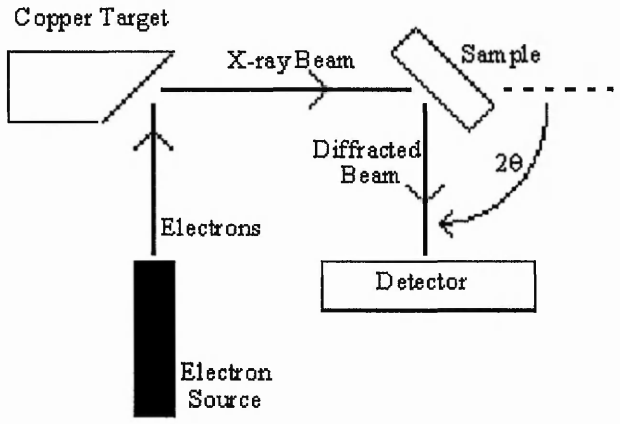

X-rays are formed by bombarding a source with high energy electrons. The Cu Kα x-rays (1.5418 Å) are produced by a primary electron creating a core hole in the K shell, which is filled by an L shell electron with emission of an x-ray quantum. The x-rays interact with, and are diffracted by, planes of atoms in a crystallite leading to constructive and destructive interference of the reflected x-rays. Constructive interference, due to diffraction of monochromatic waves that are in phase, lead to an increase in x-ray intensity, and can be related to interplanar spacings. The angles at which the radiation enters and leaves the crystal to obtain constructive interference satisfies Bragg's Law.

$$n\lambda = 2d_{hkl} \sin\theta \qquad \text{equ.2.4.}$$

Where,

λ = wavelength of the x-ray source

d_{hkl} = distance between planes

θ = diffracted angle from incidence (Bragg angle)

n = order of reflection

Characteristic reflections, d-spacings and relative intesities obtained from a pattern can be compared to standard JCPDS (Joint Committee on Powder Diffraction Standards) powder diffraction files enabling phase identification.

Peak widths yield information about the average dimensions of the crystallite and any strain within it. The diffraction lines from perfect crystals are very narrow. The Scherrer equation is used to relate line width to crystallite size.

$$S = K\lambda / \beta\cos\theta \qquad \text{equ.2.5.}$$

Where,

β = Peak width / °

S = Crystallite size / Å

K = Shape constant taken as unity in radians

θ = Bragg Angle

λ = Wavelength / Å (3)

The scans of the samples, prepared by compaction of the powder into a glass backed aluminium sample holder, were run on a Philips 1050, Hiltonbrooks modified, x-ray powder diffractometer. The diffractometer used a CuK_α source (1.5418Å) with a generator operating at 42.5KV and current of 18mA. The powder samples were typically scanned over a region of 10-80 2θ°, with a step size of 0.02° 2θ, at 0.5 seconds per step.

2.4 : X-ray Photoelectron Spectroscopy

X-ray photoelectron yields useful information on surface elemental composition and the oxidation states of the catalysts of interest. The basic principle is shown in figure 2.5.

Figure 2.5. X-ray photoelectron spectroscopy

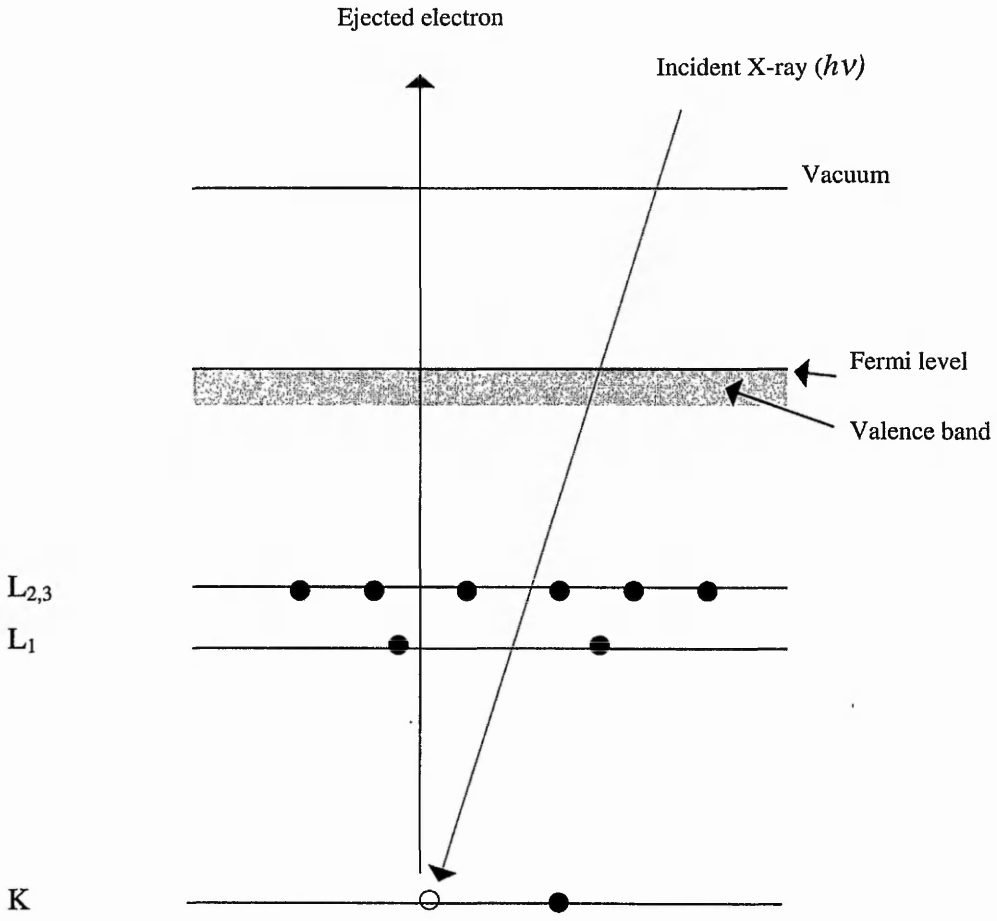

The technique is based upon the photoelectric effect. An atom absorbs a photon of energy $h\nu$ and a core or valence electron with binding energy E_B is ejected with kinetic energy.

$$E_K = h\nu - E_B + \phi \qquad \text{equ.2.6.}$$

Where,

E_K	=	Kinetic energy of the emitted photoelectron
$h\nu$	=	Incident photon energy
E_B	=	Electron binding energy
ϕ	=	Spectrometer work function

Photons of soft x-rays (Mg Kα) of 1253.6 eV irradiate a sample. The photons have a limited penetrating power in a solid sample (1-10 microns) so interact with surface atoms leading to the emission of electrons, as previously described. The binding energy may be regarded as a type of ionisation energy of the atom for the particular shell involved. Electrons from different types of atoms, and from different electronic shells within the same type of atom, are emitted with different kinetic energies and so may be distinguished. The electrons emitted can only travel short distances before losing energy in collisions with atoms. This inelastic scattering process gives rise to the surface sensitivity of XPS. There is a different probability (cross-section) for each process. Auger electrons are emitted due to the relaxation of energetic ions after photoemission. The intensity of the photoelectron N(E) is measured as a function of their kinetic energy (E_k). The XP spectrum is a plot of N(E) against E_k, or more generally E_B, the binding energies. The binding energies recorded are not only element specific but yield chemical information as well, such as the chemical state of the species, as peak positions indicate the ionic charge.

As previously stated, emitted electrons lose energy rapidly because of collision with other atoms. This relates to the notion of escape depth defined as the thickness of the material for which the probability of electron transmission without energy loss is 1/e. The intensity (I) of elastically transmitted electrons depends exponentially on the thickness (d).

$$I = I_o \exp(-d/\lambda) \qquad \text{equ.2.7.}$$

Equation 2.7. is expressed in the terms of a universal escape depth curve, where escaped depth is plotted as a function of kinetic energy (figure 2.6).

Figure 2.6. Escape depth curve

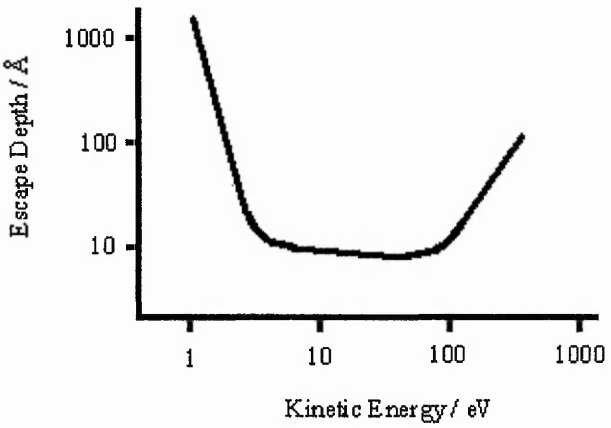

The intensity of peaks in the XP spectrum may be used, with certain assumptions, to determine the composition of the surface layer. If this is assumed to be homogeneous, then equation 2.8 describes the intensity to be expected in any XPS peak.

$$I = F_x.S(E_k).\sigma(E_k).n.\lambda(E_k)\cos\theta \qquad \text{equ.2.8.}$$

Where, I is the intensity of the XPS peak, F_x is the x-ray flux on the sample, $S(E_k)$ is the spectrometer efficiency for detecting the electron at kinetic energy E_k, $\sigma(E_k)$ is the cross-section for photoemission, n is concentration, $\lambda(E_k)$ is the escape depth of the photoelectron at kinetic energy E_k through the material and θ is the angle between the direction in which the photoelectron is emitted and the surface normal.

The major use of XPS in this project was for the determination of surface (zirconia / ceria / rare earth oxide) composition, achieved by the comparison of peak areas and the application of equation 2.9.

$$N_B / N_A = (I_B / I_A).(\sigma_A / \sigma_B).(E_A / E_B)^{1.35} \qquad \text{equ.2.9.}$$

where,

N = Elemental surface concentration

I = Peak intensity corrected for the number of scans

σ = Photoionisation cross-sectional area

E = Kinetic energy

The value 1.35 is a spectrophotometer correction function calculated by a standardisation technique using silver foil (12-14).

The experimentation was undertaken using a Vacuum Generators ESCA 3 spectrometer. The analysis chamber, containing the sample on a brass sample holder, was evacuated to approximately 10^{-7} mbar prior to photon irradiation of the sample and spectra recording. The spectra were recorded on a Pentium I PC running the programme Spectra version 6 by Borland International. The x-ray generator was operated at an emission current of 20 mA and an accelerating voltage of 10 keV, and the analyser pass energy was 20 eV.

Generally all the recorded peaks are shifted equally in their position due to sample charging. The carbon 1s peak is known to have a binding energy of 285.0 eV, therefore the peak positions can be corrected.

2.5 : Catalyst Testing

This section describes the microreactor set-up used in this work. Further details of the reactions studied and procedure may be found in chapters 5 and 6.

2.5.1 : The Microreactor

Figure 2.7 illustrates schematically the catalytic microreactor. It incorporates a horizontal stainless steel fixed bed reactor with exhaust gas analysed by chemiluminescent NOx analyser and a gas chromatograph with a thermal conductivity detector (GC-TCD). The set-up was designed to study the reactions over a number of catalyst types subject to various feed gas compositions. The studies were designed to investigate the catalytic ability of materials to perform reactions undertaken by the actual TWC, and these were the carbon monoxide - nitric oxide (CO-NO) oxidation - reduction, nitrous oxide decomposition, and the propene - oxygen - nitric oxide selective catalytic reduction (SCR) reactions.

Fig 2.7. The microreactor set-up

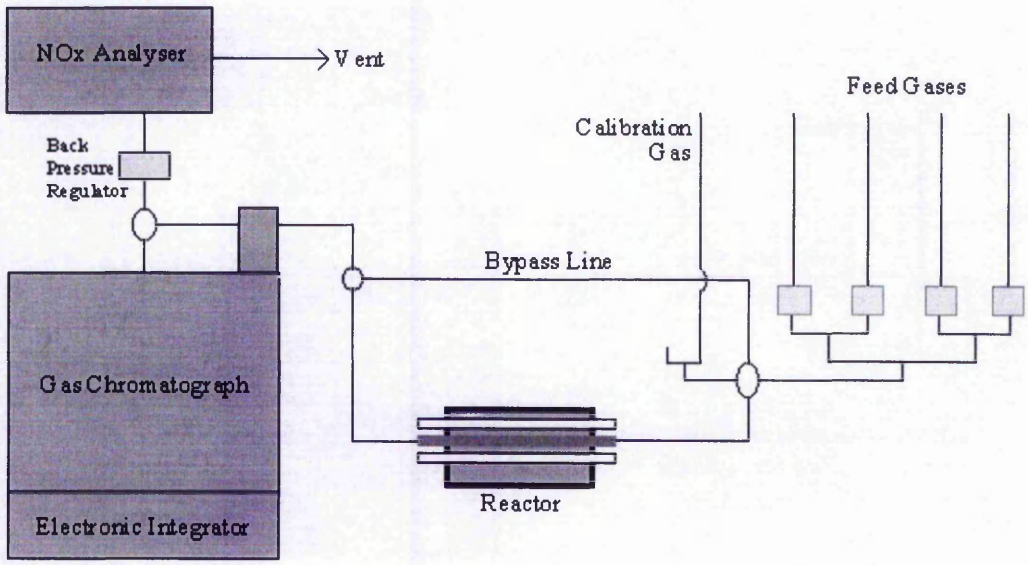

The microreactor was fed by pressure regulated lines, each of which were capable of independent isolation. Gas flow rates were controlled by the use of Brooks 5850 thermal mass flow controllers. The four independent gas lines converged to a single line, allowing thorough mixing of the gaseous components. The single line then entered a 4 port valve so that the gas could be directed through the catalyst bed or through a by-pass line for analysis. The port valve also served as the point for

calibration gas inlet. Gases passing to the reactor bed were subject to an increase in pipeline diameter from 1/8 - 1/2 inch. The catalyst bed was secured between silica wool plugs at the centre of a 1/2 inch reactor tube. A stainless steel spacer was placed at the exit side of the tube to ensure minimal bed slippage. The catalyst granules were prepared by compacting the powder precursor in a die press to a pressure of six tons. The solid was then pushed through a sieve so that granules of size 0.6 – 1mm were obtained. The reactor tube itself was situated centrally within a Carbolite tube furnace, model MTF 12/25A, with temperature controlled by a Eurotherm 91E unit.

The reactor's exhaust gas was continually monitored by GC-TCD and the NOx analyser set up in series. A back pressure regulator was placed between the two pieces of equipment to maintain atmospheric pressure in the GC sample loop and reactor as the NOx analyser functioned under pressure.

The feed gases used were supplied by Air Products. The gases used for the three types of study are shown in table 2.1

Table 2.1. Gases used in reactor studies

Study	Gases
CO - NO Reaction	5% nitric oxide in helium carbon monoxide helium
N_2O Decomposition	1.04% nitrous oxide in helium
Selective Catalytic Reduction	20% oxygen in helium 5% nitric oxide in helium 1% propene in helium

2.5.2 : Gas Analysis by Gas Chromatography – Thermal Conductivity Detection

Gas chromatography is a dynamic separation system consisting of two media, the stationary phase (column) and mobile phase (gas). The rate at which gaseous components pass through a column depends upon their physical properties and affinity

for the column. Retention time and detector signal parameters of the eluted gas allows the component type and concentration to be identified (15).

The apparatus consisted of a Pye Unicam PU4550 GC fitted with Molecular Sieve 5A and Porapak QS columns. The detector used was a thermal conductivity detector (TCD) couple to a Spectra Physics Chromjet CH-2 integrator. An oxygen trap was fitted between the molecular sieve column and TCD in order to improve the nitrogen resolution and to protect the TCD filament. A diagrammatic representation of the set-up is shown in figure 2.8.

Figure 2.8. Column arrangement

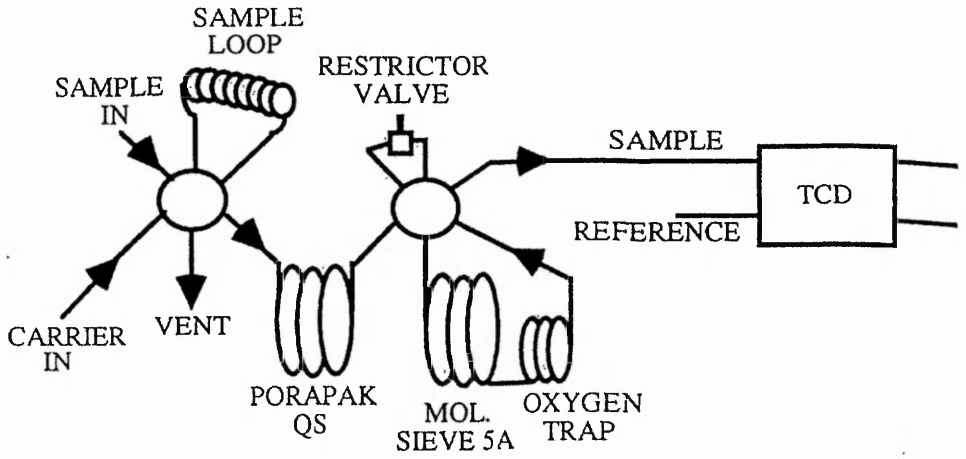

This arrangement allows for the injected sample to pass to either both columns in series or only through the Porapak QS column, bypassing the molecular sieve. Samples of reactor exhaust gas were introduced into the GC using a 1.25 ml sample loop linked to the first VICI pneumatically controlled valve. In order to control the injection procedure, and to interpret the output signal of the TCD, the integrator was programmed to automate the process. In order to analyse for nitrous oxide, nitrogen and carbon dioxide, two separate injections were required. The first injection allowed the gas to pass through the Porapak column resolving carbon dioxide and nitrous oxide. With the columns in series, the second injection allowed the oxygen and nitrogen to enter the molecular sieve column. Isolation of this column ensured the carbon dioxide

and nitrous oxide passed to the TCD. Switching the molecular sieve back in allowed the nitrogen to elute and pass to the detector. In the studies, any material retained on the Porapak column, for example water or propene, was flushed out by isolating the molecular sieve column and raising the column temperature.

In the configuration shown in figure 2.8 all gas flow throughout the columns were maintained at 30 ml/min, which was balanced by a flow of 30 ml/min through the TCD reference channel. Changes in flow rates were controlled by the use of restrictor valves.

The GC operating temperatures used were as follows; the column oven temperature was set at 50 °C and both detector and TCD filament temperatures were at 150 °C.

The thermal conductivity detector (TCD) or katharometer, briefly mentioned in section 2.2., measures the bulk property of thermal conductivity of the gaseous eluent from the GC. Thermal conductivity is described as the flow of heat from a body to an accepting material (15). The gas stream passes over heated filaments with the response of the TCD dependent upon the thermal conductivity of the gas. Changes in thermal conductivity of the gas are indicative of gas composition change and cause change of filament temperature which in turn change the resistance of the filament on the Wheatstone bridge network, figure 2.9.

The out of balance current caused by the change in filament resistance is amplified to form the recorder signal. The filament is housed in a heated block to minimise temperature variation. An identical reference cell, over which is passed pure carrier gas, is also housed in this block. The reference cell serves to improve stability and reduce baseline drift.

The detector was calibrated for carbon dioxide, nitrous oxide and nitrogen by using a calibration gas consisting of 1264 ppm CO_2, 1179 ppm NO, 1084 ppm N_2 and 1149 ppm N_2O, with helium as the make up gas, supplied by Argo. A typical calibration trace is shown in figure 2.10.

Figure 2.9. The typical TCD – Wheatstone bridge arrangement

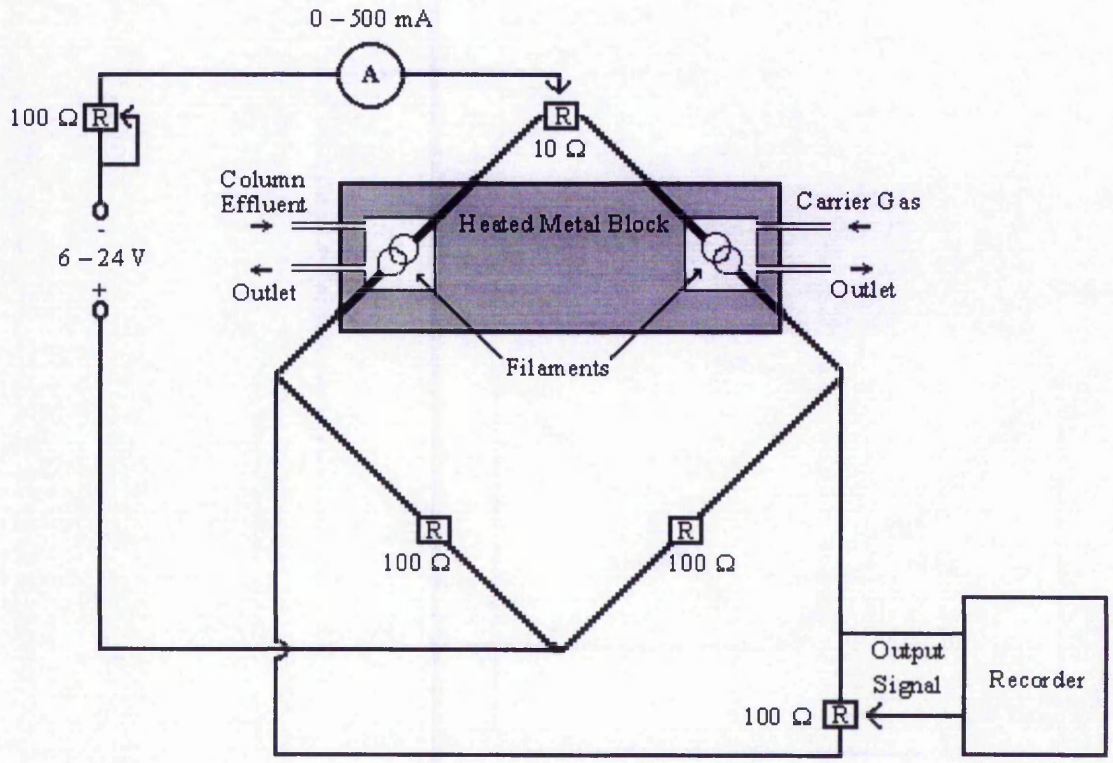

Figure 2.10. A typical calibration trace.

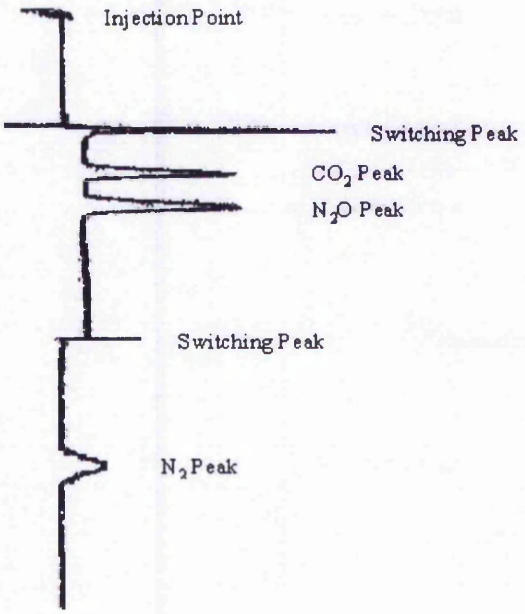

2.5.3 Gas Analysis by NOx Chemiluminescence

As previously stated the reactor's exhaust gas was continually monitored by the NOx analyser and GC-TCD set up in series. The use of NOx chemiluminescence analysis allowed for the measurement of oxides of nitrogen (NO + NO_2) alongside of the CO_2, N_2O and N_2 gases analysed by GC-TCD.The NOx chemiluminescent analyser used was the Signal Instruments Model 4000 machine.

Gas phase chemiluminescence is defined as the production of visible or infra-red light by the reaction of two gaseous species to form an excited species product that decays to its ground state by the act of photoemission (16-18). The method used by this apparatus is based upon the reaction between ozone and nitric oxide to give oxygen and nitrogen dioxide. About 10% of the nitrogen dioxide produced is in a electronically excited state. These molecules either lose energy by collision with other molecules or they lose energy by the emission of light of wavelength 0.6 – 0.3 microns.

$$NO + O_3 \rightarrow NO_2 + O_2 + \text{light} \qquad \text{equ.2.10}$$

The intensity of light emitted has been shown to be proportional to the flow of nitrogen dioxide into the reaction chamber. A photomultiplier tube with associated electronics is used to measure the light emission, from which, in turn, the NO concentration can be determined. The Signal 4000 operates at low pressure (12 mbar approx.) to favour the loss of energy by light emission by reducing the chance of collision of excited nitrogen species. The low pressure also has the benefit of reducing the interference affect that other gaseous species may have on the excited nitrogen species.

There are two major modes of operation of the NOx analyser, the NOx mode and the NO mode. When running in NO mode only the nitric oxide can be measured. When running in NOx mode the total oxides of nitrogen (NO and NO_2 / N_2O_4) can be determined. This is achieved by converting nitrogen dioxide to nitric oxide thermally or by partial reduction by carbon within the analyser. This gas is then passed to the reaction chamber as previously described. Figure 2.11 is a typical block diagram of a chemiluminescent analyser.

Fig 2.11. The chemiluminescent analyser

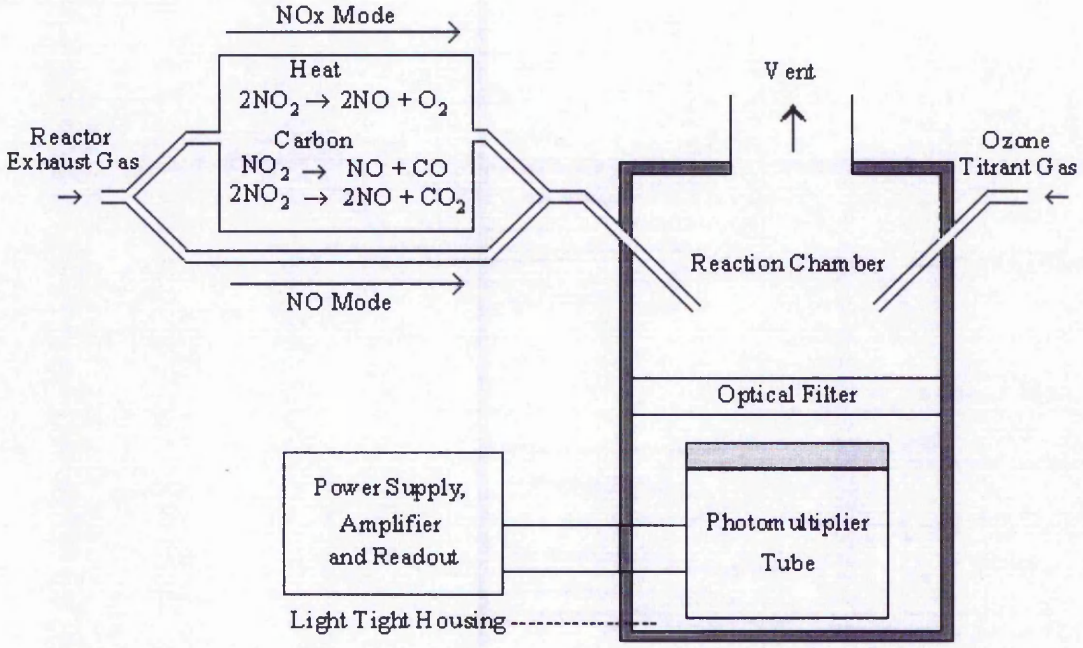

The analyser was calibrated by use of the calibration gas described in section 2.5.2. The calibration of the instrument was linear up to 10,000 ppm nitric oxide, and had a response time of less than five seconds.

2.6: References

1. G.C.Bond, 'Heterogeneous Catalysis, Principles and Applications', 2nd Ed. Oxford science Publications, 1987.
2. S.J.Gregg, K.S.W.Sing, 'Adsorption, Surface Area and Porosity', Academic Press, London. 1982.
3. J.A.Moulijn, P.W.N.M.Van Leeuan, R.A. Van Santen. 'Catalysis', Elsevier Science, Amsterdam. 1993 363-420.
4. S.Ardizzone, E.Grassi, J.Electroanalytical.Chem. 1996 417 193.
5. R.A.Keogh, R.Srinivasan,B.H.Davis, J.Catal. 1995 151 292.

6. E.E.Platero, M.P.Mentruit, Materials Letters. 1992 14 1 318.
7. E.Luccini, S.Meriani, O.Sbaizero, Int.J.Materials and Product Technology. 1989 vol. 4 167-175.
8. C.E.Hori, H. Permana, K.Y.S.Ng, A Bremner, K.More, K.M.Rahmoeller, D. Belton, Appl.Catal B. Env 1998 105-117.
9. K.Yamada, H.Tanaka, M.Yamamoto, SAE Paper 970464 1997
10. D.A.M.Monti and A.Baiker, J.Catal. 1983 83, 323-335.
11. G.Fierro,M.L.Jacono,M.Inversi, G.Moretti, P.Porta, R.Lavecchia. in 'New Fontiers in Catalysis'ed.L.Guczi, Elsevier Science 1993 1847-1850.
12. J.W.Niemantsverdriet 'Spectroscopy in Catalysis' ,VCH, Weinheim, 1993 11-77.
13. J.H.Schofield J.Electron.Spec and Related Phenomena 1976.8. 129-137.
14. C.D.Wagner, W.M.Riggs, L.E.Davis, J.F.Moulder, G.E.Muilenberg. 'Handbook of X-Ray Photoelectron Spectroscopy' Perkin-Elmer Minnesota, 1979.
15. A.Braithwaite and F.J.Smith, Chromatographic Methods, 4th Ed, Chapman and Hall, London, 1985.
16. Signal Series 4000 NOx Analyser Manual.
17. J.P.Lodge (Ed) Methods of Air Sampling and Analysis, 3rd Ed, Lewis, Michigan, 1991.
18. A.Fontijn, A.J.Sabadel, R.J.Ronco. Analytical Chemistry, Vol.42, No.6, 1970.

Chapter 3:

The Preparation and Characterisation of Ceria / Zirconia Materials by a Statistical Method Applied to the Coprecipitation Route.

'By a small sample, we may judge the whole piece.'
Miguel De Cervantes

'Some people hate the very name of Statistics, but I find them full of beauty and interest. Whenever they are not brutalised, but delicately handled by the higher methods, and are warily interpreted, their power in dealing with complicated phenomena is extraordinary.'
Sir Francis Galton

3.1: The Statistical Approach to Catalyst Optimisation

It is well recognised that the performance of any catalyst can be critically influenced by the way it is prepared (1). A complete understanding of the influence of any preparation variable can only be obtained in a systematic study where all other variables are held constant. Such a procedure is not, however practicable, since for example a study which examined 15 variables would require at least 2^{15} or 32768 experiments. Fortunately, statistical approaches are available which allow very marked reductions in the number of experiments needed. In turn they provide only an estimate of the importance of any one variable, but this is usually reliable enough for use in practical catalyst preparation.

This study uses the Plackett-Burman (PB) design (2), which has been used widely in related fields, three of which are the designs applied to hydrothermal synthesis of zeolite ERI (3), to the optimisation of the preparation of a metal-carbon catalyst for enhancement of surface area (4) and to the ceramic powder processing of magnesium oxide (5).

The PB design allows a study to be made of the influence of 15 variables in the preparation of ceria / zirconia mixed oxide catalysts in only 16 experiments. Each variable is set at one of two levels, entitled the nominal and the extreme, - and + respectively. A table is produced which indicates the setting, either nominal or extreme, of each of the variables to be used in each experiment. The method for constructing the table is described by Plackett and Burman (2), and the table used here was generated by the X-Stat software package (6). Since the design matrices are orthogonal, component effects can be estimated with the same accuracy as if attention had been concentrated on varying a single component at a time (2). The term orthogonal means mutually independent and is derived from its use in the field of mathematical vectors. Simply described, the orthogonal arrays produced are treated in such a way as to focus upon the component of interest, whereas the other variables in the array are cancelled out (7-9).

Application of the software package to the PB approach randomises the order in which the variables are changed. This is important, as it ensures that each experiment has an equal chance of being affected by things that may change over time, such as an

improvement in the technique of the experimenter, or small, systematic changes in instrumental performance (7-9).

In this study, the role of the 15 preparation variables, (discussed in detail below), has been examined through 16 catalyst preparation experiments. Each of the 16 catalysts has been characterised in a number of ways, the most important of which is surface area. The PB approach allows the influence of each preparation variable on the surface area to be quantified. For any variable, the average surface areas resulting when it is taken to its nominal and extreme values are determined and the difference is taken. The greater the result obtained, the more important that variable is in determining surface area, and examples will be discussed below.

3.2: Preparation of Ceria / Zirconia Materials

Ceria / zirconia mixed oxides were prepared by the standard approach of precipitation (10) followed by aging, drying and calcining.

Cerium carbonate hydrate 99.9% (Aldrich) and zirconium basic carbonate [0.13% SiO_2, 0.13% TiO_2, 0.16% SiO_2 (MEL)] were mixed at a ratio of 1:9 or 1:1.36, to attain an oxide ratio of 10 mol% ceria and 40 mol% ceria respectively. 250 ml of concentrated HCl and 250 ml of distilled water were mixed and added to the mixed powders, so that 10 or 60 g/l of the resulting oxide would be obtained from the solutions. The acid solution was constantly stirred on a hot plate stirrer at room temperature.

The precipitants used were 35% ammonia solution (Philip Harris) and sodium hydroxide solution, prepared from 98% min. sodium hydroxide granules (Fisons Scienific) dissolved in distilled water until a pH of 14 was achieved.

The acid solution was added dropwise to 1.5 L of precipitant, which was rapidly stirred by the action of an overhead stirrer / glass paddle set up. Extra base was added when required for the attainment of the correct pH. Following this, 50 ml / 100 vols of hydrogen peroxide (Fisons), when required, was added to the mixing hydroxide/base, prior to allowing the hydroxide/base to age.

The hydroxide was vacuum filtered and washed by the addition of copious amounts of distilled water over a period of 24 hours. The material was then dried at 110°C and calcined. Calcination took place in a porcelain calcination boat placed within a Carbolite tube furnace controlled by a Eurotherm, similar to that described in Chapter 2. When nitrogen was required as the atmosphere for calcination, the porcelain boat was placed in a silica tube within the same furnace with nitrogen at 100 ml min^{-1} passed over the sample.

The ceria concentrations in the mixed oxides were chosen to be 10 and 40 molar %, the nominal and extreme respectively. These concentrations had previously been shown to offer significantly different surface area, crystallite size, and reduction characteristics (11,12).

The nominal and extreme concentrations for the acid precursor solutions were chosen to be 10 and 60 g l^{-1}, (gram of oxide per litre of solution), chosen because it had been shown that a dilute acid solution could enhance the surface area of the final mixed oxide, as well as altering its crystal nature (12).

The different precipitants studied were sodium hydroxide, nominal, and ammonia, extreme. In the literature a number of bases have been employed for precipitation including ammonia (12-14), urea (15), potassium hydroxide (16) and sodium hydroxide (16,17) yet little study has been undertaken on the comparison of precipitant types for this material.

The temperatures at which the precursor was precipitated at, 20°C and 80°C, extreme and nominal respectively, and maintained at, 20°C and 80°C, nominal and extreme respectively, following precipitation were also investigated, although temperature of coprecipitation has been claimed to have little significance upon the phase composition and specific surface of the mixed oxide (18). Conversely the temperature of digestion (aging temperature) has been reported as being important in the formation of highly temperature stable tetragonal zirconia (19).

It is useful to determine whether the amount of time taken in adding the acid precursor to the precipitant is of importance to the quality of the final product. The rate at which acid is added to base, or base to acid, has not been fully investigated in the literature with respect to the character of this mixed oxide. Here the nominal was chosen

as slow addition, over 2.5 hours, with the extreme value being the fast addition of the acid precursor, over 0.25 hours.

One would imagine that the pH of precipitation would be vital to the character of the final mixed oxide considering the literature based upon the nature of zirconia following deposition at various acidities (20,21). It is for this reason why pH was chosen to be investigated, with the nominal being 9 and the extreme being 11. Values of pH 6.5 (15) and 10 (14) and what has been termed as 'excess ammonia' (13) have been cited, yet pH of precipitation has been stated not to have a significant influence on the nature of the final mixed oxide (18).

Aging time, or digestion time, was studied as it has been claimed to be an important parameter in the formation of high surface area zirconia (19), by a similar method of preparation. The two levels investigated were 2.5 hours (extreme) and 0.25 hours (nominal).

The addition of hydrogen peroxide at the completion of the precipitation was investigated. Little literature evidence exists for the use of hydrogen peroxide in zirconia preparation, but there is published work indicating that addition of peroxide to amorphous zirconia materials lowers the temperature of crystallisation hence lowering the thermal stability (22). The nominal level was set at no addition of peroxide, the extreme being addition of peroxide.

The influence of drying and calcining the obtained precipitate is dealt with in reasonable detail. Both the length of time and the rate of drying are investigated. To limit the rate of drying, the beaker containing the washed precipitate is either covered with aluminium foil, with small holes, (nominal) or not (extreme). The length of drying time was either set at 20 hours (nominal) or 68 hours (extreme). Both the rate and extent of water loss in the drying stage is thought to be importance (11).

All of the calcination variables, just as the drying variables, will influence the crystallisation of zirconia from the hydroxide (23), final phase of the zirconia and surface area (12). Extended time at high temperature has also been shown to be detrimental to the crystal structure of the mixed oxide (24). Calcination ramp rate, 10 (extreme) or 4°C min^{-1} (nominal), atmosphere, air (extreme) or nitrogen (nominal), calcination temperature, 900°C (extreme) or 500°C (nominal) and time at maximum temperature, 12 hours (extreme) or 2 hours (nominal) where the variables investigated.

The 15 variables, and with their nominal and extreme values, - and + respectively, is listed below; each variable is referred to by an abbreviation. Table 3.1 shows the settings of the 15 variables in each of the 16 catalysts prepared.

1) Ceria / Zirconia oxide ratio set at (-)10 or (+) 40 mol% (Ratio)
2) Concentration of the mixed acid solution acid (-)10 or (+) 60 g/l (Conc)
3) An (+) ammonia solution or (-)sodium hydroxide precipitant (PPT)
4) Precipitation at either (-) 80 or (+) 20°C (Ptemp)
5) Acid added to the base over (+) $^1/_2$ or (-) $2^3/_4$ hours (Speed)
6) A final pH of the mixed hydroxide of either (-) 9 or (+)11 (pH)
7) An aging time of (-) $^1/_4$ or (+) 2 $^1/_2$ hours (Atime)
8) An aging temperature of (-) 20 or (+) 80°C (Atemp)
9) A drying time of (-) 20 or (+) 68 hours (Dtime)
10) A (+) dry or (-) moist drying atmosphere (Datmo)
11) A calcination temperature of (+) 900 or (-)500°C (Ctemp)
12) A calcination ramp rate of (+)10 or (-) 4°C min^{-1} (Crate)
13) A calcination time, at maximum temperature, of (+) 12 or (-) 2 hours (Ctime)
14) A (-) nitrogen or (+) air calcination (Catmo)
15) The (+) addition, or not (-) of hydrogen peroxide to the hydroxide (Perox)

3.3: Results and Discussion

The 16 catalysts were characterised by surface area measurement, temperature programmed reduction, X-ray photoelectron spectroscopy, and X-ray diffraction and the results are presented in sections 3.3.1. to 3.3.4.

What will become evident is that unsurprisingly, the dominant variables in determining a range of mixed oxide characteristics are calcination temperature and ceria / zirconia ratio. It is thus useful to divide the 16 catalysts prepared into four groups:

Group 1	Calcined at 900C / 40 mol % ceria.	Catalysts 1, 12, 14, 16
Group 2	Calcined at 500C / 40 mol % ceria.	Catalysts 2, 5, 6, 13
Group 3	Calcined at 900C / 10 mol % ceria.	Catalysts 4, 7, 9, 15
Group 4	Calcined at 500C / 40 mol % ceria.	Catalysts 3, 8, 10, 11

Table 3.1. Preparation sheet

Catalyst	Ratio % Ce	Conc g/l	PPT	PTemp ° C	Speed	pH	ATime hrs	ATemp ° C	DTime hrs	DAtmo	CTemp ° C	Crate ° C/m	CTime hrs	CAtmo	Perox
1	40	10	NH_3	80	S	9	2.5	20	20	M	900	10	12	Air	NP
2	40	60	NaOH	80	S	11	2.5	20	20	D	500	4	2	Air	P
3	10	10	NaOH	20	S	9	0.25	20	20	M	500	4	2	N_2	NP
4	10	60	NH_3	20	S	11	0.25	20	20	D	900	10	12	N_2	P
5	40	60	NH_3	80	S	11	0.25	80	68	M	500	10	2	N_2	NP
6	40	10	NH_3	20	F	11	0.25	20	68	M	500	4	12	Air	P
7	10	60	NaOH	20	S	11	2.5	80	68	M	900	4	12	Air	NP
8	10	60	NH_3	80	F	9	2.5	20	68	D	500	4	12	N_2	NP
9	10	10	NH_3	80	F	11	0.25	80	20	D	900	4	2	Air	NP
10	10	60	NaOH	80	F	9	0.25	80	20	M	500	10	12	Air	P
11	10	10	NH_3	20	S	9	2.5	80	68	D	500	10	2	Air	P
12	40	60	NaOH	20	F	9	0.25	20	68	D	900	10	2	Air	NP
13	40	10	NaOH	20	F	11	2.5	80	20	D	500	10	12	N_2	NP
14	40	10	NaOH	80	S	9	0.25	80	68	D	900	4	12	N_2	P
15	10	10	NaOH	80	F	11	2.5	20	68	M	900	10	2	N_2	P
16	40	60	NH_3	20	F	9	2.5	80	20	M	900	4	2	N_2	P

3.3.1: Effect of Preparation Variables on Surface Area

The surface area of ceria / zirconia mixed oxides have been shown to be directly related to catalytic activity for the decomposition of propan–2–ol to propene (12). It is for this reason an investigation has been undertaken to determine the important parameters influencing surface area.

Table 3.2 below shows the surface area of the 16 catalysts. Figures are correct to the nearest whole number. The standard deviations (7) for the repeated runs are also shown.

Table 3.2. Surface area of the catalysts

Surface Area / $m^2 g^{-1}$	**Standard Deviation**	**Catalyst**
122	0.40	6
109	0.10	8
108	0.35	3
104	0.65	10
94	0.35	11
92	1.34	2
91	0.10	13
74	0.90	5
28	0.10	14
26	1.15	4
12	1.20	16
12	1.48	9
12	1.05	15
10	1.30	1
7	0.05	12
6	0.40	7

From table 3.2. and the discussion of group types it is seen that catalysts of group 1 and 3, i.e. those subject to a calcination temperature of 900°C have surface areas ranging

from 7 – 26 m^2g^{-1}, whereas those catalysts calcined at the lower temperature have a much greater surface area.

Because of the problems associated with averaging values it is acknowledged that the manner in which ranking is depicted in table 3.2. , and elsewhere in this chapter, could be erroneous. Where the standard deviation, shown in figure 3.2., is greater than the difference between catalysts, i.e. in the case of catalysts 2 and 13, the character should be considered the same. The statistical approach used requires two groups of data to be taken, processed and compared. In one group surface areas may be underestimated and in the other the surface areas may be overestimated, significant errors may result. The author wishes the reader to take note of this.

The Plackett-Burman approach has allowed us to determine the importance of all the preparation variables affecting the surface area of the catalysts. Table 3.3. shows the values by which the factors influence surface area.

Table 3.3. indicates that the method of preparation required to obtain a ceria / zirconia mixed oxide of higher surface area would primarily be to calcine the material at 500°C, which would give a material with a surface area 85.1 m^2/g higher than that of a material calcined at 900°C. The remaining preparation variables are shown to have a much smaller degree of influence as compared to the calcinations temperature. Preparing the catalyst by quickly adding the dilute acid precursor, containing 10 mol% ceria, to ammonia down to pH 9 at room temperature, allowing little time for aging at room temperature with the addition of peroxide are the conditions necessary in the precipitation phase of the preparation to enhance the surface area. Drying in an uncovered beaker for 20 hours, followed by calcination in nitrogen for 12 hours with a slow ramp rate, are the remaining conditions indicated by the table for the attainment of the higher surface area material.

As expected, calcination temperature has been found to be the dominant variable influencing surface area. In the mixed oxide, as in pure zirconia, calcination induces nuclei grow into observable crystallites (23). Calcination temperature thus governs the crystallite size and hence the surface area of the final zirconium based mixed oxide. The formation of the nuclei is stated as an important factor to the character of the final oxide. The remaining drying and calcining variables will thus be of importance. The loss of loosely bound water and terminal hydroxo groups and the oxolation of OH

bridges allow for nuclei formation (24,25). I believe that the drying and calcination regimes shown to be favourable in this study are responsible for the formation of fewer nuclei; which in turn would limit the formation and growth of crystallites upon calcining at 500°C for 12 hours. Why calcination of the mixed oxide for 12 hours is indicated as beneficial is puzzling however. Phase separation has been observed with ceria / zirconia mixed oxides subject to temperature aging for extended periods (26), while 50:50 mixed oxide samples showing phase separation have been shown to have smaller crystallite size than those not showing phase separation (12).

Table 3.3. The influence of variables on the surface area of the prepared catalysts

Preparation Variable (Extreme)	**Effect on Surface Area (m^2/g) with Variable at Extreme**
Ctemp (900°C)	-85.1
Ctime (12hrs)	10.7
Perox (added)	9.1
Crate (10°C min^{-1})	-8.7
Atemp (80°C)	-8.0
Atime (2.5hrs)	-6.9
Conc (60gl^{-1})	-5.7
pH (11)	-4.7
Ratio (40 mol% ceria)	-4.3
Speed (fast)	4.2
Ptemp (20°C)	3.2
Catmo (air)	-1.8
PPT (NH_3)	1.5
Datmo (dry)	1.5
Dtime (68hrs)	-0.5

The addition of the peroxide to the aging hydroxide is shown to have a beneficial effect on the surface area of the mixed oxide. Evidence suggests, however, that addition of peroxide to amorphous zirconium materials lowers the temperature of crystallisation due to the formation of peroxo-species of zirconium. The peroxo-bonds are then readily broken by thermal treatment, reducing the stability (22). The effect that hydrogen peroxide exerts on cerium/zirconium hydroxides is not understood, it may be important that the peroxide ensures that cerium is in the +4 state, i.e. has the same charge as the zirconium ion.

The remaining variables are shown to exert little influence on the final surface area of the mixed oxide as previously reported (18). Aging time and temperature are shown to offer minor influence here where in the case of pure zirconia, higher temperatures and longer times offer some enhancement to surface area, (19). The surface area differences between the 10% and 40% ceria materials are statistically insignificant.

The Plackett - Burman approach allows us to identify the preferred setting for each of the 15 variables studied. It is thus of interest to make and characterise a catalyst using only these preferred settings. We have chosen to do this while making a brief study of the influence of calcination time. With the other 14 variables set as indicated in table 3.3, the influence of calcination time is shown in figure 3.1.

The best surface area obtained is 121 $m^2 g^{-1}$, after a calcination time of 7 hours. Disappointingly, this is no better than the best value obtained in the statistically designed set of studies, which was 122 $m^2 g^{-1}$. The fact that the calcination time of 12 hours resulted in a catalyst of lower surface area also seems to disprove its importance and the argument above.

The overall conclusion on the optimum setting of each variable may, however, not be equally applicable to each catalyst type. Here we have formed a 500/10 material and applied optimum conditions to prepare a high surface area material based on data obtained from all 4 types of catalyst. The preparation variables which may aid surface area enhancement in the 900/40, 900/10 and 500/40 types may not be the same as those required by a 500/10 material. The variables for optimum surface area can thus not be straight forwardly applied to this catalyst. What is useful however is the information gleaned on the general effects the factors have on the materials' character.

Figure 3.1. surface area vs. calcination time for an 'optimal' material

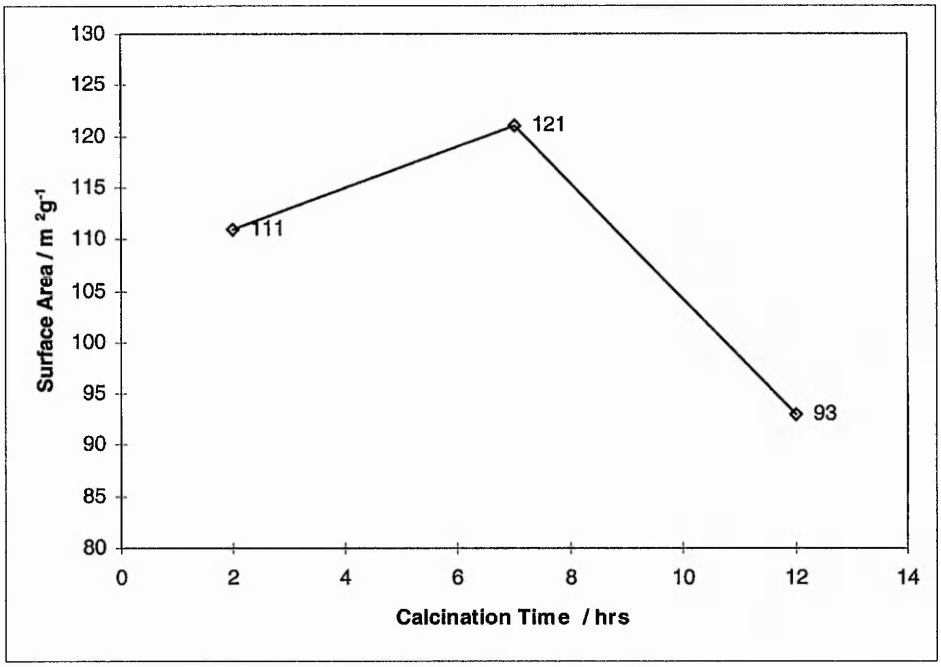

3.3.2: Effect of Preparation Variables on Crystal Structure

X-ray diffraction patterns provide evidence of how changing preparation variables affect catalyst structure. Here are described the crystallographic nature of the 16 prepared mixed oxides. A number of phases exist within the ceria / zirconia binary system, solid solutions based on the monoclinic (m) and tetragonal (t) nature of zirconia and the cubic phase (c) of ceria and phase separated tetragonal zirconia and cubic ceria (26,27,28). These structures are seen in the prepared catalysts.

Table 3.4. summarises the results obtained for this study from analysis of the individual traces and data calculated by the XRD software. Figure 3.2. shows typical diffraction patterns obtained. A high degree of confidence is ascribed to these figures. A standard sample was regularly run on the machine to ensure accuracy to within one step.

Catalyst 12, the XRD trace of which is shown in figure 3.2., is a 40 mol% Ce material calcined at 900°C. The XRD trace shows phase separation of the major tetragonal zirconia and cubic ceria peaks at the 30° 2θ position. In the case of catalyst 6, a 40 mol% Ce material calcined at 500°C, there is less well defined crystal structure,

and phase separation is not observed. Catalysts 6 and 12 have a shifted main reflection to lower 2θ°, indicative of the formation of a solid solution of ceria in zirconia.

Catalysts 8 and 9 are 10 mol% Ce materials. They show, as expected, no phase separation, and a reduced shift in lattice parameter. Catalyst 9, calcined at 900°C, displays a greater crystalline character.

What is observed on examination of the XRD traces is that with high ceria concentrations in the catalyst there is sufficient to prevent tetragonal to monoclinic phase change at 900°C, but too much to prevent phase segregation of tetragonal zirconia and cubic ceria. With lower ceria levels there seems to be insufficient to prevent the zirconia phase change at 900°C and so insufficient to limit surface area loss.

Figure 3.2. Typical XRD traces of the four main classes of mixed oxide

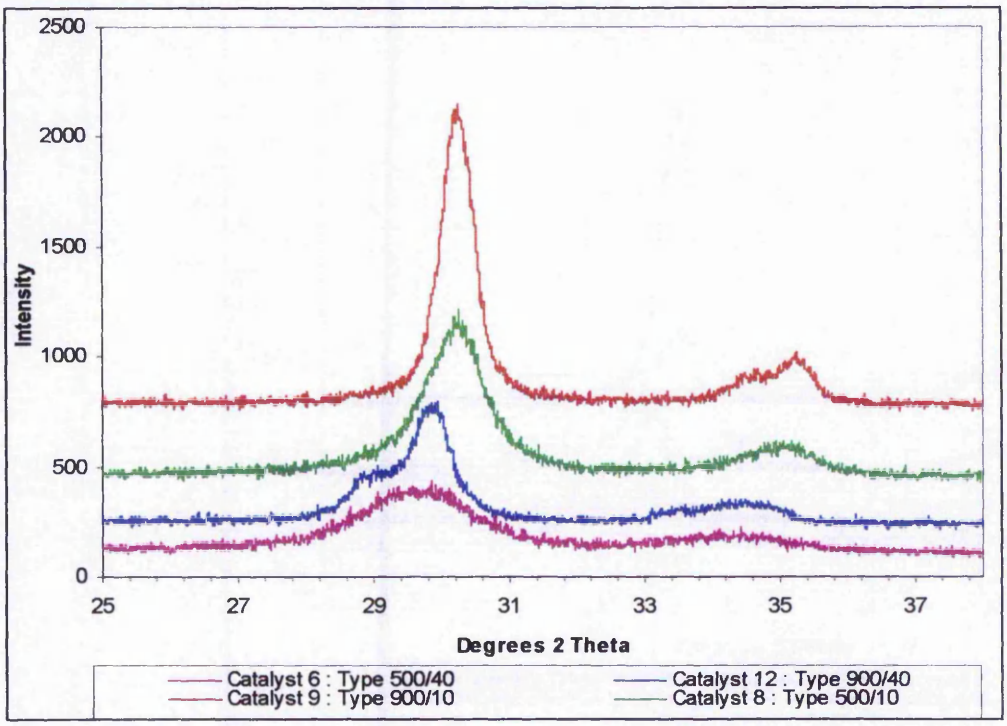

See also table 3.1. Previously it was reported that extended treatment at high temperature induces phase separation. Group 1 materials, 1, 12, 14, and 16, i.e. those

Table 3.4. Results from the XRD characterisation technique

Catalyst	XRD FWHM / 2°θ	Crystallite Size / nm	Major Reflection Position / 2°θ	Phase
1	1.268	6.41	29.64	Weak phase separation of (t) and (c)
2	2.212	3.67	29.72	No clear separation of (t) and (c)
3	1.512	5.38	30.14	No clear separation of (t) phase
4	0.458	17.80	30.16	No phase separation in the (t) to (m) phase transition
5	1.520	5.33	29.36	Weak separation of (t) and (c)
6	2.352	3.45	29.70	No separation of (t) and (c)
7	0.292	27.96	30.16	No phase separation in the (t) to (m) phase transition
8	1.146	7.11	30.12	No clear separation of (t) phase
9	0.604	13.49	30.10	No clear separation of the (t) phase
10	1.446	5.63	30.16	No clear separation of (t) phase
11	0.640	12.74	30.30	No clear separation of (t) phase
12	1.504	5.41	29.80	Clear separation of (t) and (c)
13	2.614	3.11	29.84	Clear separation of (t) and (c)
14	1.628	5.00	29.88	Clear separation of (t) and (c)
15	0.432	18.88	30.18	No phase separation in the (t) to (m) phase transition
16	0.914	8.90	29.76	No clear separation of (t) and (c)

calcined at 900°C and containing 40% ceria did differ with regards to phase separation. Catalysts 1 and 14, subject to temperature for twelve hours both show a degree of separation, 16, calcined for two hours, did not show the phenomenon. To state that this observation is of significance when the manner of preparation of the materials differed would be erroneous.

In the case of the materials containing 10% ceria FWHM and hence apparent crystallite size are seen to be closely related to surface area (table 3.2.) and so are almost totally related to the crystallinity. In the 40% ceria materials the relationship is complicated by the double peak effects of broadening and phase separation. No relationship can thus be observed linking phase separation, apparent crystallite size and surface area.

Table 3.5. shows the main factors influencing the main tetragonal zirconia peak position.

Table 3.5. Importance of variables to peak position

Preparation Variable (Extreme)	**Effect on Peak Position (2θ°) with Variable at Extreme**
Ratio (40 mol% ceria)	-0.453
Datmo (dry)	0.103
PPT (NH_3)	-0.093
Ptemp (20°C)	0.088
Perox (added)	0.088
pH (11)	-0.073
Conc ($60gl^{-1}$)	-0.068
Atime (2.5hrs)	0.053
Ctemp (900°C)	0.043
Ctime (12hrs)	0.038
Speed (fast)	0.038
Crate ($10°C\ min^{-1}$)	-0.018
Catmo (air)	0.018
Atemp (80°C)	0.013
Dtime (68hrs)	-0.003

Table 3.5. indicates that increased ceria levels in the mixed oxide significantly shifts the major reflection to lower values of 2θ°, indicative of greater levels of ceria within the zirconia lattice. The remaining parameters that also enhance this effect are the use of a concentrated acid precursor added slowly to ammonia at 80°C down to a pH of 11. The precipitate should then be subject to no peroxide addition but aged for a short period of time at room temperature. The filtered and washed precipitate, subject to drying in a covered beaker for 68 hours, should further be calcined in nitrogen with a ramp rate of 10°C min^{-1} to 500°C and maintained at that temperature for 2 hours.

Peak width is due to a number of factors. Temperature of calcination is known to influence crystallite size. A lower calcination temperature decreases crystallite size (increases peak width), whereas the presence of excess ceria within the mixed oxide is shown to cause phase separation and stabilisation of the tetragonal phase, increasing the peak width and decreasing the apparent crystallite size. Table 3.6 indicates the variables of importance to peak width.

Table 3.6. indicates that the full width at half maximum of the major reflection is increased with ceria present in the mixed oxide to a greater amount, and when the material is calcined at 500°C. The remaining variables indicated in enhancing this phenomenon are the use of a dilute acid precursor added rapidly to sodium hydroxide precipitant down to pH 11 at room temperature. The lack of peroxide addition with little aging at room temperature would complete the precipitation stage of the process. Drying in an uncovered beaker for 20 hours prior to calcination in air for 12 hours, subject to ramping of 4°C min^{-1}, completes the conditions indicated to enhance peak width.

The zirconia lattice parameter has been shown to decrease when the ceria/zirconia exists as a solid solution rather than a physical mixture (29). The decrease in 2θ has been assigned to the presence of the solid solution. The major tetragonal zirconia peak, when the bulk Ce content is 10%, is 30.17°, at 40% it is at 29.71°. The said variables are thus enhancing the solid solution phase (t) i.e. encouraging ceria take up into the bulk zirconia.

Table 3.6. Preparation variables and their importance to peak FWHM

Preparation Variable (Extreme)	**Effect on XRD Peak FWHM (2θ°) with Variable at Extreme**
Ratio (40 mol% ceria)	0.935
Ctemp (900°C)	-0.793
PPT (NH_3)	-0.342
Ctime (12hrs)	0.233
Conc ($60gl^{-1}$)	-0.195
Dtime (68hrs)	-0.189
Atime (2.5hrs)	-0.188
Speed (fast)	0.185
Atemp (80°C)	-0.153
Datmo (dry)	0.134
Crate ($10°C\ min^{-1}$)	-0.097
pH (11)	0.053
Perox (added)	-0.047
Catmo (air)	0.012
Ptemp (20°C)	0.004

By far the most important factors are calcination time and Ce/Zr ratio. With the addition of a larger bulk Ce content, XRD data shows that the main tetragonal zirconia peak/ cubic ceria peak is broader. With the 40% Ce materials, the average FWHM of the peak is 1.63°, with the 10% materials it is 0.82° 2θ. With more Ce present there is more to stabilise the tetragonal structure, also, as there is a larger volume of ceria there will be an increase in the peak intensity. The overlapping of the 2 peaks around 30 2θ° will account for a broader peak. A lower calcination temperature limits crystal growth and hence offers a smaller crystal size and a broader peak.

3.3.3: Effect of Preparation Variables on Ce/Zr Surface Ratio

The temperature of calcination and the nature of preparation of zirconia based mixed oxides has been shown to change surface composition significantly (12). The nature of the surface is important for surface area and redox properties of the mixed oxide and it is for this reason an examination of how preparation variables influence surface composition was undertaken.

The peaks scanned for the determination of surface composition are indicated in table 3.7. Each range was scanned at 1 second dwell for each 0.1 eV, 10 times. The surface composition was calculated by the application of the equations given in chapter 2.4. Figure 3.3. shows the typical XPS traces observed. Table 3.8 shows the Ce/Zr surface ratios of the 16 catalysts

Figure 3.3. XPS peaks

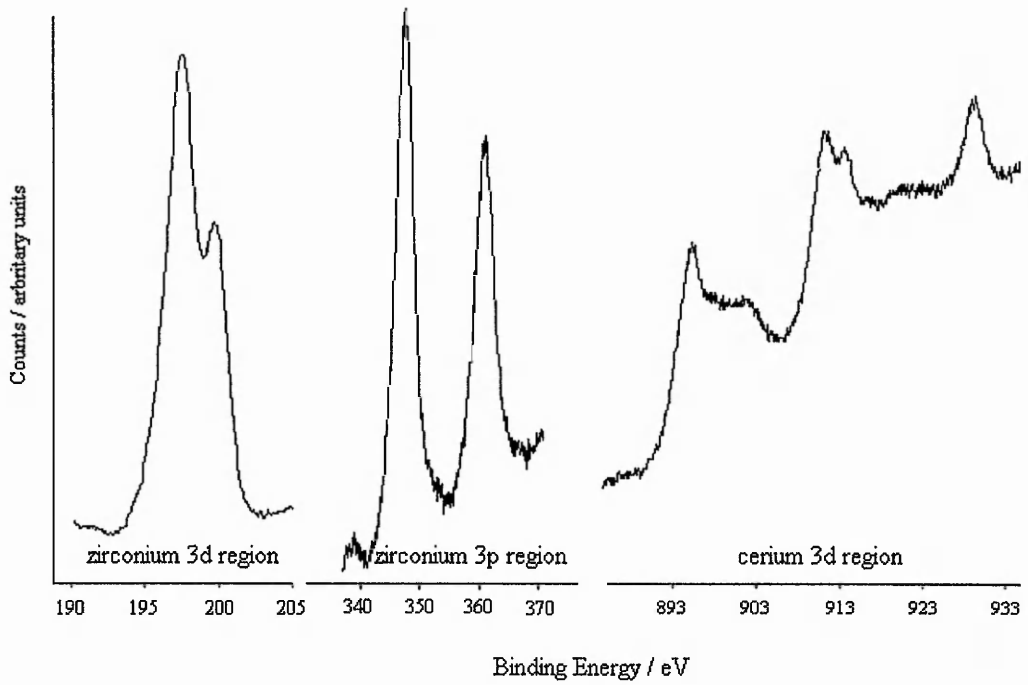

Table 3.7. XPS scanned regions

Elemental Orbital Peak	Range Scanned eV (binding energies)
Zr 3d	190 - 215
Ce 3d	880 – 955
Zr 3p	330 – 375
C 1s	295 - 310

Table 3.8. Surface composition of the catalysts

Catalyst	Ce/Zr Ratio
1	2.27
2	1.75
3	0.28
4	0.54
5	2.0
6	2.94
7	0.65
8	0.26
9	0.52
10	0.21
11	0.21
12	1.04
13	1.49
14	1.92
15	0.26
16	1.52

Table 3.9. displays the influence of the preparation variables on the surface composition of the mixed oxides.

Not surprisingly, table 3.9. shows that the ratio of ceria to zirconia is the most important variable governing the surface ratio. The other factors required in reducing the level of surface ceria are indicated as being the use of a concentrated acid solution added quickly to sodium hydroxide at room temperature to pH9 with no addition of peroxide. An extended aging time at 80°C are also stated as the preferred variables. Drying in an uncovered beaker for 20 hours prior to calcination in nitrogen, subject to a ramp rate of 10°C min^{-1}, for 2 hours at 900°C completes factors required.

Table 3.9. Preparation variables and their importance to surface composition

Preparation Variable (Extreme)	**Effect on Ce/Zr Surface Ratio with Variable at Extreme**
Ratio (40 mol% ceria)	1.53
pH (11)	0.33
Datmo (dry)	-0.33
Ctime (12hrs)	0.31
PPT (NH_3)	0.30
Conc ($60gl^{-1}$)	-0.27
Speed (fast)	-0.20
Crate (10°C min^{-1})	-0.20
Catmo (air)	0.19
Atime (2.5hrs)	-0.16
Perox (added)	0.13
Atemp (80°C)	-0.07
Dtime (68hrs)	0.06
Ptemp (20°C)	-0.04
Ctemp (900°C)	-0.02

Ratio is obviously the dominant factor. With a ratio of 40% Ce, the average surface ratio is 1.85 Ce/Zr. With the 10% Ce the average surface ratio is 0.37. When the bulk ratio is increased from 10% - 40%, the surface ratio increases by approximately 1.5. The bulk ratio is by far the most important factor as regards surface ratio, however there is a three-fold difference in the ratio of the ceria on the surface for the 10wt% samples, 0.21 – 0.65 and for the 40wt% samples, 1.04 – 2.94. The three-fold difference within the two groups must be ascribed to the influence of the other variables.

Surprisingly, calcination temperature proved relatively unimportant to the surface composition of the mixed oxide. It has been previously been shown that an increase in the calcination temperature causes surface enrichment of ceria in this mixed oxide (12). It has previously been discussed that increased time of calcination induces phase separation, here there is evidence to suggest that ceria surface enrichment also results from long periods of calcination; a rapid ramp rate will also limit the time by which the mixed oxide is subject to high temperature. Rapid addition of the mixed acid solution of high concentration is shown to be beneficial in limiting high surface ceria content. It can be envisaged that these variables could result in rapid precipitation of the mixed hydroxide in a manner by which the close contact of the two different components of the mixed solution are maintained, thus forming a more uniform mixed hydroxide. As the nature of the preparation is acid to base it seems somewhat odd that the final pH and the nature of the precipitant should be important to the surface character of the mixed oxide; as upon contact of the solution with the base spontaneous coprecipitation results. The P-B method also indicates the apparent importance of the drying method to surface composition.

3.3.4: Effect of Preparation Variables on the Reduction of the Catalysts

As discussed in chapter 1, the main reason for the presence of ceria in an automotive catalytic converter is its ability to undergo reduction and reoxidation. To determine the way in which the preparation variables influence the reduction characteristics of the ceria / zirconia mixed oxides the catalysts where subject to temperature programmed reduction (TPR), as described in chapter 2. Traces are

reproducible to an accuracy of +/- 5°C.

Figure 3.4. shows the typical TPR traces observed for pure CeO_2.

The oxygen mobility is slow in pure ceria which leads to a two-stage reduction process. The first peak, at low temperature, correlates to the reduction of the easily reduced surface ceria, whereas the high temperature peak is assigned to the more difficult bulk reduction. This is clearly seen in the figure 3.4. The relative sizes of the peaks are surface area dependent. Oxygen mobility in the ceria is enhanced by zirconia presence, this leads to a single reduction feature with the majority of the reduction occurring at lower temperature (31,32). Zirconia itself is not reducible under TPR conditions (33).

Fig.3.4. TPR of CeO_2 samples. (30).

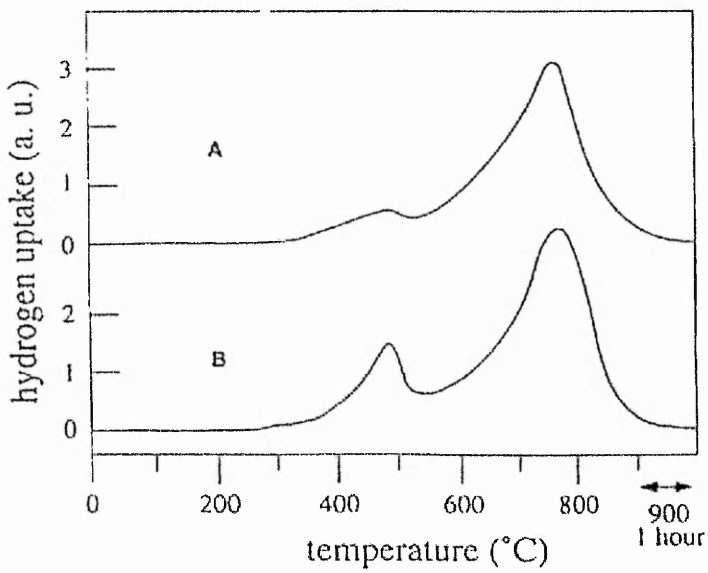

A, BET surface area 1 m^2/g; B, 10 m^2/g

Four reduction characteristics were examined on the 16 samples: amount of reduction, peak position, commencement of reduction and FWHM of the reduction profile.

Table 3.10. reports the character of the 16 catalysts.

The reduction of ceria by hydrogen follows by the equation

$$2CeO_2 + H_2 \rightarrow Ce_2O_3 + H_2O \qquad \text{equ.3.1.}$$

Percentage reduction of ceria is calculated thus...

$$\frac{\text{moles of } H_2 \text{ taken up by the catalyst}}{\text{moles of Ce IV in the mixed oxide}} \times 100 \qquad \text{equ.3.2.}$$

Figure 3.5. displays typical TPR profiles for 4 catalysts.

Figure 3.5. TPR traces

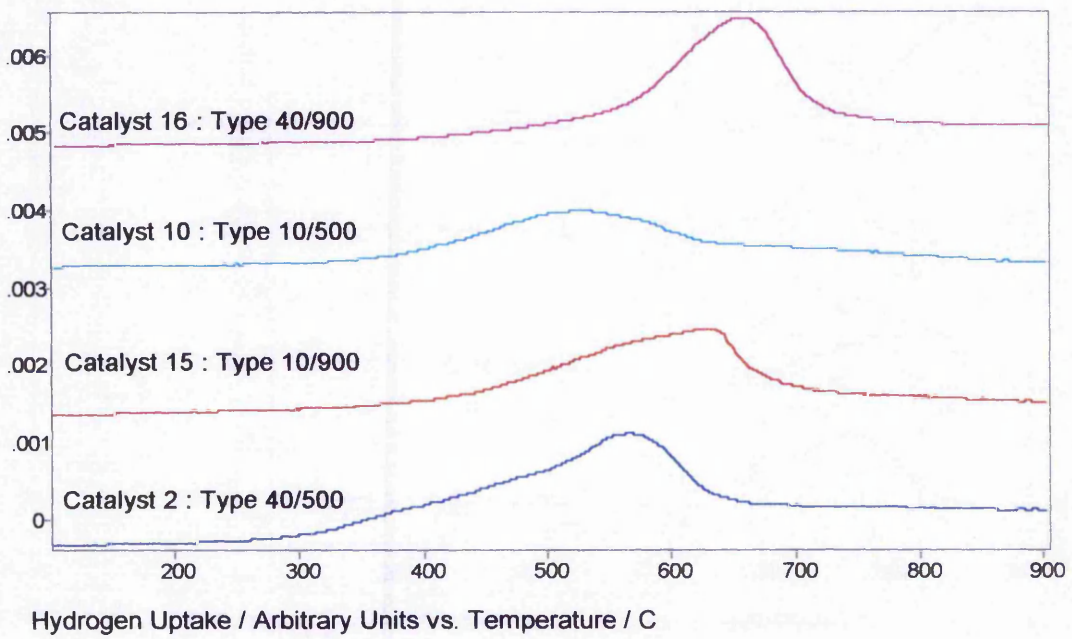

What is clear from figure 3.5. is that the greater the content of ceria in the mixed oxide the greater the hydrogen uptake i.e. the area under the peak. What is also clear is that peak position is shown to be related to the calcination temperature of the mixed oxide.

Table 3.10. Reduction characteristics of the catalysts

Catalyst And Type	Ce IV Reduction / %	TPR Peak / °C	Reduction Start / °C	TPR FWHM / °C
1 (900/40)	41.0	626	350	100
2 (500/40)	23.1	564	290	140
3 (500/10)	50.2	550	370	140
4 (900/10)	53.4	634	310	240
5 (500/40)	29.3	590	340	90
6 (500/40)	40.9	552	280	130
7 (900/10)	42.1	620	350	150
8 (500/10)	69.8	619	290	150
9 (900/10)	49.5	640	320	430
10 (500/10)	82.8	526	320	170
11 (500/10)	61.9	627	300	230
12 (900/40)	41.9	649	480	80
13 (500/40)	28.4	566	260	170
14 (900/40)	27.7	547	350	160
15 (900/10)	59.1	625	340	160
16 (900/40)	33.2	656	390	110

Table 3.11. shows how the preparation variables influence the amount of reduction the ceria component can undergo.

Table 3.11. Preparation variables and their importance to reducibility

Preparation Variable (Extreme)	**Effect on Ceria IV Reducibility (%) with Variable at Extreme**
Ratio (40 mol% ceria)	-25.4
pH (11)	-10.3
Speed (fast)	9.6
Crate (10°C min^{-1})	7.6
Ctemp (900°C)	-4.8
Ctime (12hrs)	4.7
Catmo (air)	4.0
Ptemp (20°C)	-3.8
Perox (added)	3.7
Atemp (80°C)	-3.1
PPT (NH_3)	3.0
Datmo (dry)	-2.9
Atime (2.5hrs)	-2.1
Conc (60gl^{-1})	2.1
Dtime (68hrs)	1.4

Proportionally greater reducibility of the mixed oxide, according to table 3.11., is obtained with ceria present at 10mol%. Concentrated acid precursor solution quickly added to ammonia at room temperature to pH9 and the addition of hydrogen peroxide with a short aging time at 20°C are given as the conditions necessary in the precipitation phase to enhance reducibility characteristics. Drying of the precipitant in a covered beaker for 68 hours, followed by calcination in air, subject to a ramp rate of 10°C min^{-1}, for 12 hours at 500°C completes the conditions required for proportionally greater reduction.

Table 3.12. indicates the factors governing TPR peak position.

Table 3.12. Preparation variables and their importance to TPR peak position

Preparation Variable (Extreme)	**Effect on TPR Peak Position (°C) with Variable at Extreme**
Ctemp (900°C)	50.4
PPT (NH_3)	37.1
Atime (2.5hrs)	26.9
Ctime (12hrs)	-26.4
Perox (added)	-16.1
Conc ($60gl^{-1}$)	15.6
Ptemp (20°C)	14.6
Datmo (dry)	12.6
Crate ($10°C\ min^{-1}$)	11.9
Ratio (40 mol% ceria)	-11.4
Speed (fast)	9.4
Dtime (68hrs)	8.4
Atemp (80°C)	-5.9
Catmo (air)	2.1
pH (11)	-1.1

Table 3.12. indicates that the temperature at which the ceria component of the mixed oxide reduces is decreased, primarily, by lower temperature calcination. The other preparation variables required to enhance this effect, according to the approach used, are a dilute acid precursor solution, added slowly to sodium hydroxide precursor at 80°C down to pH 11. Hydrogen peroxide should be added and the precipitant should be aged for a short amount of time at 80°C. The precipitant requires drying in a covered beaker for 20 hours. Calcination should proceed in nitrogen with a ramp rate of 4°C min^{-1} up to 500°C for 12 hours.

Both the initial point at which reduction commences and the temperature range over which reduction takes place are interesting characteristics of the prepared

materials. Tables 3.13. and 3.14. show how the preparation variables influence these characteristics.

Table 3.13. Preparation variables and their importance to commencement of reduction

Preparation Variable (Extreme)	**Effect on Commencement of Reduction (°C) with Variable at Extreme**
Ctemp (900°C)	55.0
pH (11)	-45.0
Ctime (12hrs)	-40.0
Perox (added)	-25.5
Conc ($60gl^{-1}$)	25.0
Atime (2.5hrs)	-25.0
PPT (NH_3)	-22.5
Ptemp (20°C)	17.5
Ratio (40 mol% ceria)	17.5
Datmo (dry)	-17.5
Dtime (68hrs)	15.0
Atemp (80°C)	-10.0
Crate ($10°C\ min^{-1}$)	7.5
Catmo (air)	5.0
Speed (fast)	2.5

Table 3.13. indicates that the reduction of the ceria component will begin at a lower temperature when the mixed oxide is calcined at the lower temperature. The preparation variables indicated to enhance this character are a dilute acid precursor, ceria rich, added slowly to ammonia to a pH of 11, at a temperature of 80°C. An aging temperature of 80°C for 2.5 hours following addition of peroxide complete the

precipitation stage. The washed solid should then be dried in an uncovered beaker for 20 hours before being calcined for 20 hours subject to a ramp rate of 4 °C min^{-1}.

Table 3.14. Preparation variables and their importance to TPR peak FWHM

Preparation Variable (Extreme)	**Effect on TPR Peak FWHM (2θ°) with Variable at Extreme**
Ratio (40 mol% ceria)	-86
Datmo (dry)	69
Conc ($60gl^{-1}$)	-49
Atemp (80°C)	46
pH (11)	46
Dtime (68hrs)	-44
PPT (NH_3)	39
Atime (2.5hrs)	-29
Catmo (air)	26
Ctemp (900°C)	26
Crate (10°C min^{-1})	-21
Ptemp (20°C)	-19
Speed (fast)	19
Ctime (12hrs)	-14
Perox (added)	4

According to table 3.14. high ceria loading will decrease the temperature range over which the ceria is reduced. Enhancement of this character is aided by using concentrated acid precursor added slowly to sodium hydroxide to pH 9 at room temperature. The lack of peroxide addition to the precipitant / precipitate mix at 20 °C with an extended aging time completes the precipitation phase of the preparation. Drying in a covered beaker for 68 hours and calcining in nitrogen, subject to a ramp rate

of 10°C min^{-1}, for 12 hours completes the indicated conditions required.

From tables 3.11. – 3.14. it is clearly seen that the most important preparation variables influencing the reduction characteristics are temperature of calcination and the content of ceria in the mixed oxide.

From tables 3.10 and 3.11. it is seen that although greater reduction occurs per gram of catalyst with the presence of a greater ceria content, the degree of reducibility of the ceria is lessened. Zirconia here is shown to be beneficial in aiding reduction. It is not the zirconia itself which reduces as it has been demonstrated that neither monoclinic or tetragonal zirconia reduce under TPR conditions over the range 25-1000°C (33). Oxygen mobility within the CeO_2 lattice has been shown to be enhanced by the presence of zirconia (34). Oxygen diffusion has been observed in trivalently doped tetragonal zirconia (35), oxygen mobility has been observed through the pure monoclinic form (36) and pure tetragonal zirconia has been shown to adsorb hydrogen onto its surface (37). These literature observations give an insight into to importance of zirconia in ceria reducibility. From tables 3.13 and 3.14. it can be seen that a narrower reduction profile is observed with a higher content of ceria in the mixed oxide and reduction commences at higher temperatures. These observations are a result of the decrease in reducibility by high ceria content catalysts due to the decrease in oxygen mobility through the oxide compared to their zirconia rich counterparts.

The commencement of the reduction and the peak position of maximum reduction are governed by the calcination temperature of the mixed oxide. In section 3.3.1. it was shown that the dominant factor influencing surface area, hence particulate size, was calcination temperature. Surface area is the reason by which the observations in tables 3.12. and 3.13. can be explained. When calcined at high temperature the mixed oxide has a lower surface area, thus a larger bulk volume. With a smaller surface the onset of reduction is limited. With a larger bulk volume TPR peak position is shifted to higher temperatures because the oxygen mobility through the mixed oxide is made less facile.

Here again the dominant factors influencing the reduction characteristics are calcination temperature and ceria / zirconia content. The other variables play a role in the formation of the mixed oxide, i.e. distrubution of ceria in the zirconia, surface area and crystal structure which are all important to reducibility.

3.4: Conclusions

- By the application of a statistical method to the formulation and characterisation of mixed oxide catalysts it has been shown that calcination temperature and proportion of the individual components are the dominant variables influencing character. The 16 catalysts can thus be conveniently grouped into four sets of four.

Group 1	Calcined at 900C / 40 mol % ceria.	Catalysts 1, 12, 14, 16
Group 2	Calcined at 500C / 40 mol % ceria.	Catalysts 2, 5, 6, 13
Group 3	Calcined at 900C / 10 mol % ceria.	Catalysts 4, 7, 9, 15
Group 4	Calcined at 500C / 10 mol % ceria.	Catalysts 3, 8, 10, 11

Calcination temperature is important to those characteristics of the mixed oxide governed by surface area. The ratio of the oxides is important to reducibility and crystallography. Within each of the groups however there is a reasonable degree of variation with regards to the determined character. The differences are ascribed to the other variables employed in their formulation. Delving any deeper into the Plackett-Burman derived results, in an attempt to derive any further information about the four groups, is not viable statistically and would produce meaningless data.

- The statistical approach has allowed for an inference to be made of the relative importance of each variable to the character.

- Using the Plackett-Burman method to optimise catalytic character has proved to be difficult; although surface areas were obtained using the optimised process which compared well to those already produced.

3.5: References

1. M.Bowker, 'The Basics and Applications of Heterogeneous Catalysis', Oxford University Press, 1st Ed. New York, 1998, 35-41
2. R.L.Plackett and J.P.Burman Biometrica 1946, vol 34, 255-272
3. A.Cichoki, P.Koscielniak, Microporous and Mesoporous Materials, 1999, vol 29, 369-382
4. E.A.Dawson, P.A.Barnes, Applied Catalysis A.Gen, 1992, 90, 2, 217-231
5. W.H.Lu, W.L.Wu, K.S.Chou, American Ceramic Soc. Bull. 1985, 64, 12, 1559-1562
6. X-Stat software package, J.Wiley and Sons, Chichester, 1982.
7. R.Caulcutt 'Statistics in Research and Development' 2nd ed. Chapman Hall London 1991 277-278
8. A.C.Atkinson and A.N.Donev 'Optimum Experimental Designs' Oxford Science 1992 280-282
9. S.N.Deming and S.L.Morgan 'Experimental Design :A Chemometric Approach' 2nd ed. Elsevier Amsterdam 1993 346-366
10. A.Pathak and P.Praminak Materials and Manufacturing Processes, 1993 8(4&5) 491-500
11. C.Norman, personal communication.
12. M.Keenan Ph.D Thesis, The Nottingham Trent University 1996
13. C.E.Hori, H.Permana, K.Y.S.Ng, A.Bremner, K.More, K.M.Rahmoeller and D.Belton, Appl.Catal.A.Gen. 1991 16 105-117
14. K.Hashimoto,N.Touka,R.Hamada and S.Imamura, Cat.Lett. 1998 50 193-198
15. E.Luccini,S.Merriani and O.Sbaizero, Int.J.Materials and Product Technology 1989 4 167-175
16. G.K.Chuah and S.Jaenicke, Appl.Catal.A.Gen, 1997 163 261-273
17. M.A.Aramenda, V.Borau, C.Jimenez, J.M.Marinas, A.Porras and F.J.Urbao, J.Chem.Soc.,Faraday Trans, 1997 93 1431-1483
18. A.S.Ivanova, E.M.Moroz, G.S.Litvak Keneticas and Catalysis 1992, vol 33, 5-6, 969-975
19. G.K.Chuah, S.Jaenicke, S.A.Chong and K.S.Chan, Appl.Catal.A.Gen, 1996 145

267-284

20. B.H.Davis, Comm.Am.Ceram.Soc 1984 C-186
21. B.H.Davis, R.Srinivasan and R.DeAngelis, J.Mater.Res, 1986 4 1-12
22. D.A.Powers and H.B.Gray, Inorg.Chem., 1973 12 2721
23. C.J.Norman, P.A.Goulding and I.McAlpine, Catalysis Today 1994 20 313-322
24. E.D.Whitney, J.am.Ceram.Soc, 1970 53 697
25. J.Livage, K.Doi and C.Mezieres, J.Am.Ceram.Soc 1968 51 349
26. C.J.Norman, SAE Paper 970460 1997
27. M.Yashima, K.Morimoto, N.Ishizawa, M.Yoshimura, J.Am.Ceram.Soc 1993 76 2867
28. M.Yashima, K.Morimoto, N.Ishizawa, M.Yoshimura, J.Am.Ceram.Soc 1993 76 1745
29. T.Egami, W.Dmowski, R.Brezny. SAE Paper 970461 1997
30. H.C.Yao and Y.F.Y.Yao, J.Catal 1984 86 254
31. P.Fornasiero, J.Kaspar, M.Graziani. Appl.Catal.B.Env. 1999 22 L11-L14
32. P.Vidmar, P.Fornasiero, J.Kaspar, G.Gobitosa, M.Graziani, J.Catal. 1997 171 160
33. A.S.C.Brown, J.S.J.Hargreaves, S.H.Taylor. Cat.Let. 1999 57 107-112
34. P.Fornasiero, R.D.Monte, G.R.Rao, J.Kaspar, S.Meriani, A.Trovarelli, M.Graziani. J.Catal 1995 151 168.
35. K.Park and D.R.Olander. Journal of the Electrochemical Society. 1991 vol 138 (4) 1154-1159.
36. D.Martin and D.Duprez. J.Phys.Chem. 1996 100 9429-9438
37. M.Daturi, C.Binet, S.Bernal, J.A.P.Omil, J.C.Lavalley. J.Chem.Soc.1998 94(8) 1143-1147

Chapter 4:

The Study of the Comparative Influence of Ternary Dopants on the Character of Ceria / Zirconia Mixed Oxides.

'Many hands make light work.'

Famous British phrase.

4.1: Chapter Introduction

The presence and requirement of the precious metal, support and ceria and zirconia in the catalyst have been discussed in chapters 1 and 3. Here we consider the advantages of introducing additional rare earth metals such as lanthanum, neodymium and praseodymium. The literature suggest that these may confer three benefits, namely...

- stabilisation of the alumina support (1-3)
- stabilisation of the zirconia (4-9)
- stabilisation and enhanced redox characteristics of ceria (2,3,10-19)

In chapter 3 it was shown that the physical and chemical properties of a ceria / zirconia mixed oxide were strongly dependent upon the temperature of calcination and the ratio of the respective oxide precursors. For the reasons already described, the influence of rare earth ternary additives were investigated with respect to surface area, crystallography, surface composition and reducibility of the ceria / zirconia system.

4.2: The Preparation of Zirconia / Ceria / Rare Earth Mixed Oxides

A series of zirconia based mixed oxides was prepared containing ceria (10 or 40 molar%) and one of the rare earth oxides praseodymia (Pr_6O_{11}), lanthana (La_2O_3), neodymia (Nd_2O_3) or Yttria (Y_2O_3) at a level of either 3 or 10 molar%. Sixteen materials were produced and were coded as shown in table 4.1.

The mixed oxides were prepared by the coprecipitation route, the same method previously used in chapter 3. Cerium carbonate hydrate 99.9% (Aldrich) and zirconium basic carbonate [0.13% SiO_2, 0.13% TiO_2, 0.16% SiO_2 (MEL)] powders were mixed at an appropriate ratio and added to the powder was an appropriate volume of rare earth nitrate solution shown below...

Pr nitrate solution:			19.1 g oxide obtained per 100g of solution						
Nd	"	"	21.7 g	"	"	"	"	"	
Y	"	"	18.4 g	"	"	"	"	"	
La	"	"	19.7 g	"	"	"	"	"	(MEL)

Table 4.1. Composition of prepared ternary mixed oxides

Code	Zirconia mol%	Ceria mol%	Ternary mol%	
50Z40C10P	50	40	Praeseodymia	10
57Z40C3P	57	40	Praeseodymia	3
80Z10C10P	80	10	Praeseodymia	10
87Z10C3P	87	10	Praeseodymia	3
50Z40C10N	50	40	Neodymia	10
57Z40C3N	57	40	Neodymia	3
80Z10C10N	80	10	Neodymia	10
87Z10C3N	87	10	Neodymia	3
50Z40C10L	50	40	Lanthana	10
57Z40C3L	57	40	Lanthana	3
80Z10C10L	80	10	Lanthana	10
87Z10C3L	87	10	Lanthana	3
50Z40C10Y	50	40	Yttria	10
57Z40C3Y	57	40	Yttria	3
80Z10C10Y	80	10	Yttria	10
87Z10C3Y	87	10	Yttria	3

250 ml of concentrated nitric acid and 250 ml of distilled water were mixed and added to the precursor, so that 10 g/l of the resulting oxide would be obtained from the solutions. The acid solution was constantly stirred on a stirrer at room temperature for 45 minutes. The solution was added slowly dropwise over the space of 1 ½ hours to stirring 35% ammonia solution (Philip Harris) which was rapidly stirred by the action of an overhead stirrer / glass paddle set up. Extra base was added when required for the

attainment of final pH of 10.5. Following this, 50 ml / 100 vols of hydrogen peroxide (Fisons) was added to the mixing hydroxide/base. Aging was allowed for 30 minutes.

The hydroxide was vacuum filtered and washed by the addition of copious amounts of distilled water over a period of 24 hours. The material was then dried at 110°C overnight in an oven and calcined. Calcination took place at 900°C in air for 7 hours, following a ramp rate of 10°C/min in a porcelain calcination boat placed within a Carbolite tube furnace controlled by a Eurotherm, similar to that described in Chapter 2.

4.3: Results and Discussion of the Character of the Ternary Mixed Oxides

4.3.1: The Influence of Composition on the Surface Area of the Mixed Oxide

The B.E.T. surface areas were obtained for the sixteen oxides by the method described in chapter 2. The results from this procedure are shown in figure 4.1.

Figure 4.1: Surface area as a function of zirconia content

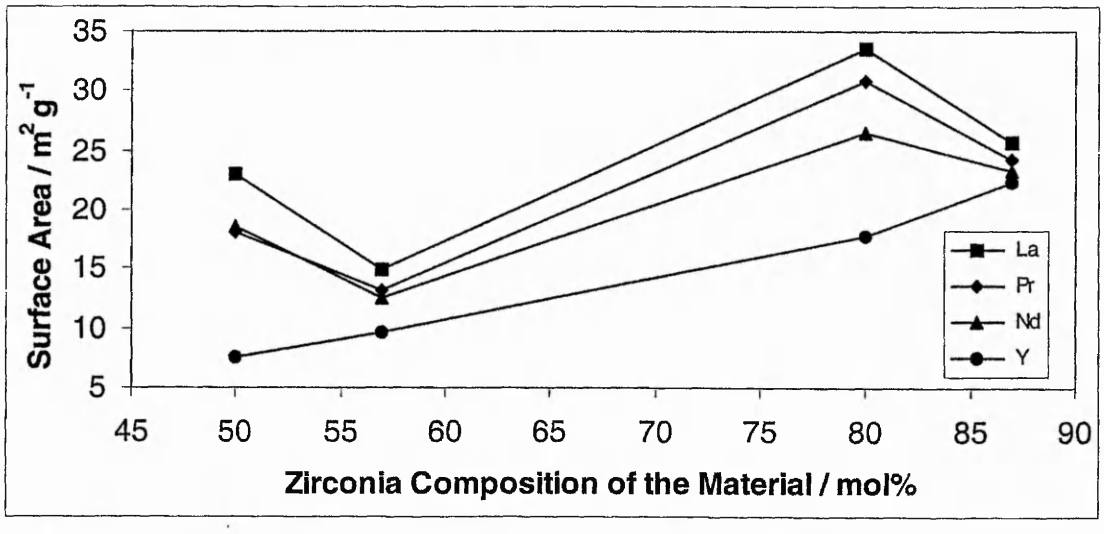

Where 50 mol% corresponds to the 50Z40C10RE, 57 mol% is 57Z40C10RE, 80 mol% is 80Z10C10RE and 87 mol% is 87Z10C3RE and where RE are the rare earths.

In chapter 3 a range of ceria / zirconia mixed oxides was produced in order to determine which key preparation variables were responsible for the character of the material. The Plackett-Burman (20) statistical approach used, applied to the coprecipitation route, meant that 8 catalysts were prepared that were calcined at 900°C. The mixed oxides containing 10 and 40 mol% ceria had surface areas which varied between 7 and 28 m^2g^{-1}, with an average of 14 m^2g^{-1}. In this chapter the addition of ternary dopants to the ceria / zirconia mixed oxide gave surface areas ranging from 8 to 34 m^2g^{-1} with an average of 21 m^2g^{-1}. A mean 50% increase in surface area is thus observed. The improvement is greater if the yttria doped samples are disregarded.

In chapter 3 it was shown that the difference in surface areas between those containing 10 and 40 mol% ceria were statistically insignificant; however in chapter 1 an 'M' shaped curve was presented showing how surface area changed with respect to the composition of the ceria / zirconia mixed oxide (21) please refer to figure 4.2. When the minor component in the mixed oxide is at approximately 15% the surface area of the mixed oxide is at a maximum. When the ceria / zirconia approaches equimolar the surface area passes through a minimum but is itself higher than the surface area of the individual components. The surface areas of zirconia based mixed oxides are greater when the ceria / rare earth component is at a level of 20 and 13% as compared to the 50 and 43%, consistent with the observations.

Figure 4.2. 'M' shaped curve of composition vs. surface area (21)

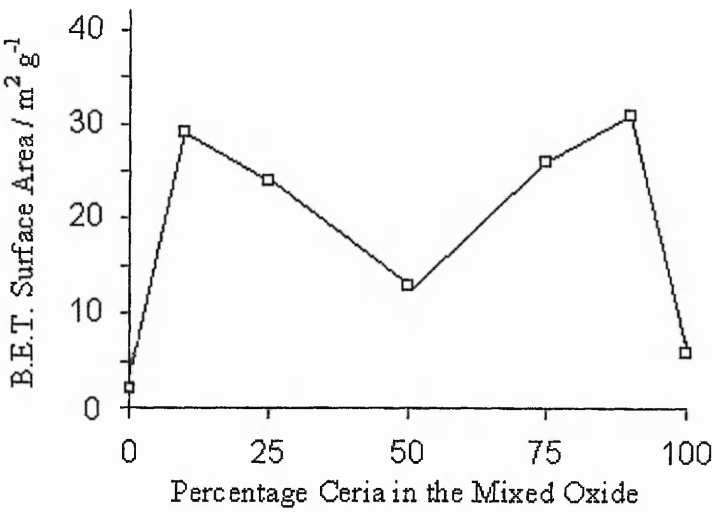

In the case of the lanthana, praseodymia, and neodymia doped mixed oxides figure 4.1. shows clear evidence for the greater stabilisation of surface area when the dopant is present at 10% rather than 3%. This is in line with a previous observation that 8 mol% lanthana was more effective in stabilising the surface area of zirconia than 4 mol% lanthana (6). The retardation of crystallisation of amorphous zirconia by the addition of lanthana and other rare earth oxides has also been reported (8) and the effect of the retardation was found to increase with increasing dopant concentration. Here there is evidence that rare earth ternaries stabilise the surface area of ceria / zirconia to a similar extent to that of zirconia alone.

The superiority of lanthana over yttria for the surface area stabilisation of zirconia alone (5,8) and for ceria alone (15, 22) has been reported and it can be clearly seen in figure 4.1. that the nature of the dopant has a strong influence on the surface area of ceria zirconia. The lanthana containing materials consistently have higher surface areas than the respective praseodymia, neodymia and yttria doped materials. As the surface area value for each material was obtained from repeated runs on the B.E.T. apparatus we are confident that the results are a true reflection of the importance of the ternary additive. Figure 4.3. relates the ionic radii of the dopants to the average surface areas where 0.893Å is the ionic radius of Y^{3+}, 0.995 = Nd^{3+}, 1.013 = Pr^{3+} and 1.061 = La^{3+}.

Figure 4.3. Ionic radii of dopant vs. surface area of material

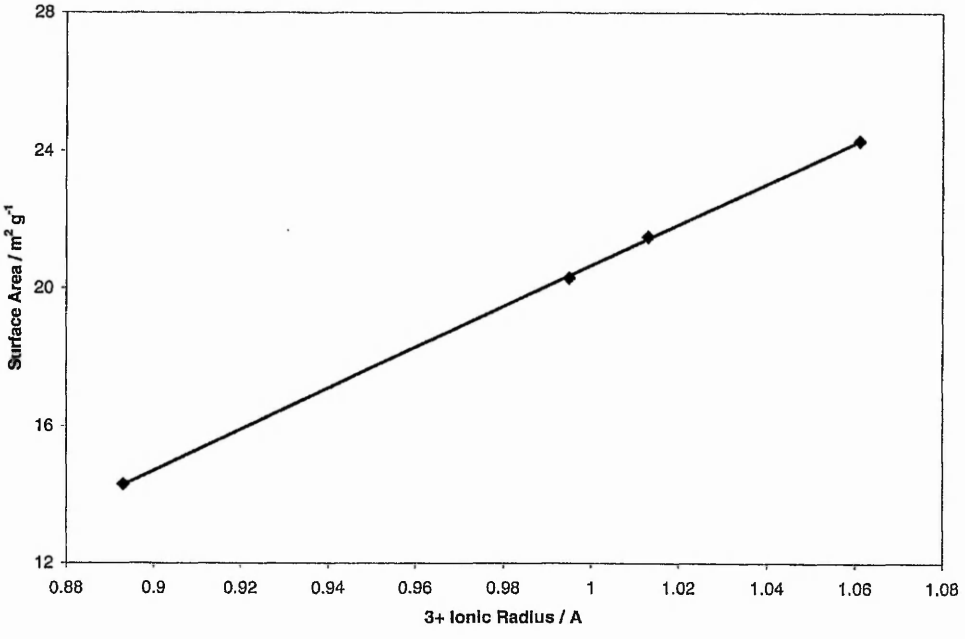

In the case of the stabilisation of zirconia it has been reported (8) that increasing the ionic radius of the rare earth metal increased retardation of crystallinity, leading to the conclusion that crystallisation of zirconia by diffusion of ions in the precursor was inhibited more greatly by doping with rare earth cations with large ionic radii. When lanthana, neodymia and yttria dopants were studied for the stabilisation of ceria (15) the same trend in surface area vs. ionic radius was observed.

Here the same surface area vs. ionic radius trend is observed, thus it can be stated that enhancement in surface area of ceria / zirconia mixed oxide is determined by the ionic radius of the rare earth ternary dopant in the same manner by which stabilisations of ceria and zirconia occur individually.

4.3.2: Crystallography Studies

X-ray diffraction studies were carried out on the sixteen ternary oxides as described in chapters 2 and 3 and figures 4.4. to 4.7. show the results. The code for the material is shown alongside each trace.

Inspection of the traces data and comparison with the JCPDS index (23) revealed no discrete phases of the rare earth oxide ternaries, suggesting formation of a solid solution of ternary additive in the ceria / zirconia mixed oxide. It is acknowledged however that the small amount of ternary additive present would make them difficult to see.

The crystallographic nature of the ceria / zirconia binary system has been much studied (24-26) and is discussed in chapter 3. With the 16 ternary oxides, no tetragonal to monoclinic zirconia phase transformation is observed, although this phase transformation was observed in a number of the binary oxide materials in chapter 3. It can be concluded that the addition of the ternaries limits the phase transformation of the zirconia component of the mixed oxide. The stabilisation effect against the phase transformation and crystallisation is believed to be the reason why higher surface areas are observed in the ternary doped materials. Inspection of the results revealed that the full width at half maximum of the major tetragonal reflection at $2\theta = 30°$ in the case of the yttria doped materials was less than the other rare earth doped systems.

Figures 4.4. The XRD traces of praeseodymia containing mixed oxides

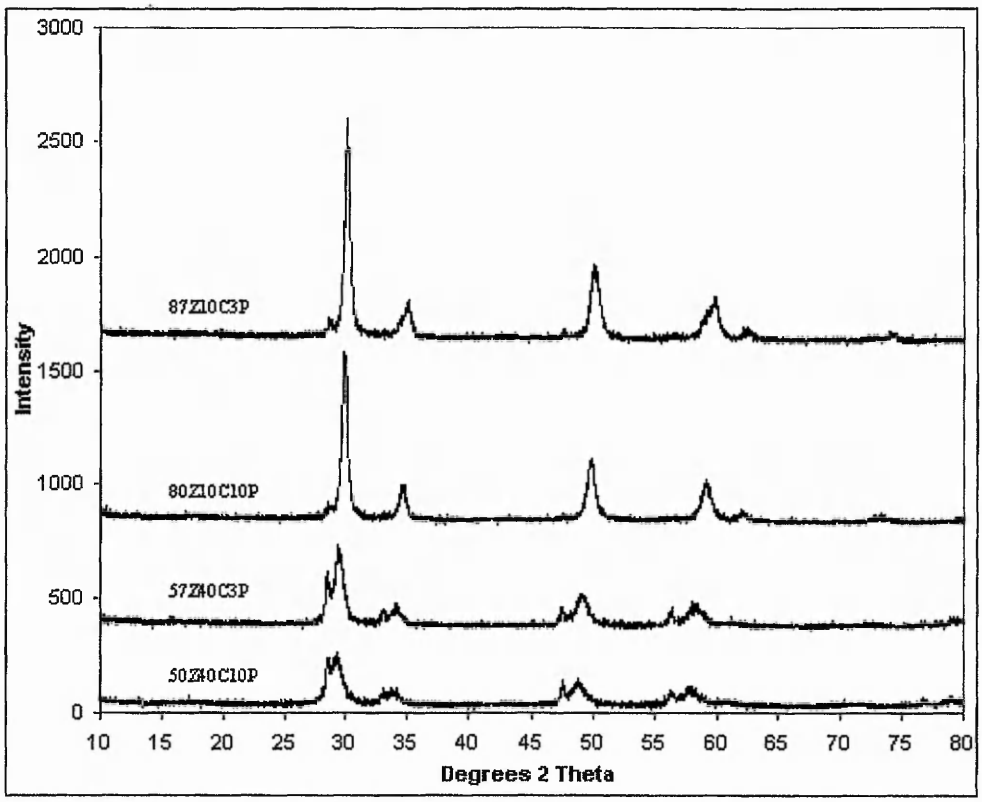

This observation is indicative of greater crystallinity in the yttria doped system and hence is the reason for the yttria doped materials having a lower surface area.

Evidence for some phase separation in all of the ternary materials studied is provided by the presence of the cubic ceria main reflection at $2\theta = 28.5°$ as well as the main tetragonal zirconia feature at $2\theta = 30°$ (25,26). Extreme conditions are known to cause this (24) and has been seen previously in yttria / ceria / zirconia mixed oxides calcined at this temperature (27). Phase separation occurred in most of the ceria / zirconia materials, calcined at 900°C, produced in chapter 3 also. In section 3.3.3. it was discussed that the presence of a solid solution of ceria in zirconia results in peak shifting. The position of the peaks are such that they are not totally independent entities as you would expect from a physical admixture of CeO_2 and ZrO_2. The peaks are closer together showing that there is still an appreciable amount of interaction between ceria and zirconia.

Figures 4.5 and 4.6. The XRD traces of neodymia and lanthana containing mixed oxides

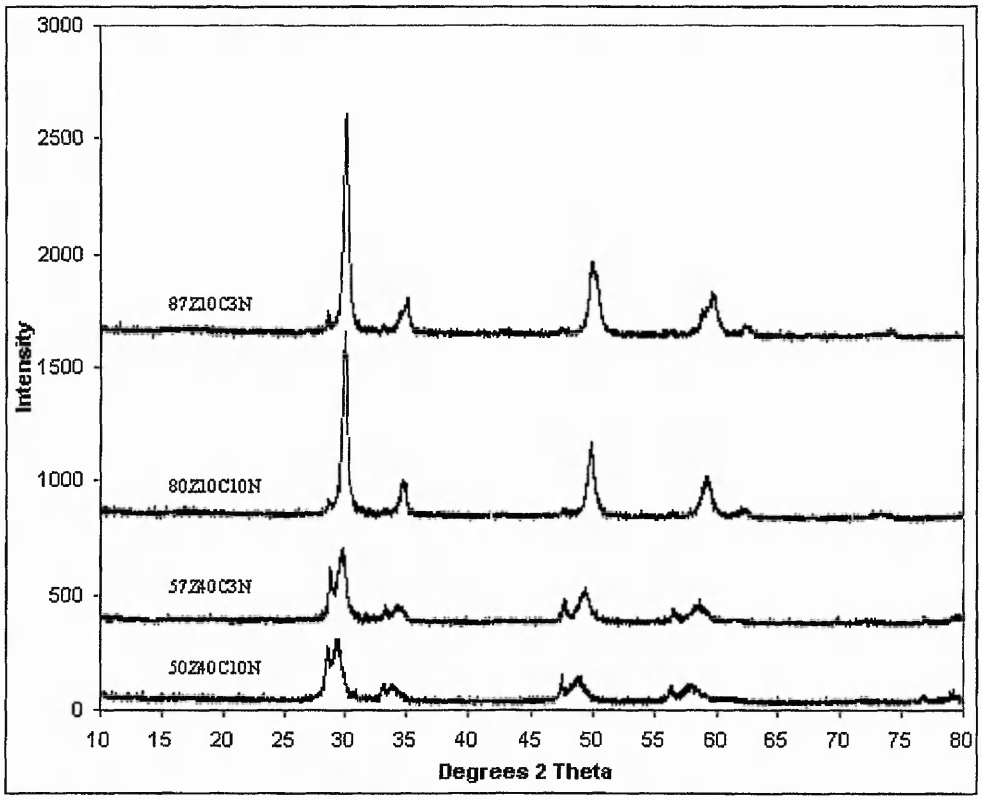

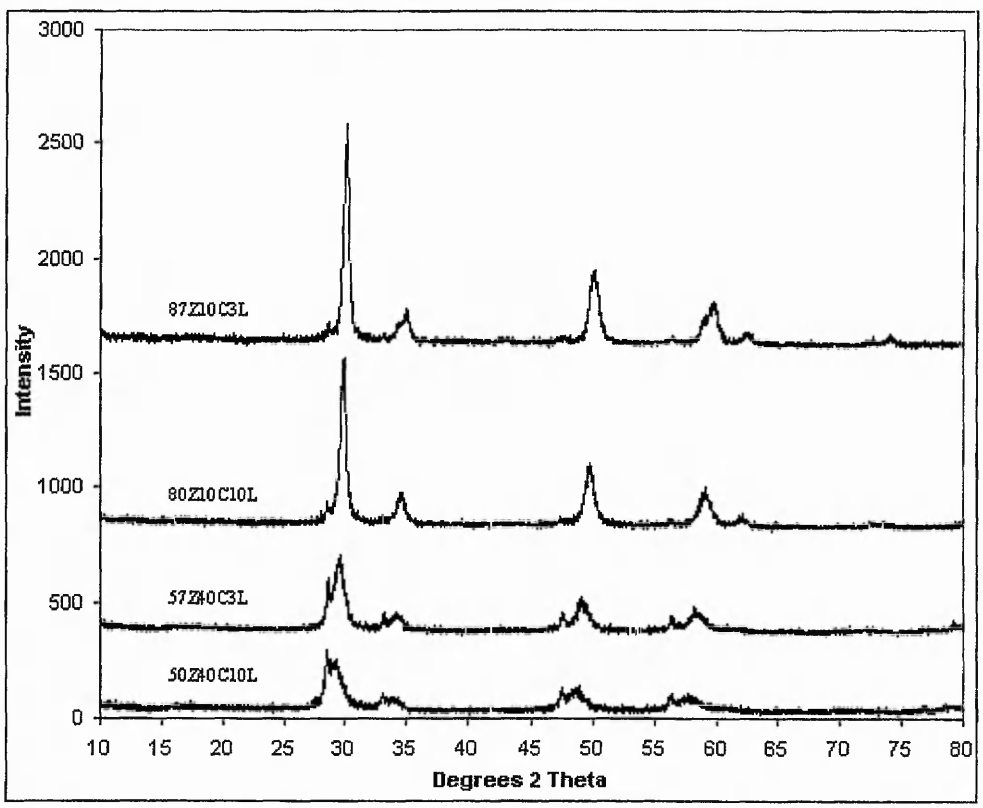

Figure 4.7. The XRD traces of the yttria containing mixed oxides

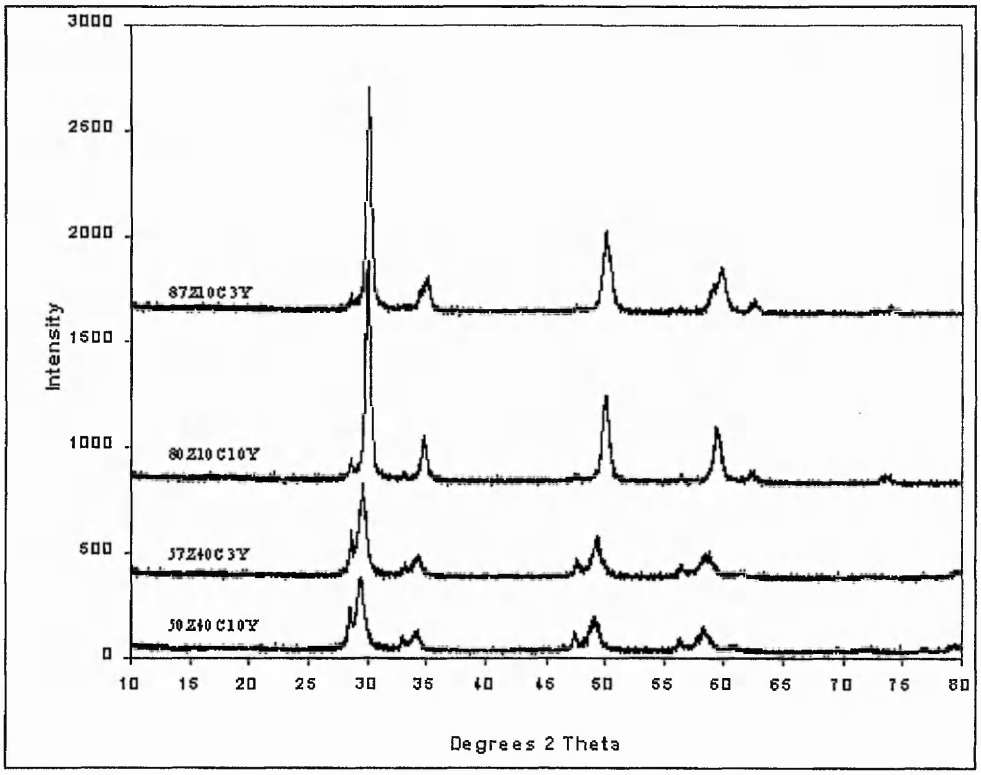

4.3.3: Surface Composition of the Ternary Doped Mixed Oxides

Previously it was reported that rare earth oxides may stabilise ceria surface area by a mechanism involved the formation of a stabiliser rich surface phase that impedes crystallisation (15). Studies using x-ray photoelectron spectroscopy (XPS) were undertaken to determine the surface composition of the mixed oxides. The peaks were identified (28) and scanned for the determination are shown in table 4.2. These are supplemental to those shown in 3.3.3. The scanning regime used was as previously described. The peaks were first identified on a broad scan and then scanning took place again to obtain a trace of the peaks of interest suitable for integration together with a good baseline. The peaks scanned were chosen on the basis of signal to noise ratio and the lack of interference from other peaks. Figure 4.8. shows typical peaks obtained.

From the method described in chapter 2.4. the surface composition of each of the sixteen materials were calculated, table 4.3. shows the results. Please note that the table shows metallic surface ratio, oxygen on the surface is neglected.

Table 4.2. Regions scanned for surface composition determination

Elemental Orbital Regions	**Range Scanned eV (binding energies)**
Pr 3d	930 - 980
Nd 3d	980 - 1035
La 3d	835 - 877
Y 3p	305 - 344

Figure 4.8. Typical XPS peaks scanned of the rare earth ternary dopants

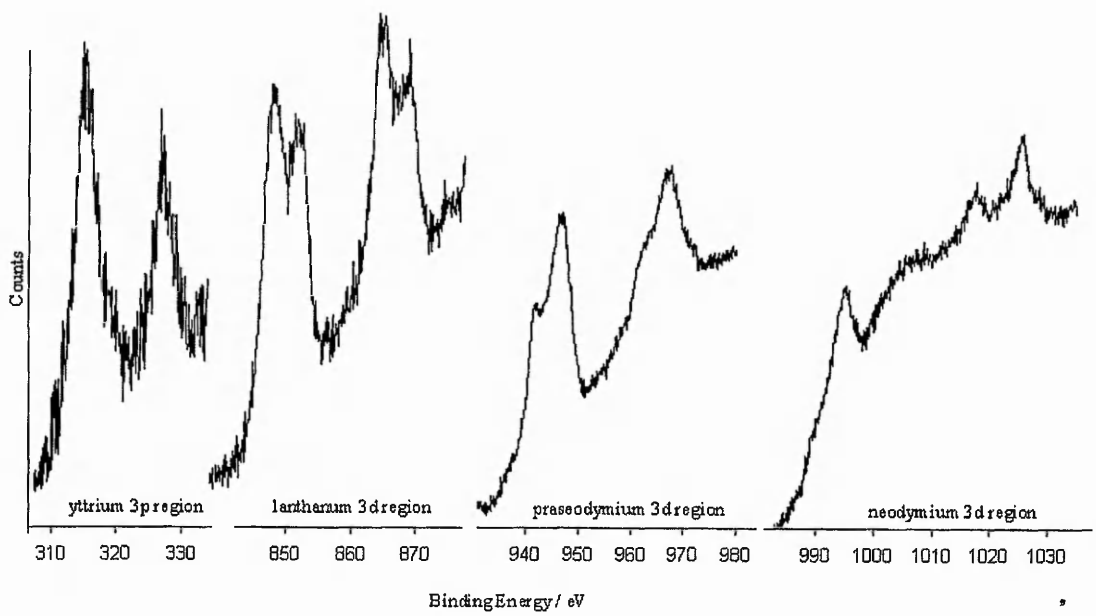

As previously seen in chapter 3, the greater the bulk component the greater the appearance of that component on the surface. Again in all cases it is seen that there is surface enrichment of ceria; and in most cases the rare earth additives also exhibit surface enrichment. From table 4.3. it can be observed that the degree of surface enrichment of the ternary is dependent upon the nature of the ternary, thus praseodymia is subject to greater surface enrichment than neodymia,lanthana, and yttria respectively.

As the method of the preparation of the materials were kept constant it can only be the different natures of the ternary additives and the interaction with the ceria / zirconia that induce the observed differences.

Table 4.3. Surface composition of ternary doped mixed oxide

Material	**Surface Composition (percentage surface metallic element)**		
	Zr	**Ce**	**R.E.**
50Z40C10P	30.0	47.2	22.8
57Z40C3P	38.6	50.2	11.2
80Z10C10P	61.0	15.0	24.0
87Z10C3P	76.9	10.8	12.3
50Z40C10N	39.8	48.2	12.0
57Z40C3N	55.0	41.3	3.7
80Z10C10N	70.9	11.6	17.6
87Z10C3N	77.7	13.2	9.1
50Z40C10L	39.7	52.2	8.2
57Z40C3L	41.9	52.0	6.1
80Z10C10L	66.9	27.3	5.8
87Z10C3L	73.7	14.3	12.0
50Z40C10Y	32.1	57.7	10.2
57Z40C3Y	43.7	50.7	5.5
80Z10C10Y	72.6	20.3	7.4
87Z10C3Y	79.6	18.1	2.4

4.3.4: Catalyst Reduction

The reducibility of the 16 catalysts were determined by temperature programmed reduction, as described in sections 2.2. and 3.3.4. Table 4.4. shows the amount of hydrogen uptake and the temperature of maximum reduction for the 16 catalysts. The degree of reduction and the temperature of maximum reduction were obtained from the curves shown in figure 4.9.

Table 4.4. Reduction characteristics of the 16 mixed oxides

Number	Material	H_2 Uptake / mol H_2 $mg^{-1}10^{-9}$	Temperature of Max Reduction / C
1	50Z40C10P	1220	610
2	57Z40C3P	1080	620
3	80Z10C10P	420	600
4	87Z10C3P	390	610
5	50Z40C10N	900	605
6	57Z40C3N	1150	610
7	80Z10C10N	450	620
8	87Z10C3N	350	635
9	50Z40C10L	990	595
10	57Z40C3L	980	610
11	80Z10C10L	440	560
12	87Z10C3L	360	620
13	50Z40C10Y	1180	640
14	57Z40C3Y	1040	625
15	80Z10C10Y	440	625
16	87Z10C3Y	370	625

Fig.4.9. The TPR traces of the 16 rare earth containing mixed oxides

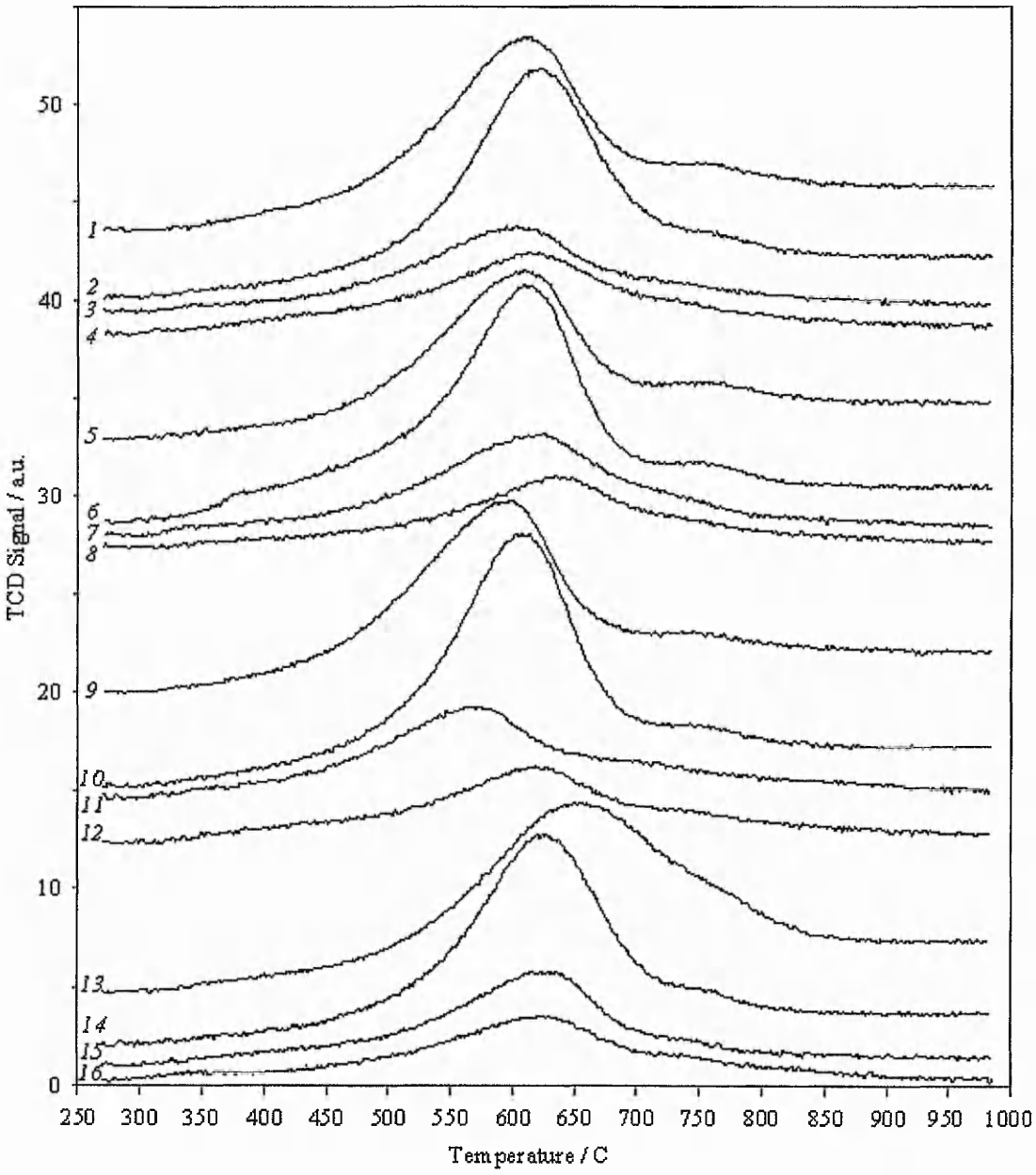

In chapter 3 it was shown that for ceria / zirconia mixed oxides the temperature of maximum reduction was lower when the surface area of the sample was higher. In section 4.3.1. the nature of the dopant was shown to strongly influence the surface area of the mixed oxide. Higher surface areas are obtained following the trend...

$$La > Pr > Nd > Y$$

The following trend for the temperature of maximum reduction is observed...

$$La\ (596°C) < Pr\ (610°C) < Nd\ (618°C) < Y\ (629°C)$$

Figure 4.10. compares the ionic radii of the dopants to the average surface areas and reduction temperatures.

Figure 4.10. Chart showing relationship between surface area, reduction temperature and dopant nature

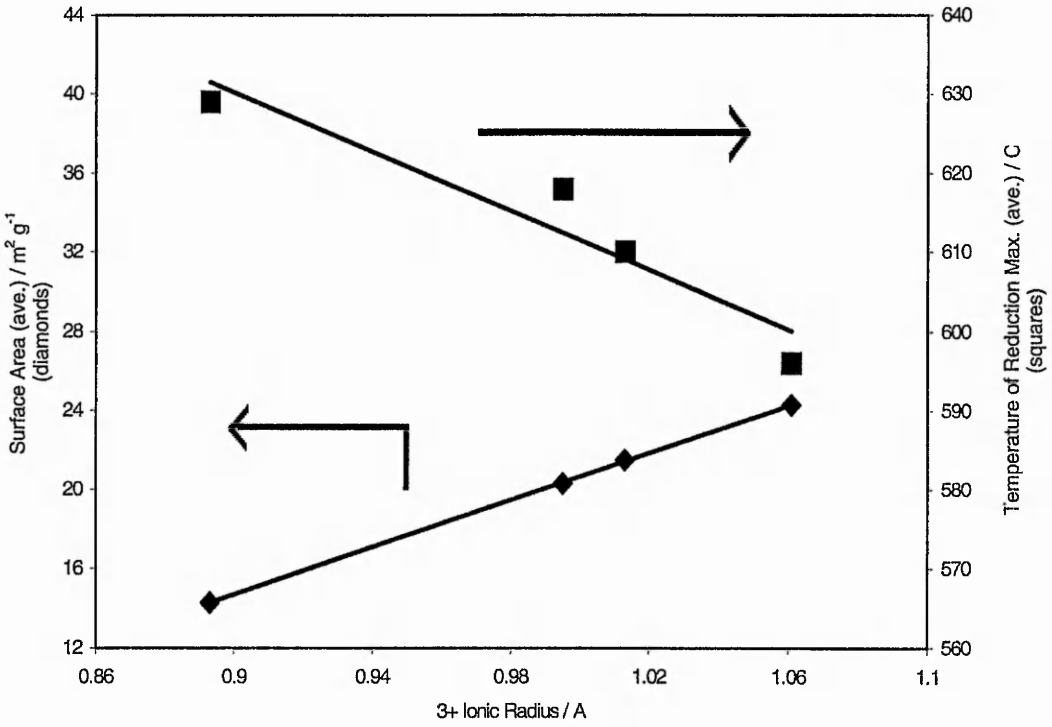

The materials reduce at lower temperatures when the ternary additive is at 10% than when at 3% in all cases except yttria. The peak reducing temperatures are generally lower than previously seen for the binary oxides of chapter 3. The lowest peak reducing temperature is displayed by the 80Z10C10L oxide. The high surface area, high amount of trivalent dopant and the nature of the dopant account for this occurrence.

No clear trend is observed with the temperature of peak reduction when the ceria levels are at either 10 or 40 mol%, which concurs with observations made in chapter 3.

The temperature of reduction seems to be clearly linked to the surface areas of the materials, as shown in figure 4.10.; the total reducibility is not however, neither is it linked to the ratio of ceria to zirconia. In all of the materials produced in this chapter the degree of total reducibility (hydrogen uptake) is increased, compared to those produced in chapter 3. Based on the average reducibility of the mixed oxides for each dopant class the influence of the rare earths are as follows...

$$Pr\ (7.8x10^{-7} molH_2mg^{-1}) > Y\ (7.6) > Nd\ (7.1) > La\ (6.9) > No\ Dopant\ (5.6)$$

It is unsurprising why the praseodymia doped mixed oxides can take up more hydrogen. Pr_2O_3 have been shown to produce oxygen vacancies when doped in ceria (IV), aiding reduction, and if the praseodymia present in the form Pr_6O_{11} this will itself reduce and take up hydrogen (13,14). The yttria doped oxides, although having poor crystal structure and low surface area have a large hydrogen take up. This must be solely attributed to the interaction of the dopant with ceria forming oxygen vacancies which aid reduction (10-12). The poor performance of the lanthana doped systems however is surprising.

4.4: Conclusions

Sixteen rare earth oxide doped ceria / zirconia materials were produced by coprecipitation and calcination at 900°C. The influence of the lanthana, yttria, praeseodymia and neodymia dopants was investigated by examining the crystallographic, reduction, surface composition and surface area characteristics of the ternary mixed oxides. A number of conclusions on the influence of the ternary additives can be stated.

- Of the ternary oxides, other than those containing yttria, the surface areas are superior to the binary ceria / zirconia mixed oxides previously prepared.
  Dopants at levels of 10mol% offered greater stabilisation of surface area.
  Enhancement of surface area was seen to be greatest with lanthana and the worst with yttria and this can be related to the ionic radius of the dopants.

- No discrete rare earth dopant phases were observed by XRD, indicative of formation of solid solutions of dopants in either ceria or zirconia. Phase separation of the ceria and zirconia were observed in all cases, thus it can be stated that the ternary rare earth oxides offer no benefit in the formation of solid solutions of ceria and zirconia. Although phase separation is observed it is concluded that an appreciable amount of interaction between CeO_2 and ZrO_2 is still present.

- Enhanced reduction characteristics are observed with the presence of dopants. The temperature of maximum reduction is related to surface area. The higher the surface area the lower the reduction temperature. The amount of reduction is dependent upon the reducibility of the dopant and the ability of the dopant to promote reduction in the ceria component.

4.5: References

1. D.Beguin, E.Garbowski, P.Primet. J.Catal. 1991 127 595
2. G.W.Graham, P.J.Schmitz, R.K.Usmen, R.W.McCabe. Cat.Lett. 1993 17 175-185
3. R.K.Usmen, G.W.Graham,W.L.H.Watkins, R.W.McCabe. Cat.Lett. 1995 30 53-63
4. T.H.Etsell, S.N.Flengas. Chem.Rev. 1970 70 339
5. P.D.L.Mercera PhD Thesis University of Twente 1991
6. R.Franklin, P.Goulding, J.Haviland, R.W.Joyner, I.McAlpine, P.Moles, C.Norman, T.Nowell. Catal.Today. 1991 10 405
7. M.Keenan. PhD Thesis. The Nottingham Trent University. 1996
8. M.Ozawa and M.Kimura. J.Less.Comm.Metals. 1991 171 195
9. C.K.Loong J.W.Richardson, M.Ozawa. J.Catal. 1995 157 636
10. S.Bernal, G.Blanco, M.A.Cauqui, G.A.Cifredo, J.M.Pintado, J.M.R.Izquierdo. Cat.Letters. 1998 53 51-57
11. S.Bernal, G.Blanco, M.A.Cauqui, G.A.Cifredo, J.M.Pintado and J.M.R.Izquierdo. J.Alloys and Comp. 1997 250 449-454
12. W.M.O'Neill, M.A.Morris. Chem.Phys.Lett. 1999 305 389-394.
13. M.Y.Sinev, G.W.Graham, L.P.Haack, M.Shelef. J.Mater.Res. 1996 11 8 1960-1971
14. A.D.Logan, M.Shelef, J.Mater.Res. 1994 9 2 468-475
15. J.E.Kubsh, J.S.Rieck, N.D.Spencer. CAPOCII. Ed. A.Crucq. Elsevier, Amsterdam. 1991 125-138
16. M.Pijolet, M.Prin, M.Soustelle, O.Touret, P.Nortier. J.Chem.Soc.Faraday.Trans. 1995 91 21 3941-3948
17. M.Pijolat, M.Prin, M.Soustelle, O.Touret ,P.Nortier. Solid State Ionics 1993 63 781
18. M.Pijolat, M.Prin, M.Soustelle, O.Touret ,P.Nortier.CAPOC3. Elsevier Science Publications 1995 325
19. S.B.Adler, J.W.Smith. J.Chem.Soc.Faraday.Trans. 1993 89 16 3123-3128
20. R.L.Plackett, J.P.Burman. Biometrica 1946 34 255-272
21. T.Yamada, T.Kobayashi, K.Kayano, M.Funabiki. SAE Paper 970466
22. K.Kushihashi, K.Maruya, K.Domen, T.Onishi. J.Chem.Soc.Chem.Comm.1992 259

23. Joint Committee on Powder Diffraction Standards File Cards. Y_2O_3 (25-1200 and 43-1036), La_2O_3 (5-602), Nd_2O_3 (6-408, 43-1023, 21-579 and 41-1089), NdO (33-937), Nd_6O_{11} (45-87), PrO_2 (24-1006), Pr_6O_{11} (42-1121) and $PrO_{1.83}$ (6-329)
24. C.J.Norman, SAE Paper 970460 1997
25. M.Yashima, K.Morimoto, N.Ishizawa, M.Yoshimura, J.Am.Ceram.Soc 1993 76 2867
26. M.Yashima, K.Morimoto, N.Ishizawa, M.Yoshimura, J.Am.Ceram.Soc 1993 76 1745
27. O.A.Kirichenko, G.W.Graham, W.Chun, R.W.McCabe. Stud.Surf.Sci.Catal. 1998 411-420
28. Y.Uwamino, T.Ihizuka, H.Yamatera. J.Elect.Spec.Relat.Phenom. 1984 34 67-97

Chapter 5:

The Influence of Supports on the De-NOx Capabilities of Rhodium Catalysts.

'CeO_2 is good!'

Robert McCabe 1997

5.1: Introduction

The aim of this chapter is to report how the activity of rhodium, in the catalytic action of nitric and nitrous oxide removal, is influenced by its zirconia based support.

Many investigations have been undertaken to determine both the kinetics and mechanism of the CO + NO reaction on rhodium. Studies have dealt with adsorption and desorption of the components of the reaction and have taken place on both single crystal and polycrystalline surfaces (1-7).

The reaction mechanism (2,7) is shown below, where ads = adsorbed. It can been seen that N_2 and N_2O are formed by a common path.

$$CO_{(gas)} \rightarrow CO_{(ads)}$$

$$NO_{(gas)} \rightarrow NO_{(ads)}$$

$$NO_{(ads)} \rightarrow N_{(ads)} + O_{(ads)}$$

$$NO_{(ads)} + N_{(ads)} \rightarrow N_{2\,(gas)} + O_{(ads)}$$

$$2N_{(ads)} \rightarrow N_{2\,(gas)}$$

$$CO_{(ads)} + O_{(ads)} \rightarrow CO_{2\,(gas)}$$

$$NO_{(ads)} + N_{(ads)} \rightarrow N_2O_{(gas)}$$

$$N_2O_{(gas)} \rightarrow N_{2\,(gas)} + O_{(ads)}$$

At temperatures above 275°C it is believed that any N_2O produced is immediately reacted with CO. CO_2 and N_2 are the only detectable products (7), yet the statement that the N_2O-CO reaction is an important step in the CO-NO reaction (7-9) has been questioned (10).

Nitrous oxide is kinetically stable at room temperature, decomposing homogeneously into its elements only above 650°C, with an activation energy of 260 kJ mol^{-1} (11,12)...

$$2N_2O \rightarrow 2N_2 + O_2$$

The active centre for N_2O decomposition is generally accepted as a charge donating site with the mechanism shown thus (11,12)...

$$N_2O_{(g)} + e^- \rightarrow N_2O^-_{(ads)}$$

$$N_2O^-_{(ads)} \rightarrow N_{2(g)} + O^-_{(ads)}$$

$$O^-_{(ads)} \rightarrow \tfrac{1}{2}O_{2(g)} + e^-$$

or $$N_2O_{(g)} + O^-_{(ads)} \rightarrow N_{2(g)} + O_{2(g)} + e^-$$

Rhodium Oxide (Rh_2O_3) (13), has been shown to be an excellent catalyst for the decomposition of nitrous oxide.

The presence of reducing gases / agents further aids N_2O destruction in the presence or absence of a catalyst (14) thus...

$$N_2O + CO \rightarrow N_2 + CO_2$$

$$2N_2O + C \rightarrow 2N_2 + CO_2$$

$$N_2O + NO \rightarrow N_2 + NO_2$$

$$N_2O + SO_2 \rightarrow N_2 + SO_3$$

Most catalysts are thermally unstable in the high surface area form in which they need to be used, and so are prepared as small particles on supports such as silica and alumina (15). Rhodium is no exception in the field of automotive catalysis and high surface area γ-alumina was the support of choice in the early days of TWC technology (2).

The interaction between rhodium particles and a γ-alumina support has been investigated with regards to the adsorption of NO (16). The metal-support interface was shown to be a site for NO dissociative adsorption, indicating that the interaction between the support and metal is of importance to the catalytic nature of the material. The loading and particle size distribution of rhodium on the support have also been shown to be important to the activity of the catalyst for the CO-NO reaction (2,17-19). It has been shown in this literature that increasing the loading of rhodium on alumina from 0.46 to 11.21% increases the rhodium particle size, decreases rhodium dispersion (percentage of rhodium exposed) and has a beneficial effect on the turnover frequency

and light off temperature (50% conversion). The benefit to turnover number may be a result of enhanced support / metal interaction. Figure 5.1. shows the relationships (17).

Figure 5.1. The relationships between rhodium loading, particle size, dispersion, turnover number and light off temperature of Rh / Al_2O_3 in the CO-NO reaction

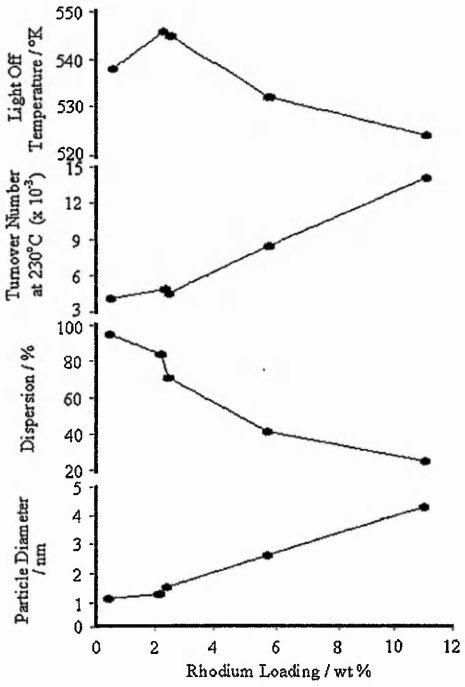

The manner in which the catalyst is treated may severely affect the physical characteristics. Rhodium dispersion is influenced at high temperature in oxidising conditions. In such conditions rhodium is rapidly oxidised resulting in dissolution into the support, resulting in a decrease in the amount of surface rhodium present. The higher the temperature, the more rapid the process. Upon reduction of the catalyst only partial recovery is attained and the rhodium is present as sintered particles (20,21).

Both NO and CO influence the nature of supported rhodium, at temperatures as low as 300°C (22). Figure 5.2. shows a schematic diagram of the microstuctural changes of Rh in NO, CO, NO and CO and H_2. After heating at 600°C in hydrogen metallic rhodium particles are formed. NO disperses rhodium into small particles on

alumina and on silica forms a rhodium film around the particles. CO, which has little effect on its own, but when subject to rhodium previously introduced to NO volatilizes the rhodium film on Rh / SiO_2 and causes sintering of the smaller particles on Rh / Al_2O_3 into the original particles. NO and CO together cause the complete loss of rhodium on silica.

Figure 5.2. Schematic diagram of the structural changes of rhodium on silica and alumina (22)

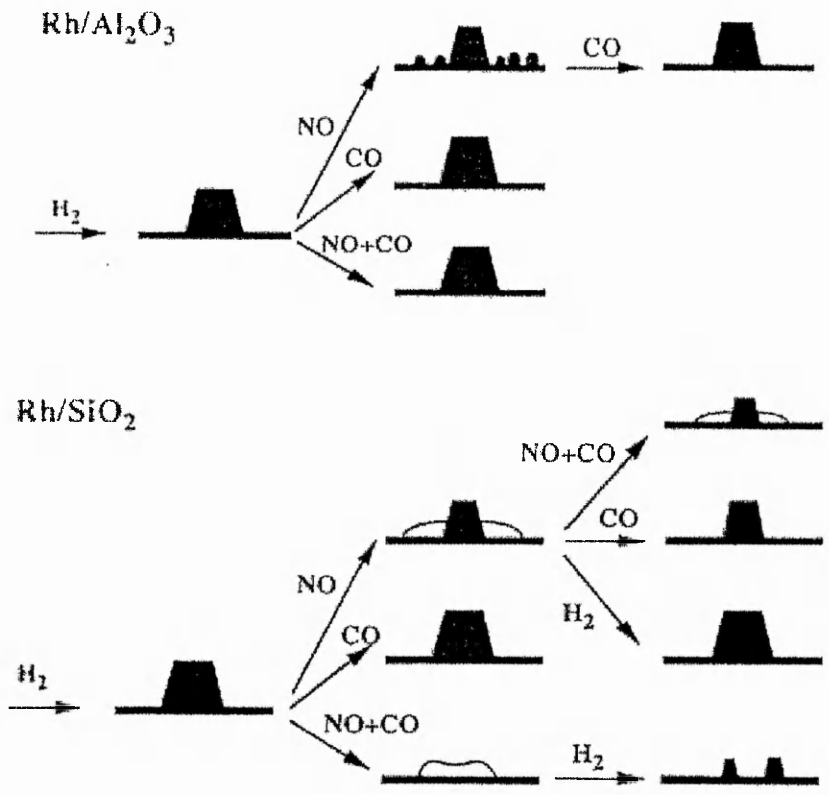

The introduction of zirconia into the washcoat favours the formation of Rh – O – Zr bonds, retarding agglomeration of rhodium and improving the thermal stability of the support, maintaining catalytic activity (23-27). Figure 5.3. shows how zirconia addition aids the maintenance of rhodium surface area on γ - alumina.

Figure 5.3. Zirconia and the retardation of rhodium agglomeration on γ - alumina (23)

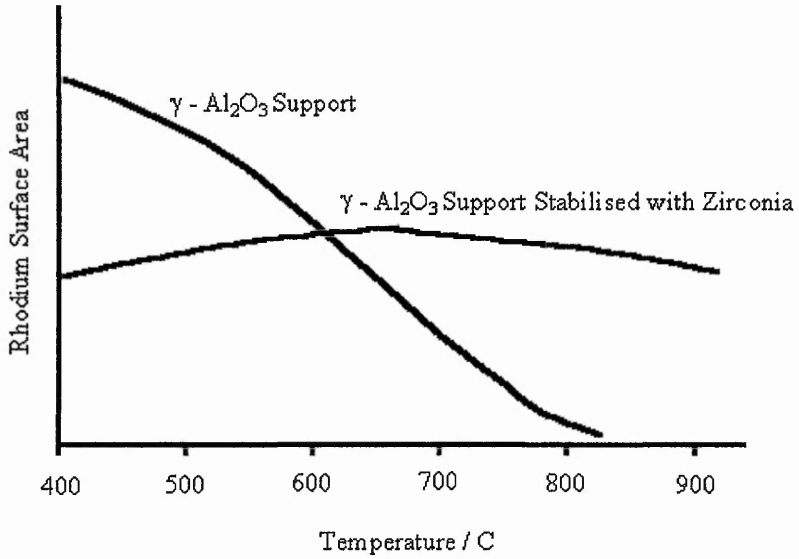

Ceria addition is also beneficial to a supported rhodium catalyst in reducing conditions, and when in contact with NO and CO (22,28,29). The introduction of ceria into the Rh / Al_2O_3 catalysts system in oxidizing conditions results in the formation of Rh^+ - O - Ce or $[Rh\text{-}O_2]^{2-}$ species (28,30) which improve the degree of metal dispersion (31). Ceria also increases the mechanical strength of alumina and prevents surface area loss (32,33).

Ceria, as well as aiding in the stabilisation of rhodium in conditions frequently encountered in three-way catalysis, could actually promote the CO-NO reaction, as shown in figure 5.4. (33). The square represents an oxygen vacancy associated with reduced ceria and adjacent to the rhodium that is suggested as the promoting influence. Reduced ceria can allow excess oxygen from the metal to 'spill over' allowing further NO decomposition.

Figure 5.4. Interaction between ceria, rhodium, CO and NO

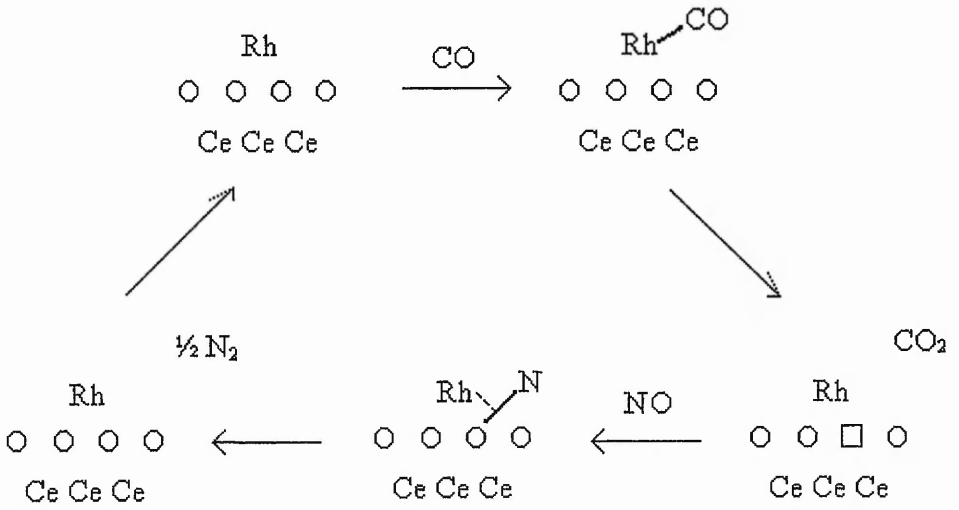

Bulk oxygen vacancies in the reduced ceria / zirconia mixed oxide are implicated in further enhancing NO decomposition by the promotion of the oxygen vacancy gradient (34-36). Figure 5.5. shows the importance of reduction of the support prior to being subject to NO at 200°C.

Figure 5.5. Conversion of NO vs. time over reduced $Ce.Zr.O_2$ catalysts (34-36)

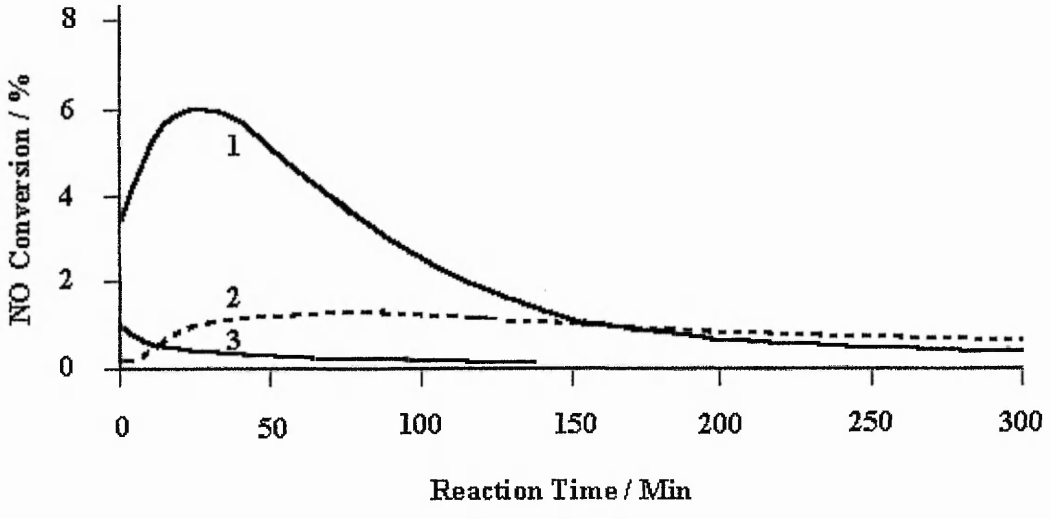

Where, 1 = Rh / $Ce_{0.6}Zr_{0.4}O_2$ prereduced in H_2 at 400°C, 2 = $Ce_{0.6}Zr_{0.4}O_2$ prereduced in H_2 at 800°C and 3 = Rh / $Ce_{0.6}Zr_{0.4}O_2$ prereduced in H_2 at 200°C.

The severe reduction procedure applied to catalyst 2 causes a great deal of bulk reduction and hence the formation of a large amount of bulk oxygen vacancies. The catalyst, in the absence of rhodium, is able catalyze an appreciable amount of NO for an appreciable amount of time. The enhancement observed when a $Rh/Ce.Zr.O_2$ is reduced at a higher temperature is self-evident.

As previously discussed in chapter 1(34-38), ceria is readily reduced by CO. In a CO rich environment, support reduction will occur yielding CO_2 as shown below...

$$xCO + CeO_2 \rightarrow xCO_2 + CeO_{2-x} \qquad (where\ x = 0 - 0.5)$$

In this chapter I report a number of studies of NO reduction by CO, using rhodium catalysts prepared on a range of supports, and studied under varying conditions. These are:-

(1) an investigation into the effect of rhodium concentration using a temperature ramping procedure to study NO reduction over $Rh / Zr_{0.6}Ce_{0.4}O_2$ catalysts.
This study was undertaken in order to determine the sensitivity of the performance of simple $Rh/CeO_2/ZrO_2$ catalysts to rhodium loading, and hence to allow the choice of a standard rhodium loading for the remaining experiments. The ramping conditions were used so as to mimic the fluctuating temperatures in the TWC.

(2) a study of the reaction involving a ramping procedure over the four ceria / zirconia support types prepared in chapter 3.
This study was undertaken in order to determine the influence of the support on the reaction in fluctuating temperatures.

(3) a study in which the catalyst is first held at 400°C for 4 hours in the reducing gas stream and then cooled to 60% NO conversion, maintained for 3 hours...
   (a) over the four material types prepared and characterised in chapter 3.
   (b) over eight ternary ceria / zirconia / rare earth oxide materials containing 40mol% ceria calcined at 900°C, prepared and characterised in chapter 4.

This study was undertaken in order to ensure that all ceria in the catalyst was in the form Ce^{3+} and to determine the influence of the support at constant temperatures where both NO and N_2O are formed.

In addition a study of nitrous oxide decomposition over the eight rare earth containing supports described above, doped with rhodium, along with eight Rh / ZrO_2 catalysts, the preparation and characterisation of which are described in this chapter, has been carried out. This was done in order to determine the influence of the support in aiding N_2O decomposition in the absence of a reductant, at temperatures where N_2O would be formed in the CO-NO reaction.

5.2: Method

5.2.1: Catalyst Preparation

The preparation of coprecipitated and deposited rhodium / zirconia catalysts

Eight 1wt%-Rh / ZrO_2 catalysts were prepared. Half of the catalysts had rhodium incorporated into the zirconia by the coprecipitation route. The remainder were made by introducing rhodium by the incipient wetness approach.

Zirconium basic carbonate (MEL) was dissolved in concentrated nitric acid (150ml) and distilled water (100ml), with or without the addition of rhodium nitrate (Johnson Matthey), so that 3g of the oxide was obtained from the acid solution. The solution was stirred under the dropwise addition of 35% ammonia solution (Philip Harris) until a pH of 10.0 was achieved. Following this, the catalyst precursors were washed under vacuum filtration, dried in an oven at 110°C for 24 hrs and calcined for 4 hours at 500°C, 650°C, 800°C and 950°C.

In the cases of oxides not already containing rhodium the incipient wetness approach of adding rhodium nitrate to the calcined zirconia, drying and re-calcining at 500°C for 4 hours was undertaken.

Incipient wetness addition

Rhodium nitrate solution (Johnson Matthey, [assay = 13.8%]) was diluted with distilled water and added to 1.5g of the four types of ceria / zirconia supports discussed in chapter 3 (500/10, 900/10, 500/40 and 900/40) so that catalysts of 1wt% rhodium were obtained. This procedure was repeated for the rare earth containing materials discussed in chapter 4 (containing 40 mol% ceria and calcined at 900°C). The solid and solutions were mixed and allowed to dry at 110°C for 1 hr. The dried mixtures were then calcined at 500°C for 4 hrs. For the investigation into the influence of rhodium content, catalysts containing respectively 0.5%, 1.0% and 3% weight of rhodium were prepared.

5.2.2: Catalyst Characterisation

No further characterisation was undertaken on the supports discussed in chapters 3 and 4 when impregnated with rhodium.

The zirconia support and the coprecipitated rhodium / zirconia were characterised by x-ray diffraction and surface area determination, as discussed in chapters 2 and 3.

5.2.3: Catalyst Testing

The testing was carried out on the microreactor described in chapter 2.

The powders were granulated (0.6 - 1 mm). The granules were loaded into the reactor tube, with a 0.5 ml bed volume, 0.6g. In all cases a gas stream flow rate of 300 ml min^{-1}, giving a GHSV of 36,000 h^{-1}, was used. All materials were pretreated under 300 ml min^{-1} of helium at 500°C for 1 hr and then cooled. The gas composition was 0.2% (0.6 ml) NO, 2% (6 ml) CO and 97.8% (293.4 ml) He.

Influence of Rhodium Level on the CO-NO Reaction

A ceria (40%)-zirconia mixed oxide that had been calcined at 900°C was loaded with varying amounts of rhodium. This support material is designated No.14 in chapter 3.

The selectivity of the reaction to N_2, rather to N_2O formation, was calculated by the equation...

$$\text{Selectivity} = \frac{N_2 \text{ formed}}{N_2 \text{ and } N_2O \text{ formed}} \times 100\%$$

Influence of the Support to the CO – NO Reaction

The importance of the support was investigated by comparison of four types of support doped with 1 wt% rhodium. The supports were ceria (40%)-zirconia mixed oxides that had been calcined at 900°C and 500°C, designated as numbers 12 and 5 respectively in chapter 3, and ceria (10%)-zirconia mixed oxides that had been calcined at 900°C and 500°C, designated as numbers 15 and 11 respectively in chapter 3.

Selectivity to N_2 formation was calculated by the equation shown above.

Investigation of 60% NO Reduction over a Reduced Support

The investigation was undertaken using the twelve catalysts prepared by the incipient wetness addition of rhodium previously described. Selectivity to N_2 formation was calculated by the equation shown above.

Nitrous Oxide Decomposition

The catalysts investigated were the rare earth materials, supporting rhodium added by the incipient wetness method and the eight 1wt%-Rh / ZrO_2 catalysts prepared by coprecipitation and deposition.

Nitrous oxide (1.04% in helium) was passed over the materials at 300 $mlmin^{-1}$, with the temperature ramping down from 400°C to 150°C at 50°C intervals. At each temperature duplicate measurements were made, reported figures are accurate to +/- 1%.

5.3: Results and Discussion

5.3.1: Characterisation of Zirconia Supports and Coprecipitated Rh / ZrO_2

As mentioned in chapter 1, zirconia can occur as a number of different phases. The ones of consideration here are the tetragonal and monoclinic. Figure 5.6. shows the XRD traces of three of the zirconia materials, the preparation of which were discussed in section 5.2.1.

The rhodium containing zirconia calcined at 500°C is purely tetragonal, exhibiting a single line at *circa* $2\theta = 30.4°$, the tetragonal 111 line. The materials calcined at 950°C contain both tetragonal and monoclinic forms. They contain the distinctive tetragonal 111 line, and the monoclinic 111 and –111 lines at *circa* $2\theta = 28.5$ and 31.5° respectively.

The determination of phase composition of each sample is achieved by relating the relative intensities of the tetragonal, 111 line, and the two monoclinic lines, 111 and –111, to the two equations equ.5.1. and equ.5.2. The volume fraction (V_m) of the monoclinic phase is calculated from the integrated intensity ratio X_m (39).

$$X_m = \frac{I_m(-111) + I_m(111)}{I_m(-111) + I_m(111) + I_t(111)} \qquad \text{equ.5.1.}$$

$$V_m = \frac{PX_m}{1 + (P-1)X_m} \qquad \text{equ.5.2.}$$

where P is a constant of value 1.31 and I_t and I_m refer to the intensities of the tetragonal and monoclinic lines.

Fig 5.6. XRD patterns showing the stabilizing effect of rhodium

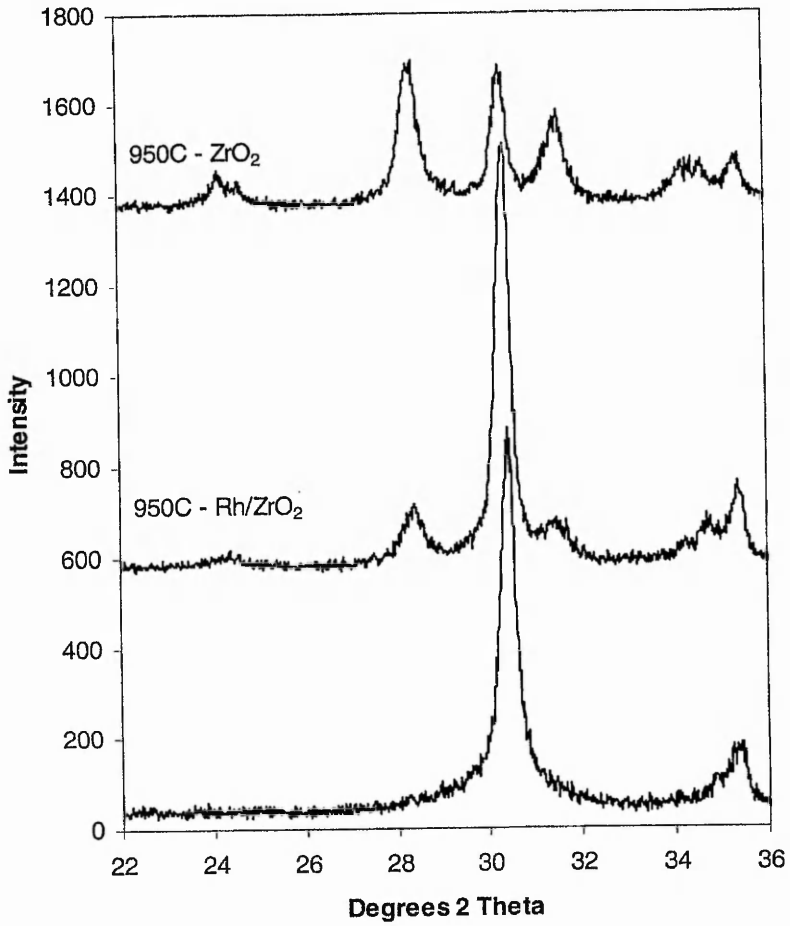

Figure 5.7. shows the values of the surface areas and percentage monoclinic volumes for the 8 prepared materials, where RZCP stands for the rhodium / zirconia coprecipitated sample.

In chapter 4 the investigation into the role of rare earth oxides in the stabilisation of surface area of zirconia was discussed. Numerous other dopants have been investigated with regards to zirconia stabilisation (40,41). This section provides clear evidence for the stabilisation of the tetragonal structure and the surface area of zirconia by 1% rhodium by comparison of the surface areas and tetragonal to monoclinic percentage to undoped zirconia. From figures 5.6. and 5.7. it is seen that the onset of the

transformation to the monoclinic phase has begun at 500°C for the undoped zirconia, yet the rhodium coprecipitated mixed oxide is perfectly tetragonal. From figure 5.7. it can be seen that at temperatures 650 and 800°C there is clear tetragonal and surface area stabilisation, imparted by the rhodium. At 950°C, although the surface areas for both samples are very low, it can be clearly seen in fig.5.6. that doping with only 1% rhodium dramatically reduces the tetragonal to monoclinic phase change.

Figure 5.7. Surface areas and monoclinic volumes of the zirconia and rhodium / zirconia materials

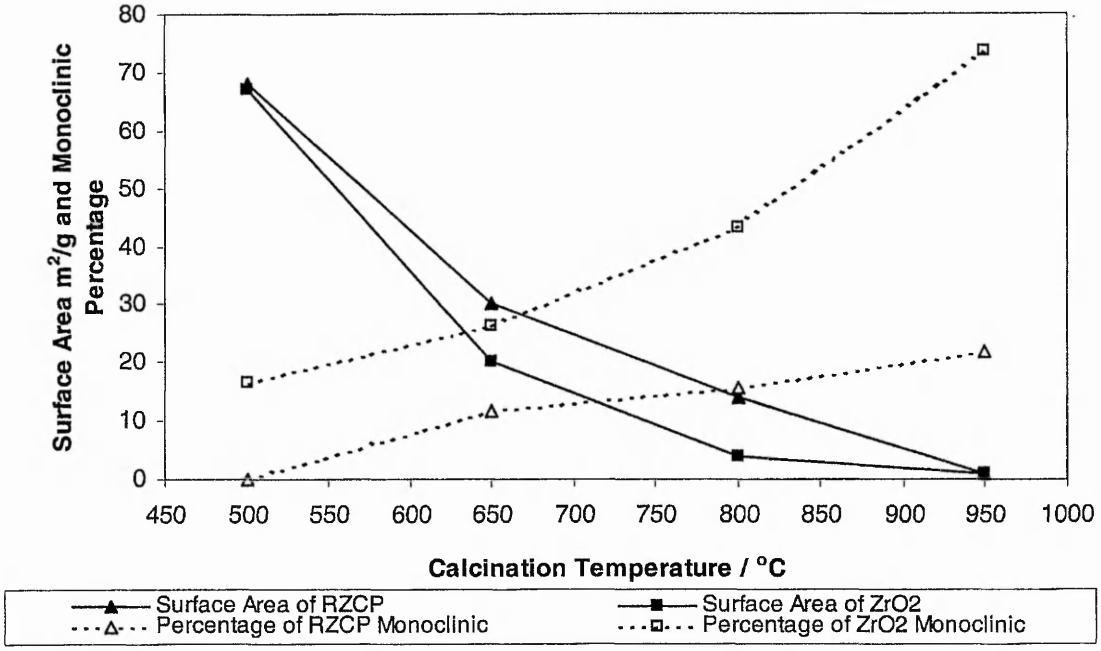

The presence of a rhodium dopant has previously been shown to modify the properties of zirconia (42). A zirconia aerogel produced by a sol-gel route and calcined at 450°C in air, containing 2 mol% rhodium, was tetragonal and had a surface area of 208 m^2g^{-1} as compared to the monoclinic undoped counterpart which had a surface area of 98 m^2g^{-1}. In this section, as in the literature case, rhodium markedly reduces phase transformation and surface area loss.

In chapter 1 it was described how the critical size theory governs zirconia phase transition (43,44). The energetics of the system can be altered by dopant addition enhancing tetragonal stability (45). Cationic dopants are stated as effective for tetragonal stabilisation if they have a large ionic radius and have a single valency (46). Rhodium in the +3 state, assuming that - Rh – O – Zr - bonds are formed and maintained within the structure, has a smaller radius than the rare earth oxides previously investigated in chapter 4 (47) but still seems quite effective for stabilisation even at the low concentration. Rhodium as Rh (I), which is stable in the presence of CO as a gem-dicarbonyl (3), is recognized by the author as a species which may exert some sort of effect on the zirconia, if present.

5.3.2: The CO-NO Reaction

5.3.2.1: Catalyst Reduction

The importance and the nature of the reducibility of ceria / zirconia in three way catalyst application has previously been discussed (chapter 1,3 and 4). Figure 5.8. shows how the TPR profiles are altered by the presence of rhodium (48,49).

The low temperature peak in profile B is attributed to surface ceria reduction, whereas the high temperature peak is attributed bulk reduction in the ceria. Comparing profiles A and B in figure 5.8. the authors (48,49) observed that rhodium promotes the reduction of the surface oxygen of the ceria by hydrogen, with the area under the low temperature peaks being too large to solely account for the reduction…

$$Rh_2O_3 + 3H_2 \rightarrow Rh_2 + 3H_2O$$

This is attributed to hydrogen spill over onto the support (50,51).

The lower temperature reduction of C compared to B is attributed to the presence of zirconia as discussed in chapters 1 and 3. For profile D, again rhodium incorporation allows reduction of the ceria / zirconia at a lower temperature. The high

temperature reduction of D and subsequent reoxidation gives trace E. The profile of E is attributed to an enhancement in the mobility of bulk lattice oxygen species (48).

Figure 5.8. TPR profiles of ceria and ceria / zirconia and rhodium impregnated ceria and ceria / zirconia (48,49)

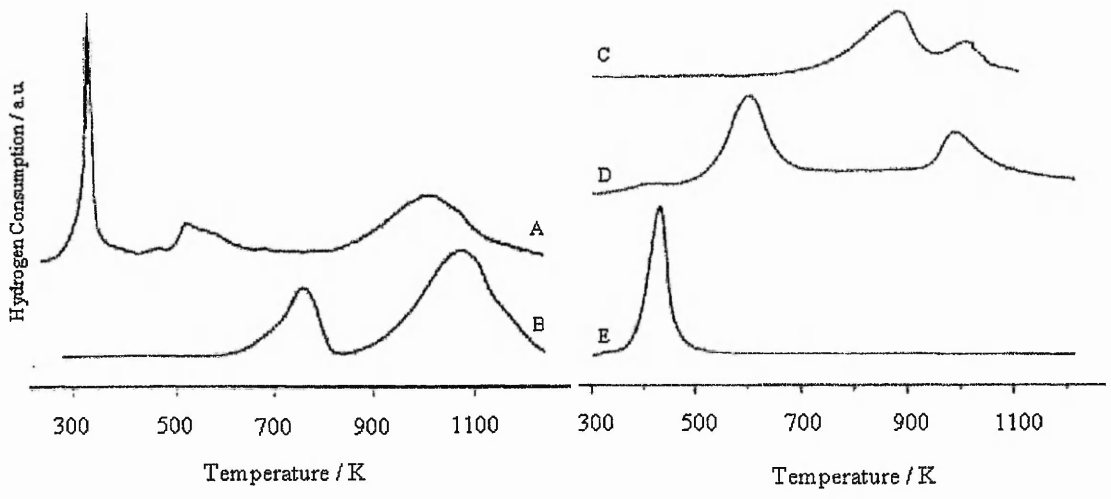

A = Rh / CeO_2 , B = CeO_2 , C = $Ce_{0.5}Zr_{0.5}O_2$, D = Rh / $Ce_{0.5}Zr_{0.5}O_2$,
E = Catalyst D after reduction and reoxidation in pulses of O_2 in Ar at 700 K.

The reduction of the catalysts in a stream of CO and NO was studied at 400°C. Figure 5.9. shows a typical trace of CO_2 production over time for the catalysts. A value of 2000ppm CO_2 is rapidly reached i.e. the obtaining of the stoichiometric reaction...

$$CO + NO \rightarrow CO_2 + \tfrac{1}{2} N_2$$

with the production of carbon dioxide via the reduction reactions...

$$CeO_2 + CO \rightarrow Ce_2O_3 + CO_2 \quad \text{and} \quad Rh_2O_3 + 3CO \rightarrow Rh_2 + 3CO_2$$

being rapidly completed.

Figure 5.9. Production of CO_2 over the 1 wt% Rh / 57Z40C3Y vs. time

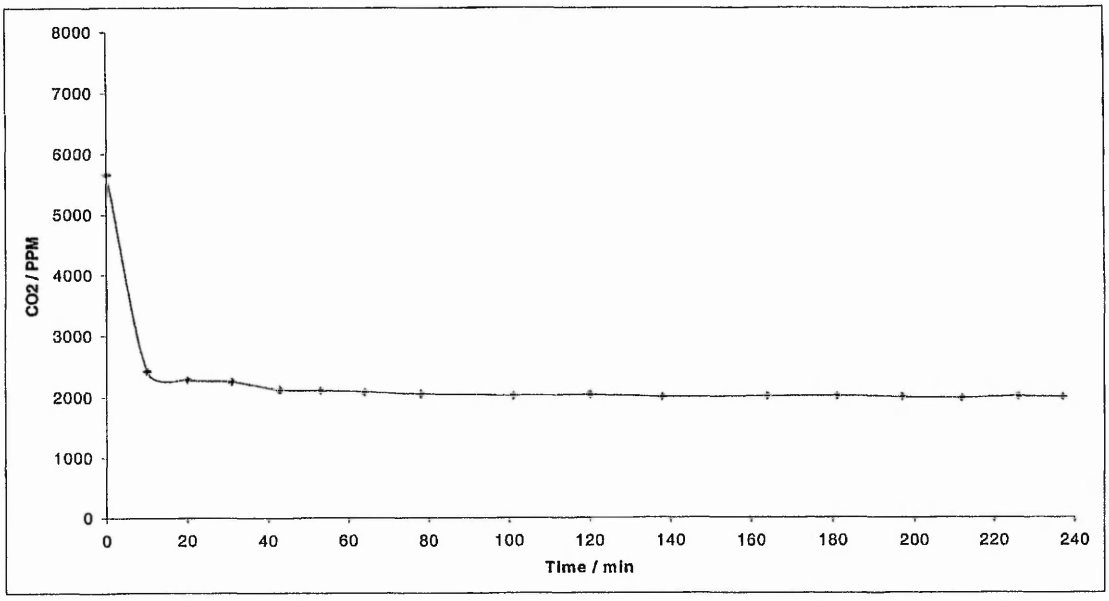

5.3.2.2: Results and Discussion

The catalyst preparation procedures are described in section 5.2. A ramping procedure of 200°C - 400°C - 200°C was used. Catalyst reduction took place over the 200°C - 400°C in the reactant gas mixture. Analysis at 40°C intervals was undertaken over the 400°C - 200°C temperature range. Two measurements were made at each temperature, and the results are considered to be accurate to +/- 1%, indicating that the catalyst behaviour, at the given temperatures, is stable.

Figure 5.10. shows the influence of rhodium loading on the CO – NO reaction. The selectivity to nitrogen and the percentage conversion of NO are shown over the studied temperatures.

From figure 5.10. it can be seen that at 400°C all catalysts convert 100% of the NO with 100% selectivity to N_2. The activity of the 0.5 wt% rhodium catalyst is very much poorer for the removal of NO at temperatures below 400°C. There seems little difference in the activity of the 1 and 3 wt% rhodium catalysts for removing NO, but the 3 wt% rhodium catalyst has greater selectivity to N_2 at low temperature.

Figure 5.10. Influence of rhodium level on NO removal and selectivity to N_2

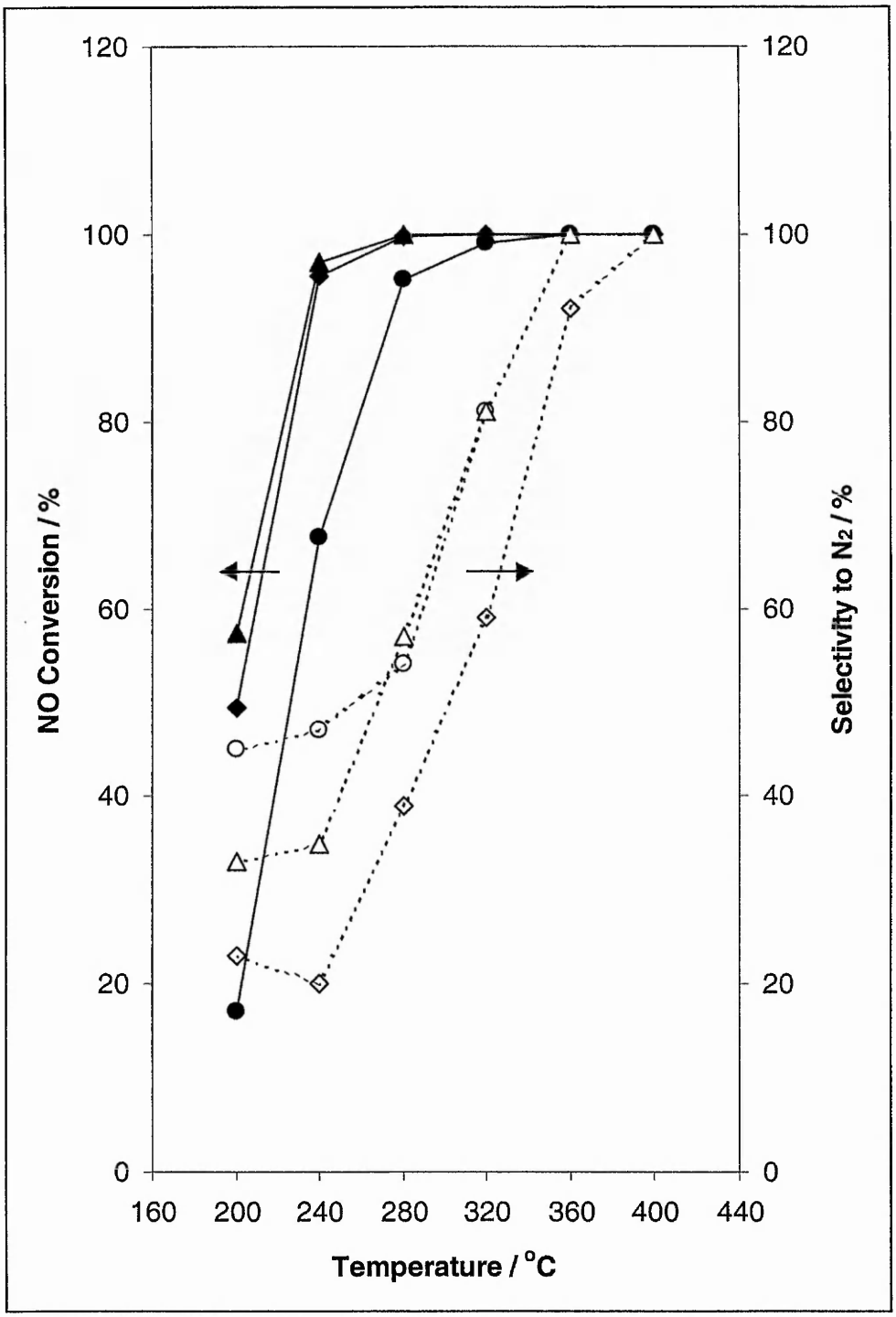

where, ● = 0.5 wt% Rhodium, ◆ = 1 wt% rhodium and ▲ = 3 wt% rhodium, on a support designated as number 14 in chapter 3.

Figure 5.11. Influence of the support for NO removal and selectivity to N_2

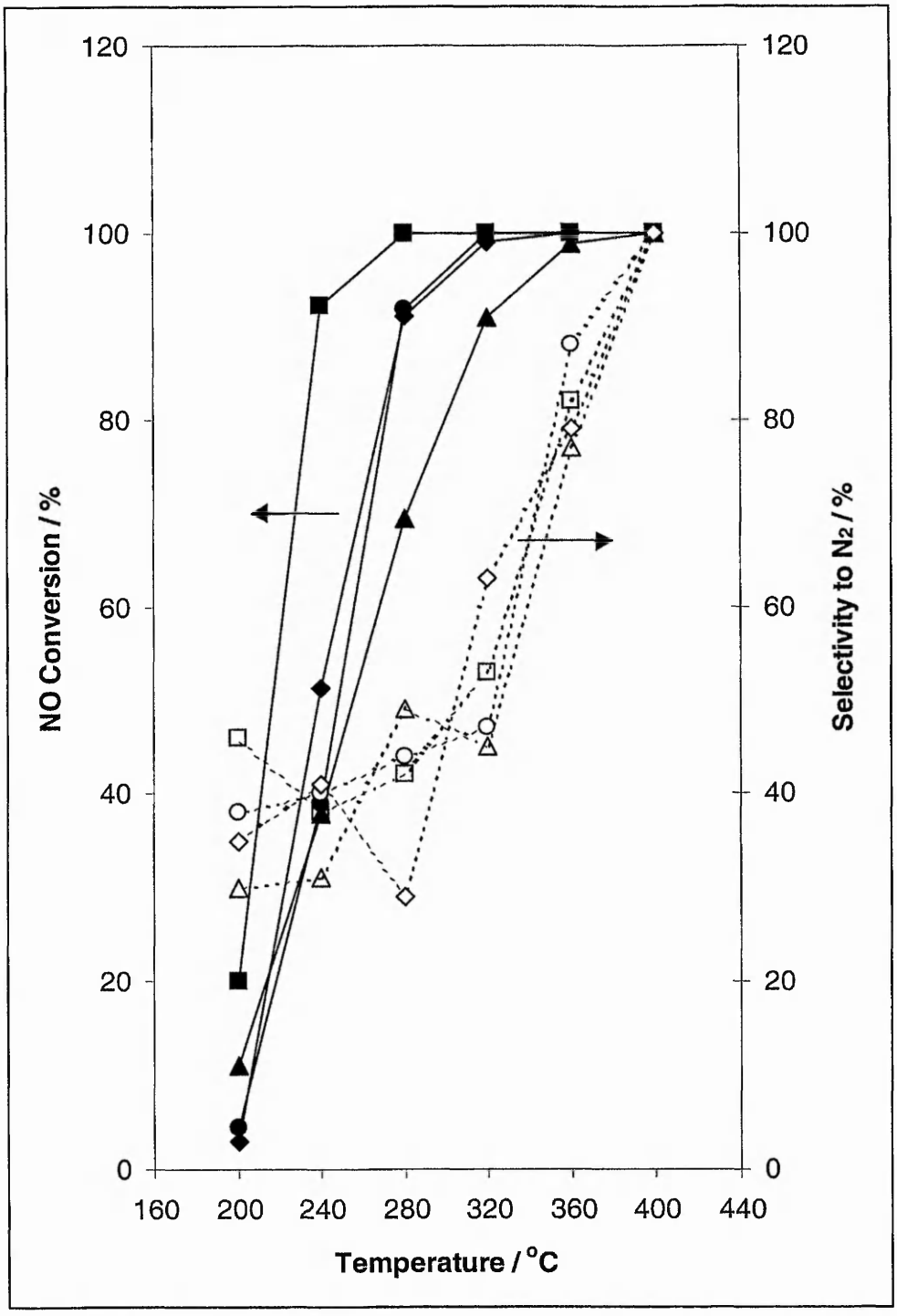

where, ● = 900 / 10, ■ = 900 / 40, ▲ = 500 / 40 and ◆ = 500 / 10 are materials designated as numbers 15, 12, 5 and 11 respectively in chapter 3, supporting 1 wt% rhodium.

NB: 900 or 500 refers to the initial calcination temperature of the support and the 40 or 10 refers to the mol% of ceria in the support.

Figure 5.11. shows the influence of the support on the CO – NO reaction. The selectivity to nitrogen and the percentage conversion of NO are shown over the identical regime with the same degree of accuracy as described above.

From figure 5.11. it can be seen that at 400°C all catalysts remove 100% of the NO with 100% selectivity to N_2. The activity of the catalysts vary widely because of the nature of the supports. The 500 / 40 mixed oxide appears to be the worst support for rhodium. It can be seen that the effectiveness of the support follows the trend:-

$$500/40 < 900/10 = 500/10 < 900/40$$

Another way to rank the effectiveness of these catalysts for NO reduction is shown by the results given in table 5.1. In each case the temperature required to give a steady conversion of 60% of the nitric oxide has been determined. By this measure, the effectiveness of all catalysts is enhanced by the presence of a ternary dopant, with the 50% zirconia, 40% ceria, 10% neodymia catalyst achieving 60% conversion at only 206°C. By contrast, of the binary supported materials only the 900/40 material achieves this conversion below 240°C.

Upon cooling down to 60% NO conversion, after support reduction, the selectivity towards N_2 formation did not vary greatly between the catalysts or over the 3 hours investigated. The applied temperature required, to attain 60% NO conversion, did need to be altered slightly (+/- 3°C) over the 3 hours.

High temperature aging of rhodium supported on ceria / zirconia has been shown to result in deep encapsulation of the metal particles (52). Penetration of rhodium into the surface of ceria has been shown to be dependent upon the initial surface area, i.e. the calcination temperature of the support (53). A ceria / zirconia mixed support calcined at high temperature is an excellent support for rhodium. There is minimal rhodium activity loss because of the favourable interaction with the support and the lack of encapsulation allows rhodium to be in a dispersed state in high concentration (54). It was for this reason that catalyst 14, a support containing 40 mol% ceria and calcined at 900°C, was chosen for the investigation into the effect of the amount of rhodium on catalytic activity. Activity differences in the three catalysts are ascribed to the level of rhodium on the surface.

Table 5.1. Results from the study of 60% NO removal over reduce supports

Support	Applied Temperature / C	Gas Composition / PPM	
		N_2O	N_2*
900/40	223	200	400
500/40	256	170	430
500/10	248	129	471
900/10	241	170	430
50Z40C10N	206	232	368
57Z40C3N	208	298	302
50Z40C10P	214	243	357
57Z40C3P	215	235	365
50Z40C10Y	214	199	401
57Z40C3Y	206	210	390
50Z40C10L	222	212	388
57Z40C3L	214	219	381

* N_2 calculated by subtraction, no other nitrogen species were observed

Studies of the CO-NO reaction of rhodium on large surface area supports (17-19 [figure 5.3.]) have shown that increasing the rhodium particle size i.e. decreasing the rhodium dispersion by increasing the rhodium loading, has a beneficial effect on the reaction rate, turnover frequency and the temperature at which light-off is achieved. Over the comparatively low surface area ceria / zirconia catalyst here only a very slight benefit, with respect to NO decomposition, is observed when the level of rhodium is increased from 1 wt% to 3 wt%. It is thus argued that the literature (17-19) has not reported catalysts with excessive rhodium content such as that seen here. Although rhodium particle size and dispersion investigations were not undertaken on the catalysts used here, it is assumed the trends remarked upon in the literature hold true for the zirconia based supports, and thus are important in the discussion of catalytic activities.

When the 1 wt% Rh / 900/40 catalysts are compared in figures 5.10. and 5.11. differences in ability of NO removal are observed. The difference in activity, most

notable at the lower temperatures used, is ascribed to the difference in the support. In the former study of the influence of rhodium the support termed 14 from chapter 3 was used. In the latter study support 12 was used. Table 5.2. highlights the main difference between the supports.

Table 5.2. The difference between catalyst support

Support Term (from chapter 3)	**Surface Area / $m^2 g^{-1}$**	**Ceria / Zirconia Surface Ratio**
14 (900/40)	28	1.92
12 (900/40)	7	1.04

Support 12 has a surface area lower than that of support 14. It is argued that a smaller surface area will insure a higher surface concentration of rhodium and hence decrease rhodium dispersion. This is thus detrimental to the activity of the catalyst for the reasons mentioned above. When rhodium is doped onto the higher surface area support 14, a sizable improvement is observed at 200°C. With support 14 conversion of NO is *circa* 50% whereas with 12 conversion is *circa* 20%. Surface area and hence rhodium dispersion may not be the only contributing factors. As discussed earlier, ceria is believed to aid NO reduction at low temperature due to spill over of oxygen from NO decomposition. At such temperatures, oxygen mobility has been reported as being rather slower so that oxygen uptake is limited to the surface of the ceria support (55). Thus the improved surface area of support 14 and the higher surface concentration of ceria will enhance the activity at lower temperature.

The significant differences in the activity of the catalyst shown in figure 5.11. are ascribed to the difference in the support type. Table 5.3. shows the surface areas and surface compositions of the 4 supports that were prepared in chapter 3 along with conversion of NO at 280°C from figure 5.11.

If previous arguments made about surface area and surface composition are valid then it could be assumed that support 5 should be superior to that of support 12 in the preparation of a catalyst for the reaction. Yet the initial calcination temperature and

surface richness of ceria are the exact reasons why the support is poor. In the catalyst preparation process, oxidation of the rhodium nitrate precursor is required. The formation of a strong interaction between oxidised rhodium and ceria has been reported leading to the incorporation of rhodium into the ceria lattice (28). Calcination of the ceria based support at high temperature increases the surface concentration of rhodium after precursor deposition and oxidation, as compared to a support calcined at lower temperature (53,54). It is thus argued that the 500/40 support removes rhodium from the surface upon calcination resulting in a poorer catalyst.

Table 5.3. Characteristics of the four support types

Support Term (from chapter 3)	**Surface Area / $m^2 g^{-1}$**	**Ceria / Zirconia Surface Ratio**	**Conversion of NO / %**
12 (900/40)	7	1.04	100
5 (500/40)	74	2.00	69.4
15 (900/10)	12	0.26	91.8
11 (500/10)	94	0.21	91.2

There is a great deal of similarity in activity among the catalysts containing 10% ceria. The benefit of surface area, in the case of catalyst 11, previously shown to aid activity, can be balanced by the argument of rhodium active surface area removal in the preparation procedure.

The 900/40 based catalysts is superior over the entire temperature range due to the surface stability of the support because of the high calcination temperature and the high level of ceria in the support, aiding NO decomposition.

The support types were compared again based on steady state activity for the removal of 60% NO by CO as shown in table 5.1. Again it was shown that a 900/40 support is superior to the others investigated. The gaseous product selectivity is shown to be very much temperature dependent.

In table 5.1. the 4 catalyst / support types are compared to the rare earth ternary doped supports containing 40mol% and calcined at 900°C, the preparation of which is discussed in chapter 4. The 8 ternary doped supports appeared superior to the comparative undoped support in catalyst formation. The surface areas of the doped

supports are greater than the undoped support, please refer to chapter 4, section 4.3.1. but no obvious relationship in surface area and reaction temperature is observed within the group, see figure 5.12. of surface area vs. reaction temperature for the ternary doped supports.

Figure 5.12. Surface area vs temperature for 60% NO for removal over ternary mixed oxide / rhodium catalysts

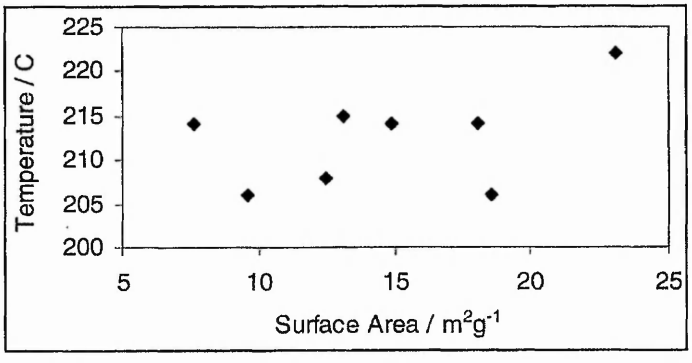

No clear relationships are observed between catalytic activity and other characteristics of the support, such as surface ceria. Figure 5.13 illustrates this lack of trend.

Figure 5.13. Surface ceria content vs. temperature for 60% NO removal over ternary mixed oxide supports

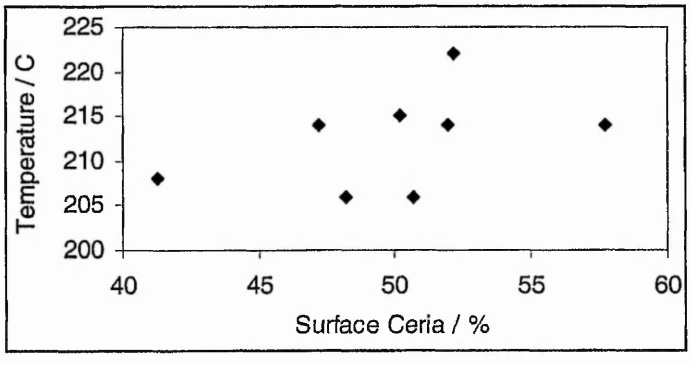

The reduction characteristics cannot usefully be related to reactivity as the presence of the precious metal significantly alters the reducibility of the mixed oxide.

In chapter 4 the character of the ternary mixed oxide was shown to be dependent upon the type of rare earth dopant and the amount. Here the activity of the catalyst in performing the CO-NO reaction is not directly linked to any single characteristic of the ternary mixed oxide. It is therefore concluded that the influence of the support in the reaction is due to a combination of a number of factors.

The product ratio of N_2 : N_2O in the CO – NO reaction is very much temperature dependent (56) with a higher ratio observed at higher temperatures. This has been attributed to a slow N_2O + CO reaction rate at low temperatures (7).

The temperature dependence can be seen in table 5.1. where the Rh / 900/40 catalyst has a lower applied temperature requirement for the removal of 60% NO and has a lower selectivity to N_2, as compared to the rhodium supported on 500/40, 500/10 and 900/10 catalysts. Figure 5.14. shows a plot of applied temperature and selectivity for the 8 rare earth oxide containing supports

Figure 5.14. Nitrogen selectivity vs. temperature for 60% NO removal over ternary mixed oxide supports

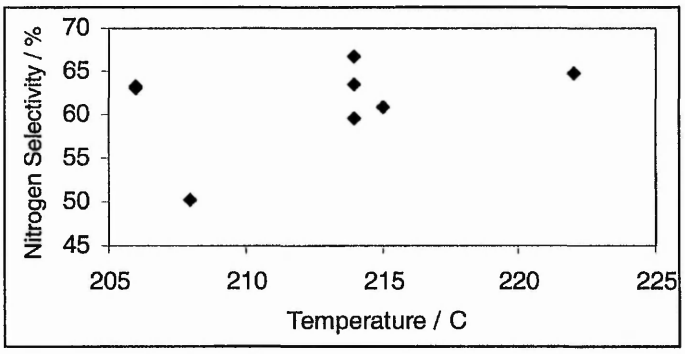

No clear relationship within the rare earth containing supports is observed with regards to selectivity and temperature. Figures 5.15. and 5.16. show plots of the character of the support against nitrogen selectivity, at 60% NO removal, in order to

determine the manner in which the support is influencing the catalytic nature of rhodium. From figure 5.15. it is seen that surface area is not important with respect to selectivity.

Figure 5.15. Nitrogen selectivity vs. surface area over ternary mixed oxide supports

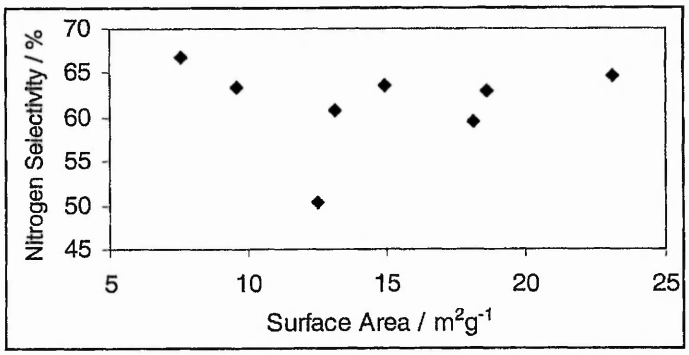

Figure 5.16. Nitrogen selectivity vs. Surface ceria content over ternary mixed oxide supports

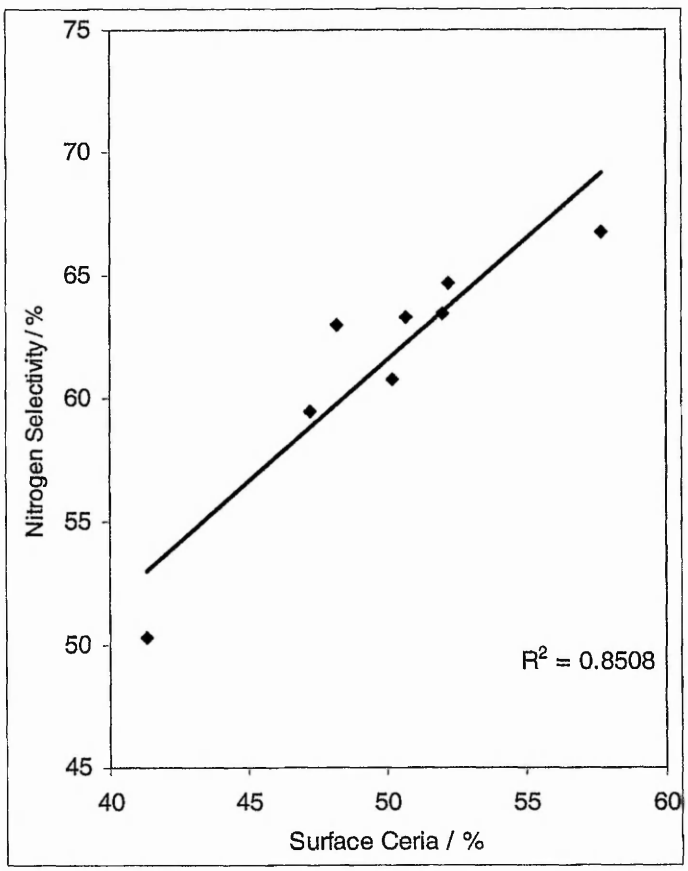

A clearer relationship is observed in figure 5.16. The greater the surface content of ceria the greater the selectivity to nitrogen. As discussed earlier ceria aids NO reduction at low temperature due to spill over of oxygen from NO decomposition. At such temperatures oxygen mobility has been reported as being slow and that oxygen uptake is limited to the surface of the ceria support (55). The presence of ceria enhances the NO dissociation rate and N_2 desorption rate at low temperature (56); thus the greater the surface ceria concentration the greater the rate of the following reactions:-

$$NO_{(gas)} \rightarrow NO_{(ads)}$$

$$NO_{(ads)} \rightarrow N_{(ads)} + O_{(ads)}$$

$$2N_{(ads)} \rightarrow N_{2\,(gas)}$$

reactions, rather than the reaction:-

$$NO_{(ads)} + N_{(ads)} \rightarrow N_2O_{(gas)}$$

5.3.3: Nitrous Oxide Decomposition Studies

5.3.3.1: Decomposition of N_2O over Rh/ZrO_2 Catalysts

The method of preparation of the catalysts and the testing regime were previously mentioned in this chapter. The catalysts are coded 500i, 650i, 800i, 950i, 500c, 650c, 800c and 950c. The coding refers to the temperature of calcination (°C) and the manner by which rhodium was deposited on the zirconia (i = incipient wetness, c = coprecipitation).

Figure 5.17. shows the decomposition curves for N_2O over the 8 rhodium / zirconia catalysts. Figure 5.18. displays the temperatures for 50 or 25% conversion obtained from figure 5.17.

Figure 5.17. 'S' shape curves of the decomposition of N_2O over the Rh / ZrO_2 catalysts

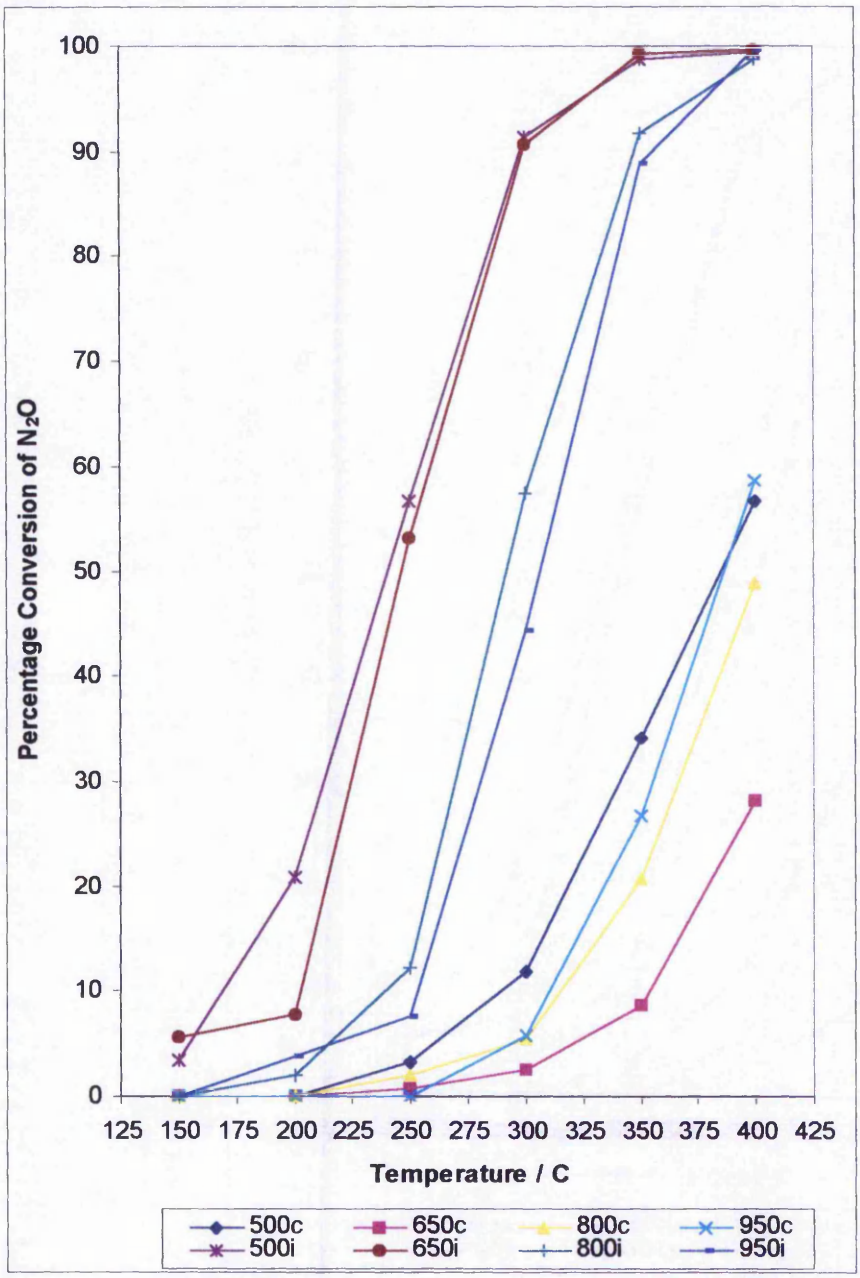

Figure 5.18. Temperature /K for conversion of N_2O vs. surface area for the Rh/ZrO_2 catalysts

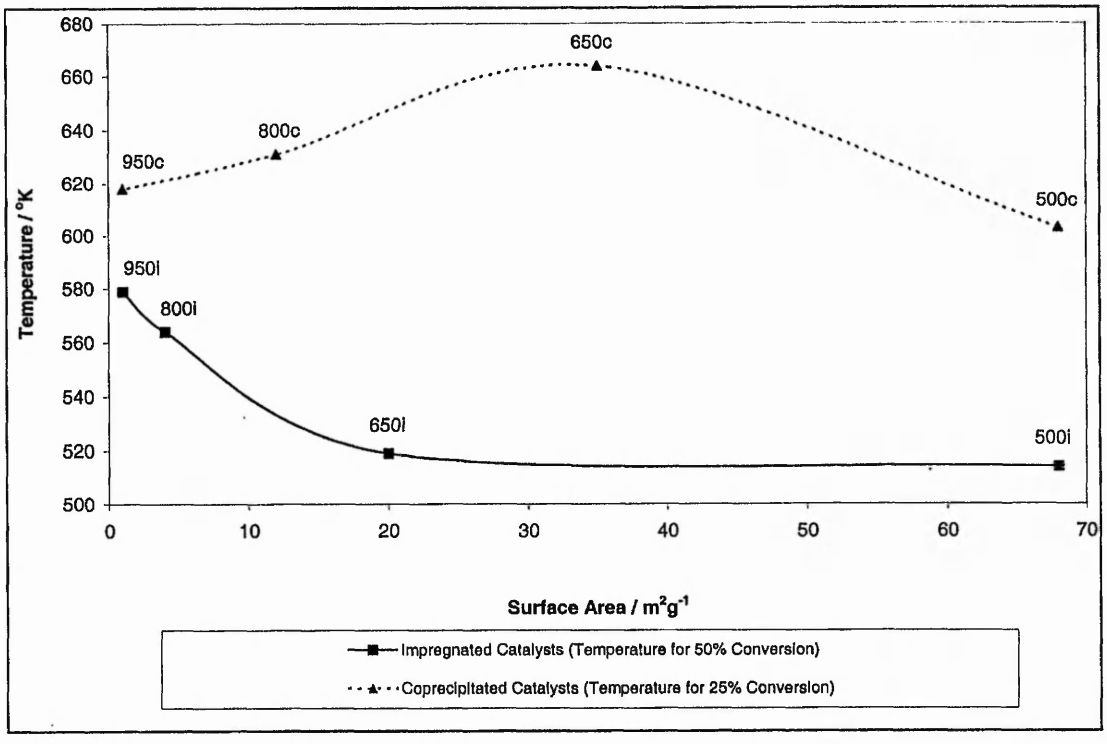

From figures 5.17. and 5.18. it can been seen that, for the catalysts prepared by the incipient wetness addition of rhodium to the surface of zirconia, conversion is very much related to the surface area of zirconia. There is a 65°K temperature increase requirement to attain 50% conversion when comparing the 950i catalyst to the higher surface area 500i. It can thus be stated that the catalytic activity of the rhodium is enhanced by being placed on a higher surface area support.

A previous study has indicated that the activity of rhodium supported on zirconia is comparable to Rh / Al_2O_3 for the nitrous oxide decomposition reaction (57). The coverage of rhodium on the surface of the support has been shown to be important in sections 5.3.2., 5.1. figure 5.1. and elsewhere (17,18,57) for de-NOx catalysts. If it is assumed that dispersion is described as the percentage of rhodium exposed and that there are no unfavourable rhodium – zirconia surface effects (58) then it can be assumed that a higher surface area will support a higher dispersion of the active component and a

catalysts of greater activity is obtained. In section 5.3.2. it was shown that there is a point where the addition of greater rhodium levels does not benefit the catalytic activity.

The observation that, for N_2O decomposition, the surface area of the zirconia support is important for catalytic activity could lead to the conclusion that all of the action takes place on the support rather than on the rhodium. However, the impregnated and coprecipitated catalysts that were calcined at 500°C have equal surface areas but vastly different catalytic activities hence this possible explanation is disproved. There is also no relationship between catalytic activity and surface area in the coprecipitated catalysts.

Coprecipitating rhodium with zirconia reduces further still the surface coverage of rhodium. The fact that it appears that the catalysts are poorer in conversion is a result of low surface coverage. The 950c catalyst offers enhanced catalytic conversion as compared to its 650c counterpart. This can be attributed to increased levels of rhodium at the surface due to surface enrichment of the rhodium due to high temperature calcination, which has previously been observed for silica and lanthana dopants in zirconia (59).

5.3.3.2: Decomposition of N_2O over Rh/Ce/Zr/Rare Earth Oxide Catalysts

Figure 5.19. shows the 's' shaped curves for the decomposition of N_2O over the eight Rh/Ce/Zr/rare earth catalysts. Figure 5.20. shows the relationship between surface area and T50, the temperature at which 50% of N_2O is converted. Table 5.4. gives the general data for the eight catalysts.

It can be seen from figure 5.20. that there is a relationship between the surface area of the ceria / zirconia / rare earth oxide support and the temperature at which 50% of the N_2O is decomposed.

The ceria / zirconia / rare earth oxide supports calcined at 900°C had superior T50 values than that of the pure zirconia support calcined at 800°C. Literature evidence suggests that the preferred support for rhodium in this reaction is a ceria / zirconia mixed oxide, which is superior to a zirconia support (53,54), which in turn is superior to a ceria support (58). The ceria / zirconia support, calcined at high temperature, was

explained as being the best support in terms of allowing rhodium to be in a highly dispersed state but in high concentration (53).

Figure 5.19. Curves of the decomposition of N_2O over the Rh/Ce/Zr/rare earth catalysts

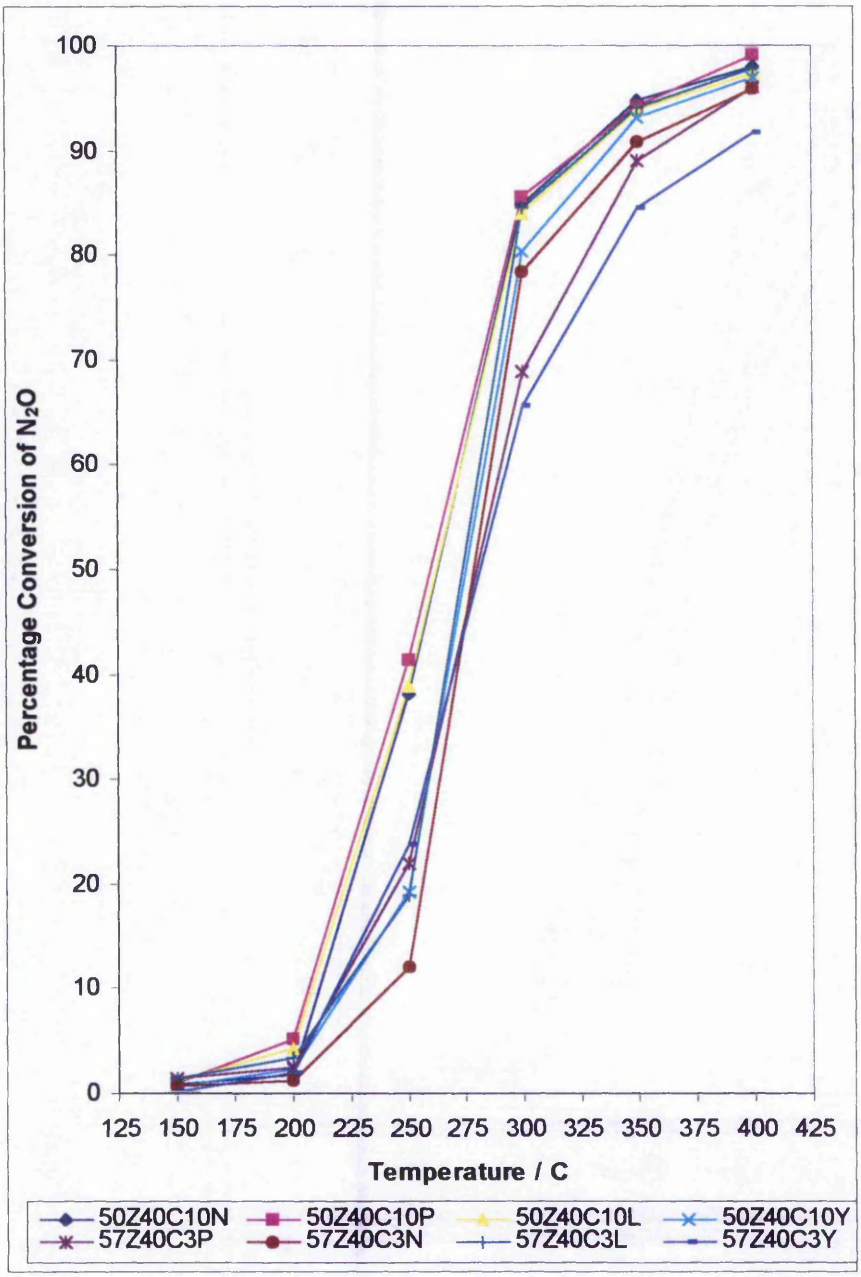

As seen in chapter 4 the addition of a rare earth dopant to the ceria / zirconia mixed oxide alters surface area, crystalline structure, surface composition and reduction characteristics depending upon the nature and amount of ternary. It is thus not unexpected to find subtle differences in the catalytic ability of rhodium impregnated on such supports.

Figure 5.20. Graph of the temperature of decomposition of N_2O vs. the surface area of the Rh/Ce/Zr/rare earth catalysts

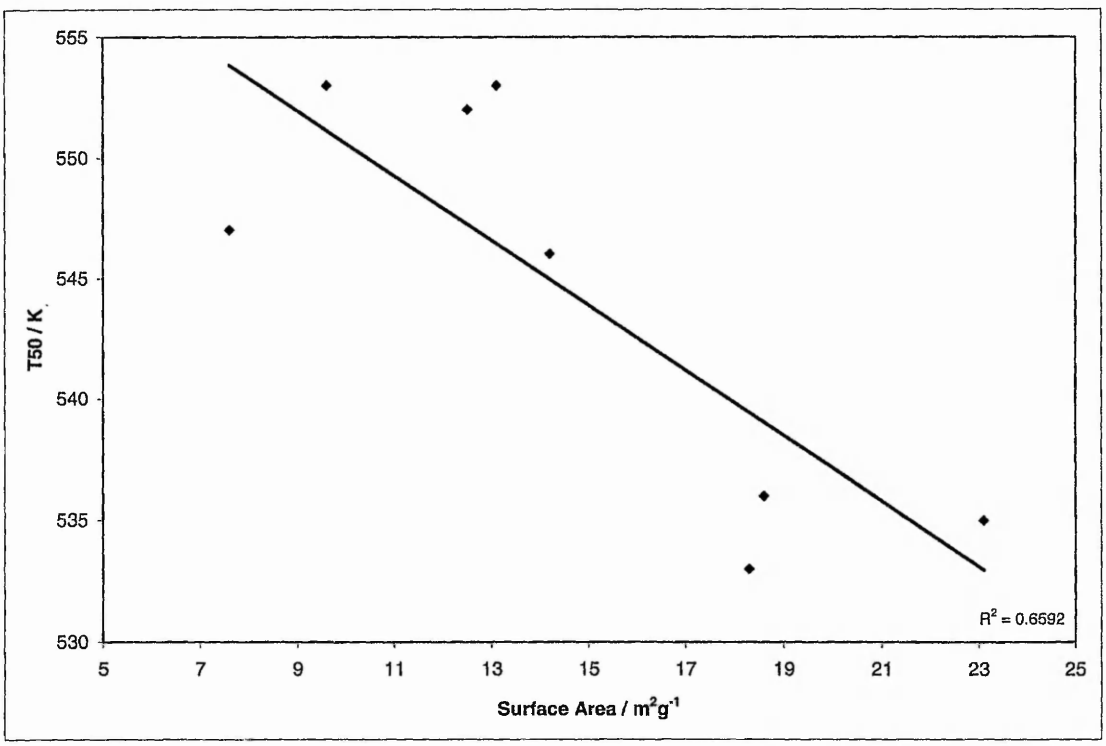

Table 5.4. Table of catalytic and material data for the Rh/Ce/Zr/rare earth catalysts

Material Type	Material	B.E.T. Surface Area / m^2g^{-1}	Conversion at Temperature / K
Rare Earth	57Z40C3N	12.5	T50 = 552
3% Doped	57Z40C3P	13.1	T50 = 553
Support for	57Z40C3L	14.2	T50 = 546
Rh	57Z40C3Y	9.6	T50 = 553
Rare Earth	50Z40C10N	18.6	T50 = 536
10% Doped	50Z40C10P	18.3	T50 = 533
Support for	50Z40C10L	23.1	T50 = 535
Rh	50Z40C10Y	7.6	T50 = 547

5.4: Conclusions

Binary ceria / zirconia and ternary ceria / zirconia / rare earth oxides, the preparation and characterisation of which were discussed in chapters 3 and 4, were investigated as supports for rhodium for the CO-NO reaction. Rhodium / zirconia catalysts were also prepared, characterised and compared to the rhodium / ternary ceria / zirconia / rare earth oxides for the decomposition of nitrous oxide.

The main conclusions from these experiments are:-

- The presence of rhodium species stabilise the surface area of tetragonal zirconia, when prepared as a 1wt% Rh / ZrO_2 mixed oxide by coprecipitation, and decreases the extent of the tetragonal to monoclinic phase transformation.

- The nature of the support significantly influences the activity of the rhodium based catalyst in performing the CO-NO reaction.
    - A ceria rich surface and high surface area are beneficial to the activity and selectivity of the catalyst.
    - The addition of ternary rare earth oxide to the support is shown to be beneficial to catalytic activity. Improvements in catalytic activity are not simply related to increases in the support surface area.

- For N_2O decomposition, the surface area of the support is directly related to catalytic activity when a catalyst is prepared by impregnation. The surface area of the support is argued to influence the dispersion of rhodium.

- For Rh / ZrO_2 catalysts prepared by coprecipitation, it is argued that, surface enrichment of rhodium under high temperature treatment improves the catalytic activity for N_2O decomposition.

5.5: References

1. M.Bowker, R.W.Joyner. in 'Insights into Speciality Inorganic Chemicals',Ed.D.Thompson, Royal Society of Chemistry, Cambridge. 1995 145-167
2. K.C.Taylor. Catal.Rev-Sci.Eng.1993 457-481
3. V.I.Parvulescu, P.Grange, B.Delmon. Catalysis Today 1998 46 233
4. W.C.Hecker, A.T.Bell. J.Catal. 1983 84 200
5. W.C.Hecker, A.T.Bell. J.Catal. 1984 85 389
6. W.C.Hecker, A.T.Bell. J.Catal. 1983 84 220
7. R.W.McCabe, C.Wong. J.Catal 1990 121 422
8. B.K.Cho. J.Catal. 1992 138 255
9. B.K Cho. J.Catal. 1994 148 697
10. V.P.Zhdanov. J.Catal. 1996 162 147
11. J.C.Bailar et al Eds. 'Comprehensive Inorganic Chemistry', Pergamon Press, Oxford, 1984 316
12. Greenwood and Earnshaw. 'Chemistry of the Elements'. 1984
13. E.R.S.Winter. J.Catal. 1970 19 32
14. F.Kapteijn. J.R.Mirasol. J.A.Moulijn. Appl.Catal.B.Env. 1996 9 25
15. M.Bowker. 'The Basis and Application of Heterogeneous Catalysis', Oxford Science Publications, Oxford, UK. 1998
16. T.R.Ward, P.Alemany, R.Hoffman, J.Phys.Chem 1983 97 7691
17. J.Kaspar, C.D.Leitenburg, P.Fornasiero, A.Trovarelli, M.Graviani, J.Catal. 1994 146 136
18. S.H.Oh, C.C. Eikel, J.Catal. 1990 128 526
19. W.C.Hecker, R.B.Breneman. CAPOC. Stud.Surf.Sci.Catal. 1986 30 257
20. D.D.Beck, C.J.Carr, J.Catal. 1993 144 296
21. J.G.Chen, M.L.Colaianni, P.J.Chen, J.T.Yates, G.B.Fisher, J.Phys.Chem. 1990 94 5059
22. J.M.Schwartz, L.D.Schmidt. J.Catal. 1994 148 22-29 and references therein
23. P.Moles, 'Zirconia – Current and Future Uses' MEL Leaflet
24. European Patent EP 0262962 Englehard Corp.

25. United States Patent USP 4233289 Ford Motor Co.
26. Japanese Patent JP 63,077,544
27. Japanese Patent JP 63,020,036
28. A.Trovarelli. Cat.Rev. 1996 38 4 439
29. K.R.Krause, L.D.Schmidt. J.Catal. 1993 140 424
30. S.Bernal, F.J.Botana, J.J.Calvino, G.A.Cifredo, J.A.P.Omil, J.M.Pintado. Catal.Today. 1995 23 219
31. L.L.Murrel, S.J.Tauster, D.R.Anderson. Stud.Surf.Sci.Catal. 1991 71 275
32. Z.R.Ismagilov, R.A.Shkrabina, N.A.Koyabkina, F.Kapteijn. Catal.Today. 1995 24 269
33. B.Harrison, A.F.Diwell, C.Hallett. Plat.Met.Rev. 1988 32 73
34. G.RangaRoa, P.Fornasiero, R.DiMonte, J.Kaspar, G.Vlaic, G.Balducci, S.Meriani, G.Gubitosa, A.Cremona, M.Graziani. J.Catal. 1996 162 1-9
35. G.RangaRoa, P.Fornasiero, J.Kaspar. S.Meriani, R.DiMonti, M.Graziani. COPAC4 Reprints. 1997 73-83
36. G.RangaRoa, J.Kaspar, S.Meriani, R.DiMonte, M.Graziani. Cat.Let. 1994 24 107-112
37. G.Srinivas, S.S.C.Chuang, S.Debnah. in 'Environmental Catalysis' Ed. J.Armor, A.S.C. Washington D.C. 1994 157-167
38. R.S.Fenoglio, R.Cataluna, J.Soria, J.S.Conesa. EuropaCatI Book of Abstacts. 1993
39. H.Toroya, M.Yoshimura, S.Somiya. J.Am.Ceram.Soc. 1984 67 C-119
40. P.Li, I.W.Chen, J.E.P.Hahn. J.Am.Ceram.Soc. 1994 77(5) 1281-1288
41. T.H.Etsell, S.N.Flengas, Chem.Rev.1970 70 339
42. P.A.Sermon, V.A.Self, Y.Sun. J.Sol-Gel. Sci.Tech. 1997 8 851
43. R.C.Garvie. J.Phys.Chem 1978 82 218
44. R.C.Garvie. J.Phys.Chem 1969 65 1238
45. C.J.Norman, P.A.Goulding, I.McAlpine. Catalysis Today. 1994 20 313-322
46. P.D.L.Mercera. Ph.D. Thesis. Twente University. 1991
47. D.R.Lide (Ed.). 'Handbook of Chemistry and Physics' 81st Ed. 2000 CRC Press. Boca Raton. U.S.A.
48. G.Vlaic, R.D.Monte, P.Fornasiero, E.Fonda, J.Kaspar, M.Graziani. CAPOC IV. Elsevier, Amsterdam. 1997 P8

49. P.Fornasiero, G.R.Rao, J.Kaspar, F.L.Erario, M.Graziani. J.Catal. 1998 175 269
50. A.Trovarelli, G.Dolcetti, C.D.Leitenburg, J.Kaspar, P.Finetti, A.Santoni. Faraday Trans. 1992 88 1311
51. H.C.Yao, Y.Yu. J.Catal. 1984 86 254
52. G.W.Graham, H.W.Jen, W.Chun, R.W.McCabe. J.Catal. 1999 182 228
53. S.Imamura, R.Hamada, Y.Saito, K.Hashimoto. H.Jindai. J.Mol.Catal.A.Chem. 1999 139 55
54. S.Imamura, T.Yamashita, R.Hamada, Y.Saito, Y.Nakao, N.Tsuda, C.Kaito. J.Mol.Catal.A.Gen. 1998 129 249
55. B.K.Cho. J.Catal. 1991 131 74
56. S.H.Oh. J.Catal. 1990 124 477
57. K.Yizaki, T.Yarimizu, K.Oayagi, S.I.Ito, K.Konimuri. Catal.Today 1998 45 129
58. R.Burch, P.K.Loader. Appl.Catal.A.Gen. 1996 143 317
59. M.Keenan. Ph.D Thesis. The Nottingham Trent University. 1996

Chapter 6:

Catalysts for the Selective Catalytic Reduction of Nitrogen Oxides.

'...and it must be said that an easier solution could be to eliminate diesel engines.'

Michael Bowker 1998

6.1: Chapter Introduction

In chapter 1 it was indicated that de-NOx catalysis was difficult over precious metals in the presence of excess oxygen; thus for vehicles that are of the lean-burn type, other approaches are required for NOx abatement. The preferential reduction of nitrogen oxides, in lean conditions, in the presence of a catalyst, is known as selective catalytic reduction (SCR).

Many coal fired boilers in power plants, have, for some time now, been fitted with such NOx abatement technology. The catalyst typically used is based on titanium dioxide with the active components of vanadium, tungsten and molybdenum oxides. The reductant used in these circumstances are ammonium ions. The addition of ammonia however leads to environmental problems resulting from ammonia escape from the stack.

The air / fuel ratio used in the diesel engine qualifies it to be described as a 'lean-burn' device. Combustion is much more efficient than in a petrol driven engine - at least 90% of the fuel is completely burnt as compared to as little as 70% in the petrol engine (1). The combustion efficiency offers greater fuel economy to the driver, decreased, uncatalysed, carbon monoxide and hydrocarbon emission in the exhaust and less CO_2 production, per mile, as compared to a petrol engine. NOx emissions can be controlled but exhaust gas recirculation is required. The type of combustion and fuel used in diesel technology leads to emission of particulates and polyaromatic hydrocarbons. Technology can allow the particulates to be burnt catalytically or trapped by a centrifugal mechanism, but these techniques are not in general use (1).

A number of catalysts and reductants have been investigated with regards to the application of SCR technology to automotive systems. The reductants investigated have included ammonia, hydrogen, carbon monoxide and hydrocarbons. The stationary NOx abatement system mentioned is not applicable to vehicles as it would require the carriage of urea and the control of addition of the ammonium based compound to the exhaust gas. The car is already carrying a source of hydrocarbons in the form of fuel. This, coupled with the fact that carbon monoxide is an inefficient reductant in the present of oxygen, has attracted much attention to the possibility of the SCR reaction of hydrocarbons and NOx in automotive catalysis (2,3). The use of copper containing

zeolites as catalysts for the SCR reaction has been much studied (4,5). Zeolites are three dimensional, porous, crystalline structures based on silica and alumina.

A zeolite is an aluminosilicate. The framework structure encloses cavities, which may contain free moving ions and water, allowing for reversible hydration and ion exchange. The structures are based on an indefinitely extending network of SiO_4 and AlO_4 tetrahedra sharing all the oxygens, two Al atoms are never adjacent and there is no Al-O-Al bonding. Because of the channel dimensions and geometry of zeolite systems, they have attracted interest for allowing reactants to enter and diffuse, leading to shape selectivity in catalaytic reactions (6). The replacement of Si^{4+} with Al^{3+} in the lattice leads to a charge inbalance that may be proton stabilised. These sites are acidic and catalytically active. The protons associated with the active sites can be exchanged by a range of metal ions (6) this action allows for the modification of catalytic behaviour. The zeolite ZSM-5 has a ring structure depicted in figure 6.1. The pore structure is based on a ten membered ring, with the pores having a diameter of approximately 5.5 Å.

Figure 6.1. The framework structure of ZSM-5

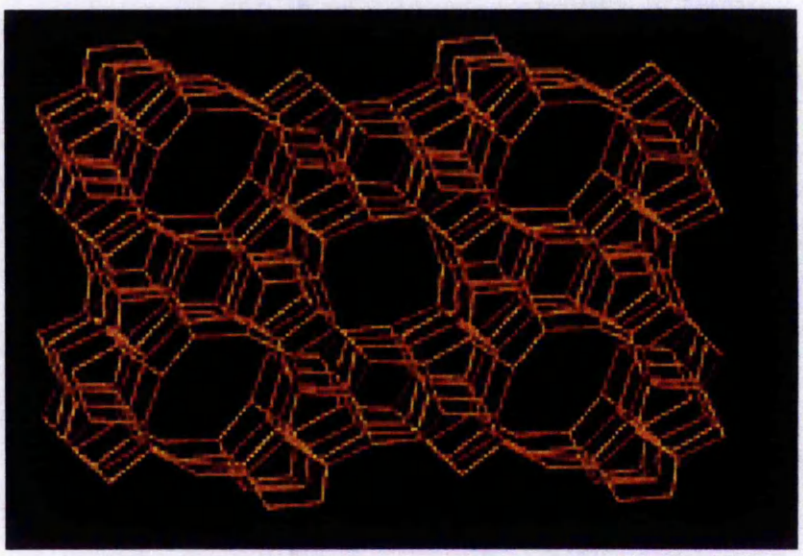

The screening of many metal exchanged zeolites as catalysts for the SCR reaction has lead to an interest in Cu-ZSM-5 because of its high activity; yet there are numerous inherent problems with using this catalyst in real conditions. Such problems have not stopped research into this material, not for attainment of an excellent SCR catalyst in real conditions, but for the sake of interest and knowledge. The combustion process produces steam. The presence of water has been shown to cause catalyst deactivation due to the alteration of coordination and position of the metallic active site and structural dealumination leading to changes of acidity and formation of $CuAl_2O_3$ which is not active for the reaction (7,8).

The lack of stability of zeolites in the presence of water has attracted authors to re-evaluate precious metal catalysts for the SCR reaction. Supported platinum catalysts have been widely investigated (9-15). In these studies there has been shown to be a strong dependence on activity to the loading of the metal (9), support – metal interaction (10-13) and nature of reductant (15).

Studies have compared the activities of the noble metals in the SCR reaction (12,16). Rhodium and palladium on both alumina and silica have been shown to be less active than the supported platinum counterpart in the propane – NO SCR reaction (12); however, the temperature of peak activity was shown to be significantly different. In the case of rhodium activity was at a maximum at 300°C, 100°C lower than that of the platinum catalyst. Palladium was shown to be the least active catalyst in this study and in an investigation studying iridium, platinum, palladium, rhodium and ruthenium catalysts for the propene – NO SCR reaction (16). Here it was reported that at temperatures in the region of 275°C platinum / alumina catalyst had a greater activity than rhodium / alumina catalysts, but at 350°C the Rh and Ru were superior. A benefit of greater selectivity to N_2 rather than N_2O was also reported with the use of rhodium instead of platinum.

Copper containing aluminophosphate has been reported as a comparable catalyst to Cu-ZSM-5 in the SCR reaction (17). Dehydration of zeolites, which may require temperatures in the region of 350°C, opens up the channel structure (6). AlPO-5, as shown in figure 6.2., has an open framework structure containing channels of molecular dimensions. The $AlPO_4$ group is based on aluminophoshate with the general formula:-

$$[\,(AlO_2)_m(PO_2)_m\,]\cdot{}_nH_2O$$

Further features distinguishing zeolites from $AlPO_4$s is that in these aluminophospates the Al : P ratio is constant: they may contain aluminium in coordination other than tetrahedral and they have a neutral framework and so such cannot act as acid catalysts (6).

AlPO-5 is one of the simplest of the microporous aluminophoshates that has been prepared and was the first in the group whose structure was determined (6). AlPO-5 is a large pore molecular sieve with a unidimensional pore system of diameter approximately 8Å. This 12-membered channel is surrounded by 4- and 6-rings. Modification of the preparation of microporous aluminophoshpates has allowed for the incorporation of metal ions into the tetrahedral framework sites.

Figure 6.2. The framework structure of AlPO-5

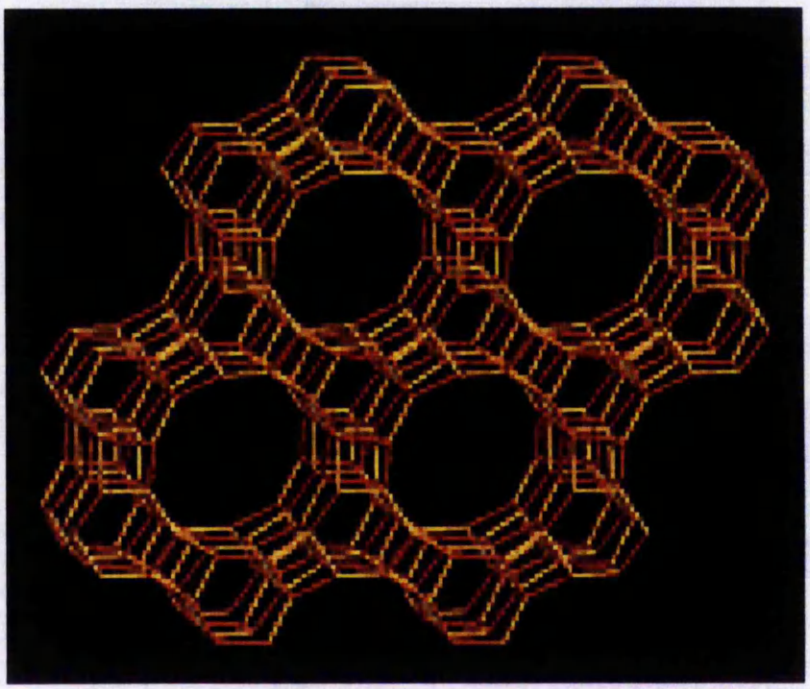

6.2: Study Aims

It is the aim of this study to investigate the performance of Cu-AlPO-5 catalysts, prepared by two routes, in the SCR reaction. These aluminophoshate catalysts were prepared and characterised by researchers at the University of Trondheim. A rhodium / zirconia catalyst and a Cu-ZSM-5 catalyst were investigated under the same conditions for comparison.

6.3: Experimental

6.3.1. Catalysts preparation

The catalysts were prepared as shown in figure 6.3. overleaf.

The two copper – aluminophosphate characters were shown to be different because of the method of preparation (18). This is discussed in section 6.4., with respect to the activity of the catalyst. Atomic absorption analysis showed that the (AC) and (IW) samples contained 5.0 and 5.7 wt% copper respectively.

The Cu-ZSM-5 catalyst was one that was previously prepared (5). The method of preparation involved the one-step ion exchange process, giving a material with a metal loading of 3.2 wt%. The material is said to be over-exchanged, in that the catalyst contains more copper ions than required to replace the charge balancing Na^+ or H^+ within the structure assuming a 2:1 stoichiometry. In the framework of ZSM-5, the exchange of Na^+ or H^+ for Cu^{2+} is known to be the best method of preparation to obtain a Cu-ZSM-5 with good catalytic activity in the SCR reaction (19), with exchange level shown to be of importance (20). Within the Cu-ZSM-5 copper ions are present as both isolated species and small clusters linked by extra-lattice oxygen eg (Cu^{2+} - O - Cu^{2+}) pairs as the active site. Over-exchange has been shown to enhance the formation of these sites within the ZSM-5 structure (21).

The forth catalyst investigated was the 1 wt% rhodium / zirconia material prepared by coprecipitation and calcined at 650°C, as described in chapter 5.

Figure 6.3. Catalysts preparation

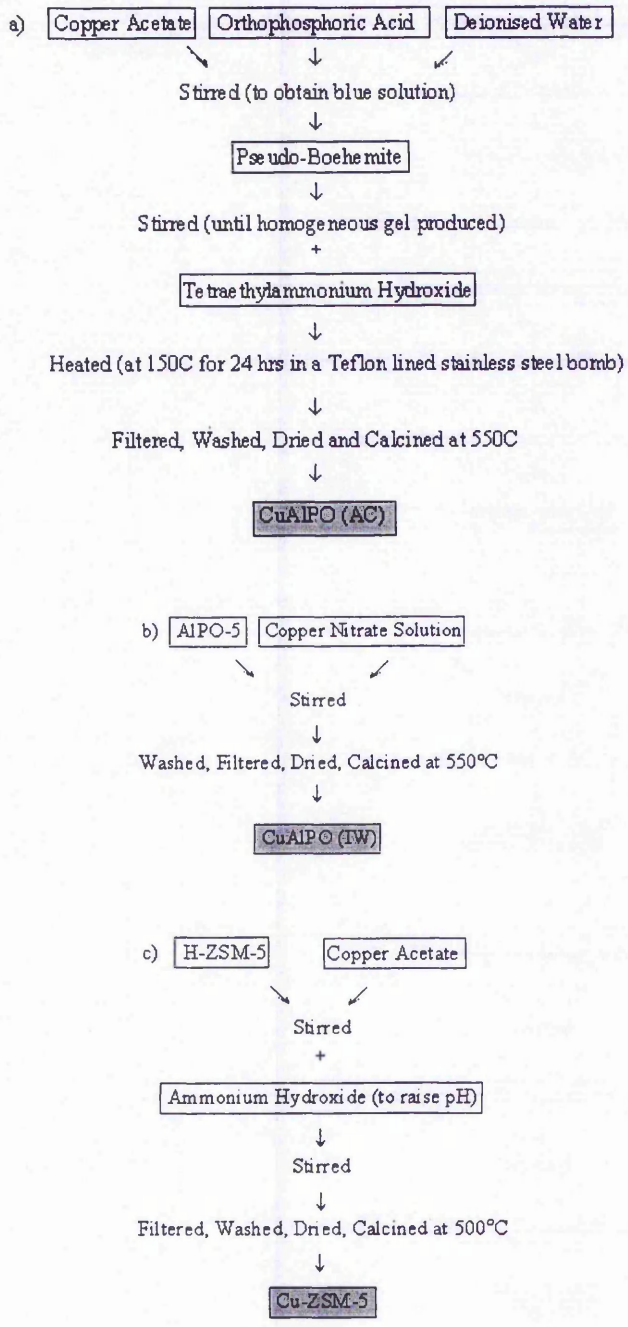

6.3.2: Catalyst Testing

The microreactor set-up used was that described previously in chapter 2. It allows the conversion of propene and nitric oxide to nitrogen, nitrous oxide and carbon dioxide to be monitored.

Prior to loading the catalysts into the reactor tube, the powders were granulated and screened to a particle size of 0.6 – 1.0 ml. A bed volume of 1 ml was used, with a gas flow rate of 300 ml / min (GHSV = 18,000h^{-1}). The catalysts were pretreated at 500°C for 1 hour in 2% oxygen in helium. The catalysts were tested over a temperature range of 500-200°C, in 2% O_2, 2000ppm NO, 1220ppm propene and helium balance. Two samples of the exit gas were analysed at each temperature. The performance of the catalyst was described by the conversion of propene to carbon dioxide and nitric oxide to nitrous oxide and dinitrogen, through the following equations…

$$\text{Percentage Conversion of NO} = \frac{2 \times \text{ppm } N_2 \text{ and } N_2O \text{ Produced}}{\text{ppm NO in Feed Gas}} \times 100\%$$

$$\text{Percentage Conversion of Propene to } CO_2 = \frac{\text{ppm of } CO_2 \text{ Produced}}{3 \times \text{ppm Propene in Feed Gas}} \times 100\%$$

The activity of a catalyst can be represented either by the mass of reactant converted per unit mass or volume of catalyst per unit time, or by the number of molecules reacting per unit time per active site. The latter is often referred to as the turnover frequency or the turnover number (22). Here turnover number is used at optimum conversion temperature for each catalyst, in an attempt to compare the activity of the active components of the catalysts for the de-NOx process. Turnover number thus is said to be amount of molecules per second of NO removed, per active metal ion (either copper or rhodium).

6.4: Catalyst Results

The propene and NO conversions for the four catalysts are shown in figures 6.4. and 6.5. respectively. Each point is shown with an accuracy of + / - 1%.

From figure 6.4. it can be seen that in the case of the Cu-AlPO-5 (IW) catalyst, i.e. the material by which copper was deposited by the incipient wetness approach, there is little conversion below *circa* 400°C, as compared to the catalyst prepared by the acetate route, Cu-AlPO-5 (AC). Both AlPO based catalysts are out-performed by the rhodium / zirconia and Cu-ZSM-5 catalysts.

Figure 6.4. Propene conversion to CO_2 for the four catalysts

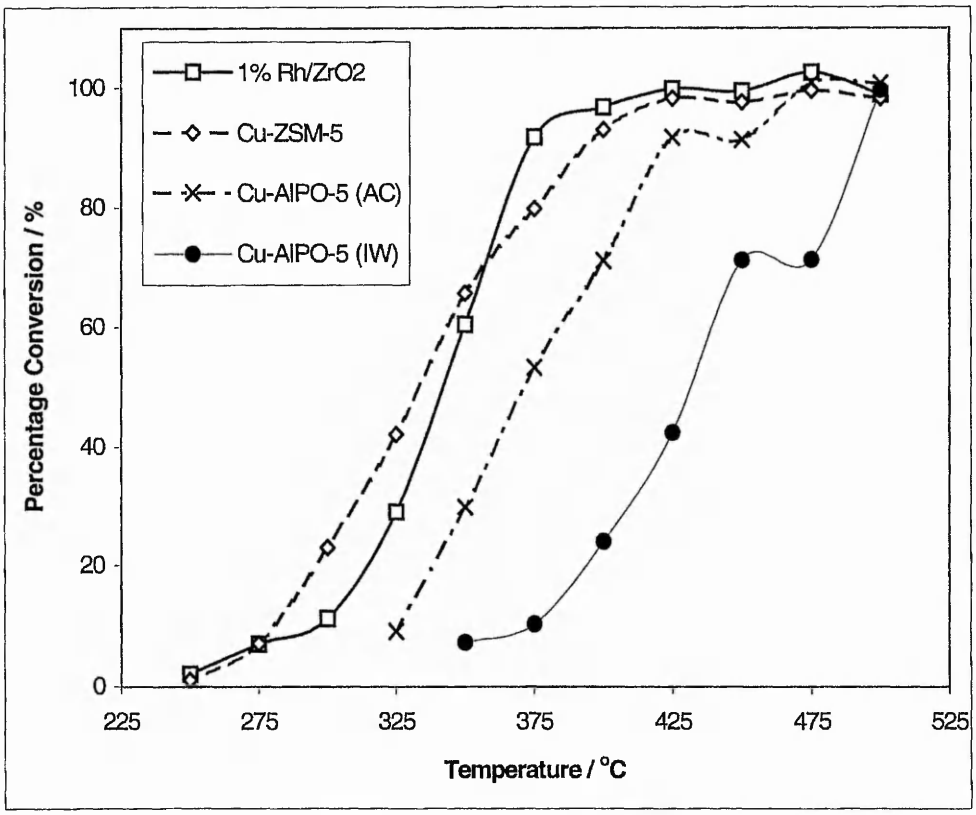

In figure 6.5. the SCR characteristics of Cu-ZSM-5 are clearly shown to be excellent, and superior to the other three catalysts. The rhodium / zirconia material too is shown to be superior to the Cu-AlPO-5 catalysts.

There is a great difference in the activity of the two types of aluminophosphate materials. Cu-AlPO-5 (AC) maintains higher propene conversion levels over a wider temperature range and also exhibits different trends in NOx conversion as compared to Cu-AlPO-5 (IW). In the case of Cu-AlPO-5 (AC), NOx conversion increases to a maximum at 375°C followed by slow decline to 500°C. With Cu-AlPO-5 (IW) NOx conversion falls at temperatures lower than 500°C.

The most interesting point of this investigation is the difference in de-NOx ability between the AlPO materials, attributed to changes in the preparative route.

Figure 6.5. NO conversion for the four catalysts

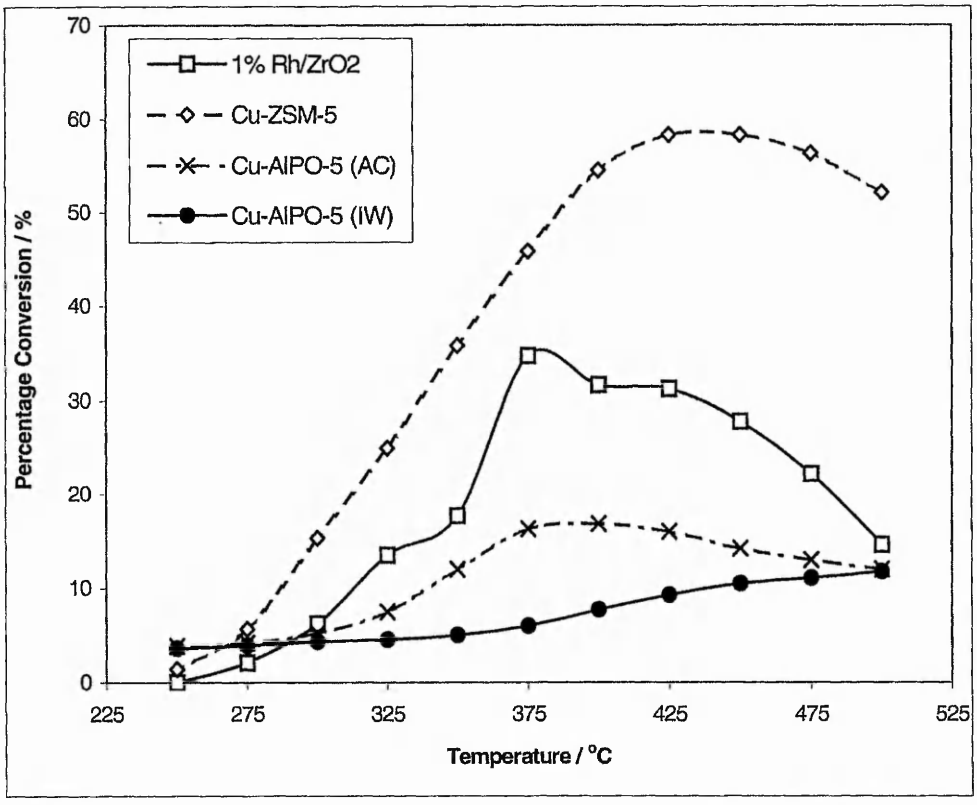

Table 6.1. shows the turnover numbers at the temperatures of maximum conversion of NO. It can be seen that activity of the copper is strongly related to the environment i.e. zeotype, and mode of preparation.

Table 6.1. Turnover numbers at temperature of maximum conversion

Catalyst Type	Turnover Number	Temperature at Maximum Turnover / °C
Cu-ZSM-5	0.00205	425
Rh / ZrO_2	0.00133	375
Cu-AlPO (AC)	0.00038	375
Cu-AlPO (IW)	0.00023	500

6.5: Discussion

From the results shown in section 6.3. it can be clearly seen that significant differences exist in the activity of the four investigated catalysts. Here the differences, and the reasons for these, are discussed.

For a good SCR catalyst there exists conditions where the reactivity is not dominated by the total oxidation of the reductant by oxygen, in this case propene. Thus the reaction:-

$$C_3H_6 + 2NO + {}^7/_2O_2 \rightarrow N_2 + 3CO_2 + 3H_2O$$

will dominate over:-

$$C_3H_6 + {}^9/_2O_2 \rightarrow 3CO_2 + 3H_2O$$

Thus, with respect to the ability of the catalyst in performing the reaction, the materials can be ranked in order of their activity:-

$$\text{Cu-ZSM-5} > \text{Rh / } ZrO_2 > \text{Cu-AlPO (AC)} > \text{Cu-AlPO (IW)}$$

As previously stated, in the introduction, within the Cu-ZSM-5, copper ions are present as both isolated species and small clusters linked by extra-lattice oxygen eg (Cu^{2+} - O - Cu^{2+}) pairs as the active site (5,6,21). XANES and EXAFS techniques have been used to determine *in-situ* structural changes in Cu-ZSM-5 (23-25). Here it was shown that fresh exchanged zeolites had fully coordinated Cu (II) ions, because of the presence of water, randomly distributed. Coordination modification occurred on calcination with copper being implanted on the zeolite framework oxygen. Activation in helium indicated an autoreduction of Cu (II) to Cu (I). This was also shown to occur in oxidising environments. In *in-situ* conditions the Cu (II) to Cu (I) to Cu (II) cycle was shown to be important to the SCR reaction thus...

$$O - Cu\ (II) + C_3H_6 \rightarrow Cu\ (I).C_3H_6$$

$$Cu\ (I).C_3H_6 + NO + O_2 \rightarrow O - Cu\ (II) + N_2 + CO_2 + H_2O$$

The activity of protonic zeolites for the SCR reaction has been well documented and it is claimed that the Bronsted acid sites are the active centres for the process (26,27). The ion-exchange process, for the formation of Cu-ZSM-5, reduces the number of Bronsted sites, and thus activity becomes associated with the Cu (I) Lewis acid sites (4).

The chemical nature of the AlPO catalysts are very different from that of Cu-ZSM-5. It is for this reason that catalytic activity is very different.

The x-ray adsorption techniques of XANES and EXAFS were used to characterise the AlPO catalysts (18). They showed that autoreduction of Cu(II) to Cu(I) did not occur upon calcination in either AlPO catalyst and that the active species, Cu^{2+} - O - Cu^{2+}, was not observed. These facts, combined with the statement in the introduction that AlPO's are devoid of acid sites (6), reveal why the activity of the Cu-AlPO's was observed as being much poorer than Cu-ZSM-5.

Zirconia has acidic properties (28-31). It has been described as a weakly acidic oxide which demonstrates primarily Lewis acidity, together with partial Bronsted acidity (31), but it is the nature of the rhodium that has been stated as being the reason for the reasonable activity in SCR conditions (32). Isolated Rh^{3+} species, produced by interaction with the support, are stated as the best rhodium species for the SCR of NO

by propene. The rhodium / zirconia catalyst used in this investigation, the preparation method of which is described in chapter 5, has been argued to have a strong Rh – Zr interaction because of the importance of the presence of rhodium in stabilising the tetragonal phase. It has also been assumed that because of the interaction, rhodium species will be present in an isolated manner on the surface of the material.

The activity of the two Cu-AlPO's in the SCR reaction are very different, as can be seen from figures 6.5. and 6.6. and table 6.1. Cu-AlPO (AC) has a greater turnover number than Cu-AlPO (IW) and has a temperature / reaction profile that is very much superior. The differences are put down to the nature of the incorporated copper in the structure, because of the mode of preparation. EXAFS showed that copper was incorporated into the structure of Cu-AlPO (AC) by [(AlPO) – $(O)_4$ – Cu] linkage, whereas in Cu-AlPO (IW) copper was shown to exist in several environments (18). Thus in Cu-AlPO materials, it is the presence of [(AlPO) – $(O)_4$ – Cu] groups which enhance catalytic activity.

6.6: Conclusions

In this chapter it has been shown that the AlPO-5 structure is much less effective a vehicle for copper for the SCR of NO by propene than ZSM-5. The activity of each copper unit, as determined by turnover number, was shown to be much greater in the case of Cu-ZSM-5. The nature of the copper within the AlPO structure however was shown to be different due to the mode of preparation. The difference in the nature of the incorporated copper was shown to be important to the catalytic nature of the material.

6.7: References

1. R.Gould. Volvo Leaflet "Building Cars for a Better Environment" 1989
2. G.W.Spitznagel, K.Huttenhofer, J.K.Beer 'Environmental Catalysis' Ed.J.N.Armor American Chemical Society 1994 172-189
3. R.J.Farrauto, R.M.Heck, Catalysis Today 1999 51 351-360
4. J.Connerton. Ph.D. Thesis. The Nottingham Trent University 1999
5. N.W.Hayes. Ph.D. Thesis. The University of Liverpool 1995
6. R.Szostak. Molecular Sieves - Principles of Synthesis and Investigation. Van Nostrand Reinhold. 1989 205-277
7. B.Wicherova, Z.Sobalik, M.Skokanek. Appl.Catal.A.Gen. 1993 103 269
8. J.Y.Lan, G.D.Lei, W.H.M.Sachtler, H.H.Kung. J.Catal. 1996 161 43
9. R.Burch, P.J.Millington, A.P.Walker. Appl.Catal.B.Env. 1994 4 65
10. M.Inaba, Y.Kintaichi, H.Hamada. Catal.Lett. 1996 36 223
11. T.Inoue, K.Tomishige, Y.Iwasawa. J.Chem.Soc.Faraday.Trans. 1996 92 461
12. H.Hamada, Y.Kintaichi, M.Sasaki, T.Ito. Appl.Catal. 1991 75 L1
13. M.Sasaki, H.Hamada, Y.Kintaichi, T.Ito. Catal.Lett. 1992 15 297
14. T.Tanaka, T.Okuhara, M.Misoso. Appl.Catal.B.Env. 1994 4 L1
15. R.Burch, D.Ottery. Appl.Catal.B.Env. 1996 9 L19
16. A.Obuchi, A.Ohi, M.Nakamura, A.Ogato, K.Mizuno, H.Ohuchi. Appl.Catal.B.Env. 1993 2 71
17. J.Dedecek. A.Vondrova. J.Cejka. Collect.Czech.Chem.Comm. 1998 63 1755
18. I.D.Burton, J.S.J.Hargreaves, D.G.Nicholson, M.H.Nilsen, M.Stockenhuber. J.Mater.Chem. 2000 11 1441-1446
19. Z.Chajar, M.Primet, H.Praliaud, M.Chevrier, C.Gauthier, F.Mathis. Appl.Cata.B.Env. 1994 4 199
20. S.Sato Y.Y.U, H.Yahiro, N.Mizuno, M.Iwamoto Appl.Catal 1991 70 L1
21. W.Grunert, N.W.Hayes, R.W.Joyner, E.S.Shpiro, M.R.H.Siddiqui, G.N.Baeva. J.Phys.Chem. 1994 98 10,832
22. M.V.Twigg. 'Catalyst Handbook' Wolfe Publishing London England 1989
23. D.J.Lui, H.J.Robota. Appl.Catal.B.Env. 1994 4 155
24. D.J.Lui, H.J.Robota. Cat.Lett. 1993 21 291

25. D.J.Lui, H.J.Robota. 'Reduction of Nitrogen Oxide Emissions' Ed. U.S Ozkan. ACS Symposium Series. 1995 587 147
26. H.Hamada, Y.Kintaichi, M.Sasaki, T.Ito. Appl.Catal. 1990 64 L1
27. H.Hamada, Y.Kintaichi, M.Sasaki, T.Ito. Appl.Catal. 1991 70 L15
28. M.A.Aramendia, V.Borau, C.Jimenez, J.M. Marinas. A.Porra, F.J.Urbano. J.Chem.Soc.Farad.Trans. 1997 93 1431
29. K.Tanabe. Mater.Chem.Phys. 1985 13 347
30. K.Shibata, T.Kiyoura, J.Kitagawa, T.Sumiyoshi, K.Tanabe. Bull.Chem.Soc.Jpn. 1973 46 2985
31. Y.Nakano, T.Lizuka, H.Hattori, K.Tanabe. J.Catal. 1979 57 1
32. R.Burch, P.K.Loader. Appl.Catal.A.Gen. 1996 143 317